

**INTRACORONARY THERMOGRAPHY**  
**A VULNERABLE PLAQUE DETECTION TECHNIQUE?**

ANNA GEERTRUIDA TEN HAVE

ISBN 90-9020879-8

©2006 by A.G. ten Have

Printed by PrintPartners Ipskamp.

All rights reserved. No part of this publication may be reproduced, stored in a retrieval system, or transmitted, in any form, or by any means, electronic, mechanical, photocopying, recording, or otherwise, without the prior consent of the author.

**INTRACORONARY THERMOGRAPHY**  
**A VULNERABLE PLAQUE DETECTION TECHNIQUE?**

**INTRACORONAIRE THERMOGRAFIE**  
**EEN DETECTIEMETHODE VOOR VULNERABELE**  
**PLAQUES?**

**PROEFSCHRIFT**

ter verkrijging van de graad van doctor aan de  
Erasmus Universiteit Rotterdam  
op gezag van de  
rector magnificus

Prof.dr. S.W.J. Lamberts

en volgens besluit van het College voor Promoties.  
De openbare verdediging zal plaatsvinden op

vrijdag 8 september 2006 om 13:30 uur  
door  
Anna Geertruida ten Have  
geboren te Wolvega

## **PROMOTIECOMMISSIE**

PROMOTOREN: Prof.dr.ir. A.F.W. van der Steen  
Prof.dr. P.W.J.C. Serruys

OVERIGE LEDEN: Dr. R. Krams  
Dr. S. Verheyne  
Prof.dr.ir. F.N. van de Vosse

COPROMOTOR: Dr.ir. F.J.H. Gijsen

This work has been supported by the Stichting Technologische Wetenschappen (RPG.5442).

### **SPONSORS**

Financial support by the Netherlands Heart Foundation and the J.E. Jurriaanse Stichting for the publication of this thesis is gratefully acknowledged.

The printing of this thesis was also made possible by Volcano Corporation, Bristol-Myers Squibb Medical Imaging, Cardialysis, Boston Scientific, STW, ICIN, Pfizer and Contract Medical International.

# CONTENTS

<b>1</b>	<b>Vulnerable plaque and its detection</b>	<b>9</b>
1.1	Coronary heart disease . . . . .	10
1.2	Atherosclerosis . . . . .	10
1.3	Vulnerable plaque . . . . .	11
1.4	Detection of the vulnerable plaque . . . . .	12
1.4.1	Anatomical features . . . . .	12
1.4.2	Other characteristics . . . . .	13
1.5	Scope and outline . . . . .	14
<b>2</b>	<b>Heat generation, transfer and detection</b>	<b>17</b>
2.1	Introduction . . . . .	18
2.2	Heat . . . . .	18
2.2.1	Heat generation . . . . .	20
2.2.2	Heat transfer . . . . .	22
2.2.3	Heat detection . . . . .	24
2.3	Previously used catheters and reported studies . . . . .	25
2.3.1	Needle thermistor . . . . .	26
2.3.2	Hydrofoil thermistor catheter . . . . .	27
2.3.3	Thermistor catheter . . . . .	29
2.3.4	Basket thermocouple catheter . . . . .	30
2.3.5	Thermocouple guidewire . . . . .	31

2.3.6	Detection of temperature distributions using a mathematical model . . . . .	32
2.4	Conclusions and recommendations . . . . .	33
2.4.1	Heat source . . . . .	33
2.4.2	Heat transfer . . . . .	34
2.4.3	Heat detection . . . . .	35
2.4.4	Closing remarks . . . . .	35
<b>3</b>	<b>Influence of plaque geometry and flow</b>	<b>37</b>
3.1	Introduction . . . . .	38
3.2	Methods . . . . .	39
3.2.1	Geometrical model . . . . .	39
3.2.2	Equations . . . . .	41
3.2.3	Boundary conditions . . . . .	42
3.2.4	Tissue parameters . . . . .	43
3.2.5	Solution procedure . . . . .	43
3.2.6	Flow Influence Factor . . . . .	44
3.3	Results . . . . .	45
3.3.1	Mesh independence and boundary conditions . . . . .	45
3.3.2	Dependence of $\Delta T_{flow}$ and $\Delta T_{noflow}$ . . . . .	45
3.3.3	Flow Influence Factor . . . . .	47
3.4	Discussion . . . . .	49
3.4.1	Dependence of $\Delta T_{flow}$ and $\Delta T_{noflow}$ . . . . .	50
3.4.2	Flow Influence Factor . . . . .	54
3.4.3	Remarks . . . . .	55
3.5	Conclusions . . . . .	57
<b>4</b>	<b>Influence of vulnerable plaque composition</b>	<b>59</b>
4.1	Introduction . . . . .	60
4.2	Methods . . . . .	61
4.2.1	Geometrical model . . . . .	61
4.2.2	Equations . . . . .	62
4.2.3	Boundary conditions and material properties . . . . .	63
4.2.4	Solution procedure . . . . .	64
4.2.5	Analysis of results . . . . .	64
4.3	Results . . . . .	65
4.3.1	Heat generation . . . . .	65
4.3.2	Influence of thermal properties of the lipid core . . . . .	67
4.3.3	Heat exchange by the vasa vasorum . . . . .	68
4.4	Discussion . . . . .	70
4.4.1	Heat generation . . . . .	70

4.4.2	Influence of insulating properties of lipid core . . . . .	71
4.4.3	Influence of location of vasa vasorum . . . . .	72
4.4.4	Limitations . . . . .	73
4.5	Conclusions . . . . .	73
<b>5</b>	<b>Influence of catheter design</b>	<b>75</b>
5.1	Introduction . . . . .	76
5.2	Methods . . . . .	76
5.2.1	Geometrical model . . . . .	76
5.2.2	Boundary conditions . . . . .	78
5.2.3	Material parameters . . . . .	79
5.2.4	Numerical solution procedure . . . . .	79
5.2.5	Analysis of results . . . . .	80
5.3	Results . . . . .	80
5.3.1	General observations . . . . .	80
5.3.2	Pullback and optimal sensor location . . . . .	82
5.3.3	Influence of catheter location . . . . .	82
5.3.4	Influence of catheter diameter . . . . .	85
5.4	Discussion . . . . .	85
5.5	Recommendations for catheter design . . . . .	87
<b>6</b>	<b>Temperature measurement of advanced murine atherosclerotic plaques</b>	<b>89</b>
6.1	Introduction . . . . .	90
6.2	Methods . . . . .	91
6.2.1	Mice . . . . .	91
6.2.2	Experimental set-up and protocol . . . . .	93
6.2.3	Histology . . . . .	95
6.2.4	Analysis . . . . .	95
6.3	Results . . . . .	98
6.3.1	General . . . . .	98
6.3.2	Temperature . . . . .	98
6.3.3	Histology . . . . .	99
6.3.4	Temperature vs. histology . . . . .	99
6.4	Discussion . . . . .	104
6.5	Conclusions and recommendations . . . . .	106
6.6	Acknowledgements . . . . .	106

<b>7</b>	<b>Conclusions: heat generation, transfer and detection</b>	<b>107</b>
7.1	Introduction . . . . .	108
7.2	Summary . . . . .	108
7.3	Discussion . . . . .	110
7.3.1	Heat generation . . . . .	110
7.3.2	Heat transfer . . . . .	111
7.3.3	Heat detection . . . . .	112
7.4	Conclusions and future perspective . . . . .	114
	<b>References</b>	<b>115</b>
	<b>Samenvatting</b>	<b>125</b>
	<b>Dankwoord</b>	<b>129</b>
	<b>Curriculum vitae</b>	<b>131</b>





# VULNERABLE PLAQUE AND ITS DETECTION

The first chapter gives an introduction to intracoronary thermography as a vulnerable plaque detection technique. It starts with a description of coronary heart disease, the number one cause of death worldwide. It then focusses on atherosclerosis, a progressive, inflammatory disease mainly found in the large arteries. Its developmental stages can be subdivided according to the AHA classification. One of the developmental stages of atherosclerosis concerns the vulnerable plaque, of which the so-called TCFA is the most common type. The chapter then continues with vulnerable plaque detection methods, based on anatomical features and other characteristics of the vulnerable plaque. Anatomical features of the vulnerable plaque include a thin fibrous cap, a large lipid pool and macrophage infiltration. Other characteristics used for vulnerable plaque detection are high-strain spots, inflammatory markers and increased temperature. The chapter concludes with the scope and outline of this thesis.

## 1.1 CORONARY HEART DISEASE

Cardiovascular disease, causing 16.7 million deaths annually worldwide, is currently known to exist typically in developed countries (WHO 2003, Mackay 2004). In fact, twice as many deaths from cardiovascular disease now occur in developing countries as in developed countries. Coronary heart disease, one manifestation of cardiovascular disease, is the leading cause of death worldwide, causing around 7.2 million deaths per year worldwide. Since 1990, more people have died from coronary heart disease than from any other cause.

Risk factors for coronary heart disease can be divided into modifiable and non-modifiable risk factors (WHO 2003, Mackay 2004). The most important modifiable risk factors include high blood pressure, tobacco use, high cholesterol, alcohol, obesity, low fruit and vegetable intake and physical inactivity. Non-modifiable risk factors are advancing age, heredity or family history, gender and ethnicity. Presence of risk factors differs among countries. Approximately 75% of cardiovascular disease cases can be attributed to conventional, modifiable risk factors, which makes it a disease typical for developed countries, even though coronary heart disease is decreasing in many of them. In developing and transitional countries it is increasing, partly as a result of increasing longevity, urbanization and lifestyle changes. In absence of elevations of these risk factors, coronary heart disease is a rare cause of death.

## 1.2 ATHEROSCLEROSIS

Coronary heart diseases are the diseases of the blood vessels supplying the heart muscle with blood. When the heart, or part of it, is deprived of oxygen, ischemia occurs, which is most frequently caused by advanced stages of atherosclerosis. Atherosclerosis is a progressive, inflammatory disease characterized by accumulations of lipids and fibrous tissue in the large arteries. Sites predisposed to lesion formation include branch points of arteries, such as bifurcations and side branches, which experience disturbed flow. These sites usually show adaptive intimal thickening, which can be interpreted as an attempt to maintain normal conditions of flow and wall tension by a range of physiological stimuli in the tissue (Stary 1992, Falk 1995, Libby 2002).

Even though the stages of atherosclerotic disease cannot be neatly separated, atherosclerosis can be divided into a number of developmental stages, according to the AHA classification (Stary 1994, Stary 1995, Stary 2000). The normal, healthy intima consists of endothelial cells, smooth muscle cells and isolated macrophages embedded into the extracellular matrix, and is separated from the media by the internal elastic lamina (Stary 1992). The very initial

changes of the intima, showing an increase in the number of macrophages and the appearance of foam cells, are named type I lesions (Stary 1994). These can develop into type II lesions, in which layers of macrophage foam cells and lipid droplets within intimal smooth muscle cells are seen. Also, minimal coarse-grained particles and heterogeneous droplets of extracellular lipid is visible. This category includes the first grossly visible lesion, called the fatty streak. Type III lesions are those linking type II lesions to the advanced lesion types, and are characterized by separate pools of extracellular lipid in addition to the components of type II lesions.

Advanced lesions, type IV through VIII, are those in which intimal lipid accumulation is associated with intimal disorganization, thickening, and complications such as fissure, hematoma and thrombosis (Stary 1995, Stary 2000). Advanced lesions may produce symptoms, but the lesions that precede them are clinically silent. A type IV lesion shows intimal disorganization due to a lipid core, and is also called atheroma. This lesion type is usually eccentric and minimally narrowing the lumen. The periphery of the lesion may be vulnerable to rupture, due to the abundant presence of macrophages. When fibrous tissue increases in the nearly normal intimal cover of endothelial cells of lesions of type IV, the lesion evolves to a type V lesion. Type VI lesions originate from one or more additional features of disruption of the lesion surface of either a type IV or V lesion. These features include hematoma, hemorrhage and thrombotic deposits. These complicated lesions usually obstruct the lumen and are symptom producing. Instead, type IV and V lesions may also develop into lesions in which calcification predominates, type VII lesions, or into lesions in which fibrous tissue changes predominate, type VIII lesions.

### **1.3 VULNERABLE PLAQUE**

Plaque disruption with superimposed thrombosis is the main cause of acute coronary syndromes, such as unstable angina, myocardial infarction and sudden death. Plaques that are at increased risk of thrombosis and rapid stenosis progression are called vulnerable plaques, and can be divided into plaques prone to rupture, plaques prone to erosion and plaques containing a calcified nodule (Virmani 2000, Schaar 2004a).

Plaque rupture is the most common cause of coronary thrombosis, and in retrospective studies it was shown that these plaques were inflamed, thin cap fibroatheromas (TCFA). The TCFA, labeled a type IV lesion in the AHA classification scheme, is characterized by a lipid-rich atheromatous core, a thin fibrous cap with macrophage and lymphocyte infiltration together with decreased smooth muscle content, and expansive remodeling (Falk 1995, Virmani

2000, Schaar 2004a).

The necrotic core area of a TCFA comprises on average  $23 \pm 17\%$  of the cross-sectional plaque area and is on average  $1.7 \pm 1.1 \text{ mm}^2$  in size. This necrotic core is of  $120^\circ$  circumference in 75% of the lesions. The cap thickness that distinguishes high-risk vulnerable plaques from stable plaques is  $65 \mu\text{m}$ . The length of a TCFA is on average 8 mm, varying between 2 and 17 mm (Burke 1997, Kolodgie 2004).

## 1.4 DETECTION OF THE VULNERABLE PLAQUE

Vulnerable plaques are high-risk plaques, being at risk to rupture, so their timely detection and optimized treatment is necessary to prevent acute clinical events. Obtaining knowledge on the developmental stages of these plaques, and thereby knowing their natural history, is therefore necessary. This requires both identification of the plaque and the ability to study its anatomical features and its other characteristics non-destructively over time. Currently, no single technique exists that can conclusively identify a vulnerable plaque, though many techniques are currently in development.

### 1.4.1 ANATOMICAL FEATURES

Anatomical features of a vulnerable plaque include the large lipid pool, a thin fibrous cap and presence of macrophages. Several imaging techniques aim at identifying and evaluating these features.

Lipid cores appear as an echolucent zone in intravascular ultrasound (IVUS) images. A firm relationship has not yet been proven, since other tissue components may have identical acoustic properties and thus appear similar (Nissen 2001). Spectral analysis of IVUS radiofrequency data is currently in development, and can discriminate between fibrous tissue, fibrolipidic tissue and tissue containing calcium. Sensitivity values of 89, 41 and 68% were reached, respectively (Nair 2002). It was shown that using computed tomography one can detect plaques and distinguish between calcified and non-calcified plaques (Ferencik 2006). For identifying lipid cores, 64-slice computed tomography (CT) revealed encouraging results, although use is currently limited due to a high interobserver variability for determining plaque volume (37%). The interobserver agreement to identify atherosclerotic sections was good (0.75) (Leber 2006). Due to the high spatial resolution required and the motion artefacts related to the beating heart, lipid core identification in coronary arteries by magnetic resonance imaging (MRI) is not yet feasible (Yuan 2004). Lipid core identification by MRI in larger and less mobile arteries such as the aorta

and carotid artery were shown to be possible (Fayad 2000, Shinnar 1999). Optical coherence tomography (OCT) has shown to distinguish the lipid core from other tissue by its appearance in the image, being signal poor and delineated poorly with respect to the surrounding tissue (Yabushita 2002). Using Raman spectroscopy, one can determine both the presence and composition of a lipid core. This method is currently hampered, though, by long collection times necessary to obtain good signal to noise ratios (van de Poll 2002).

Imaging of the cap of a TCFA requires a high spatial resolution. OCT, having a spatial resolution of 10  $\mu\text{m}$ , is currently the only method that can fulfil this criterion for coronary vulnerable plaques in vivo (Jang 2005). The thin cap appears as a thin signal-rich band overlying a large signal-poor region. The major disadvantage of OCT is the need for flushing the artery.

Presence of macrophages in the cap of a vulnerable plaque can be determined with OCT (MacNeill 2004). Macrophage density was larger in unstable patients, both for fibrous and lipid-rich plaques and sites of plaque rupture demonstrated a greater macrophage density than non-ruptured sites. Using nuclear imaging, presence of macrophages can be determined in vivo and non-invasively, by the radiolabeled tracer uptake by macrophages. One of the main challenges in this field is the poor resolution of this approach, which favors combining it with other imaging modalities (Davies 2005).

## 1.4.2 OTHER CHARACTERISTICS

Vulnerable plaque is currently recognized as an inflammatory disease, so inflammatory markers secreted by the plaque could point at presence of high risk vulnerable plaques. C-reactive protein, metalloproteinases secreted by macrophages and pregnancy associated plasma proteins are suggested markers, but other markers exist that are under study (Schwartz 2003). The disadvantage of the current inflammatory markers is that they respond to a range of inflammatory diseases, which disables detection of local inflammation seen in vulnerable plaques. In addition, they cannot determine the location of a plaque due to their systemic nature.

A functional feature by which vulnerable plaques can be detected is the high strain resulting from the differing tissue elastic properties of soft and hard tissues. Palpography can measure this strain by using cross-correlation analysis of radiofrequency ultrasound signals recorded at different intravascular pressures. The number of high strain spots was shown to be lower for stable angina patients than for unstable angina patients and patients that presented acute myocardial infarction (Schaar 2004b).

Inflammation, as described by Celsus, shows signs regarding pain,

swelling, redness and heat (Rocha e Silva 1978). This led to the assumption that vulnerable plaques could be detected by thermographic methods (Casscells 1996). Thermal heterogeneity in the coronary vessels exists, as is suggested by the number of in vivo publications on this topic (Stefanadis 1998, Verheye 2002a, Diamantopoulos 2003a, Krams 2005). Intracoronary thermography is the topic of this thesis.

## 1.5 SCOPE AND OUTLINE

Detection of vulnerable plaques, or more generally the treatment of atherosclerosis and other coronary artery diseases, can lead to optimal diagnosis and treatment of patients. This is advantageous, not only from an ethical point of view by saving lives, but also from an economical point by the ability to save money. Coronary artery disease and the developmental stages of atherosclerosis were described in this first chapter, as were ways to detect vulnerable plaques. Intracoronary thermography, one of the vulnerable plaque detection techniques, is the focus of this thesis.

After 1996, the year in which the first publication appeared that suggested the possibility of vulnerable plaque detection using intracoronary thermography, many data have been published. Large discrepancies can be noted in the published data, though, and the reported temperatures are of decreasing value. The data were obtained under differing experimental conditions, using different catheters, which could explain part of this discrepancy and decreasing trend in reported temperatures. The influence of other unknowns, such as blood flow, catheter design and plaque composition, might also play a role in the clarification. Due to these reasons, the use of intracoronary thermography as a vulnerable plaque detection technique is under debate. To elucidate the parameters that influence intracoronary temperature measurements, and to suggest ways to overcome the difficulties in this field, we have performed a number of studies, which are described in this thesis. These will help to answer the main question: can intracoronary thermography be used as a vulnerable plaque detection technique?

To better understand the parameters of influence on thermographic measurements, we have taken the task of identifying parameters that could contribute to an explanation of the mentioned discrepancy and decreasing trend in reported temperatures. We have done so by studying the field of intracoronary thermography from a more fundamental point of view, and the results of this study are described in chapter 2. The parameters were not only deduced from both the ex vivo and clinical studies that were published, but also from the biological principles regarding heat generation and from the physical

principles regarding heat transfer and heat detection.

The influence of a number of these parameters have been studied numerically. These studies are described in chapters 3, 4 and 5. In chapter 3, the influence of the blood flow through the lumen and the geometry of the heat source was studied. The influence of plaque composition is described in chapter 4. In this chapter, results describing the influence of the location of the heat source in the plaque and the lipid-density of the plaque on temperature distribution on the lumen wall are given. The study described in chapter 5 deals with the influence of the catheter on the intracoronary temperature readings. Results showing the influence of its presence and its design are given.

From the results of the numerical studies described in chapters 3 through 5, it became clear that for optimal application of intracoronary thermography, more information about the heat source causing the thermal heterogeneity is needed. Knowledge of its location and heat production values appeared to be key factors. For this, murine aortic arches containing atherosclerotic plaques were studied with an infrared camera. The results of this study are described in chapter 6. Chapter 7 concludes this thesis with a discussion of the studies that were performed, and describes the implications of them. In addition, it hands a future perspective for intracoronary thermography.







## CHAPTER 2

# HEAT GENERATION, TRANSFER AND DETECTION

Intracoronary thermography is a potential vulnerable plaque detection technique of which the development is ongoing. This chapter discusses the past and present status of this technique from a more fundamental perspective, in which heat generation, heat transfer and heat detection are considered. Details of the presumed heat source, the macrophage clusters in vulnerable, atherosclerotic plaques, are discussed. Heat transfer by ways of conduction, convection by blood flow and radiation are considered. Ways to detect heat that are currently used are discussed and suggestions for both improvement of existing thermography catheters and utilization of unexplored possibilities are given.

BASED ON: ten Have AG, Gijzen FJ, Wentzel JJ, Slager CJ, Serruys PW, van der Steen AF. Intracoronary thermography: heat generation, transfer and detection. *EuroIntervention* 2005;1:105-114.

## 2.1 INTRODUCTION

It is suggested that increased plaque heat is a feature of plaques that are denuded and inflamed and consequently at risk of thrombosis (Casscells 1996). This heat might be due to increased metabolic activity of inflammatory cells, such as macrophages, or due to enzymatic extracellular matrix breakdown. Detection of heat could thus possibly lead to detection of vulnerable plaques.

The use of vulnerable plaque detection has recently been discussed (Madjid 2004). The benefit of locating individual vulnerable plaques in a multifocal disease is a topic of debate. Detecting individual vulnerable plaques can be valuable for a number of reasons. Firstly, the natural history of the vulnerable plaque is not fully known and to obtain more information on the development of a vulnerable plaque one needs to be able to locate the individual vulnerable plaques. Secondly, pharmacological treatment of vulnerable plaque needs to be verified. And thirdly, there will be a group of people, of which the number is unknown, that will rely on invasive treatment due to failure of pharmacological treatment for whatever reason. In addition, effects of pharmacological agents can take a while to become effective, in which period it might be necessary to detect the individual plaques, perhaps to even treat them invasively. For these reasons one needs vulnerable plaque detection techniques that are well validated.

After the first publication in this relatively new field in cardiology, the detection of vulnerable plaques using thermographic methods (Casscells 1996), many thoughts and results on this detection technique have been published. In figure 2.1 some of the published temperatures have been plotted versus time. The temperatures differences that were published have decreased over time, but are still of significant value to conclude that thermal heterogeneity exists *in vivo*. Based on these values it is worthwhile to continue studying the exact details of the origin and the consequences of this thermal heterogeneity. This review tries to determine what needs to be measured and which pitfalls arise when measuring temperatures *in vivo*. In addition, it suggests ways to overcome these problems.

## 2.2 HEAT

A heat source embedded in arterial wall tissue will generate heat, which is transferred to its surroundings, thus causing a temperature difference, which can be detected. The temperature difference depends on a large number of parameters and processes. First of all, it depends on the amount of heat that is generated and on the location and the size of the source. Secondly, on how the

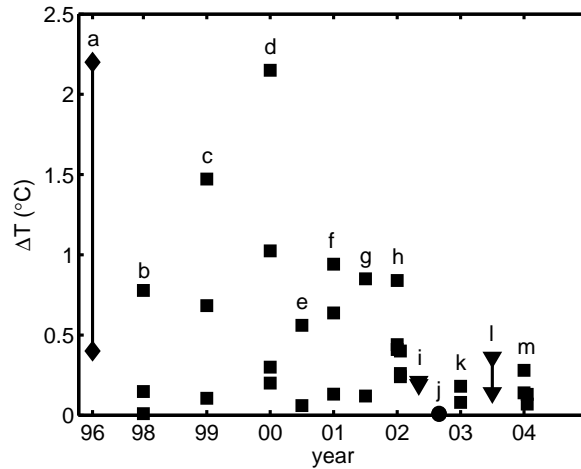


FIGURE 2.1: A selection of published intracoronary thermography data. Temperatures measured either ex vivo on human atherosclerotic tissue (a) or in vivo in human coronary arteries (b through m). Solid lines: reported temperature ranges, symbols: reported mean values. Diamonds: needle thermistor, squares: hydrofoil thermistor catheters, downward triangles: basket thermocouple catheter, circles: thermistor catheter. a: Casscells et al (Casscells 1996), b: Stefanadis et al (Stefanadis 1998), c: Stefanadis et al (Stefanadis 1999), d: Stefanadis et al (Stefanadis 2000), e: Toutouzas et al (Toutouzas 2000), f: Stefanadis et al (Stefanadis 2001), g: Toutouzas et al (Toutouzas 2001), h: Stefanadis et al (Stefanadis 2002), i: Webster et al (Webster 2002), j: Verheye et al (Verheye 2002c), k: Stefanadis et al (Stefanadis 2003b), l: Schmermund et al (Schmermund 2003), m: Toutouzas et al (Toutouzas 2004).

heat is transferred, and thirdly, on how it is measured.

### 2.2.1 HEAT GENERATION

The mechanism by which the observed heat production of plaques occurs is unknown, but most evidence points towards high metabolism of macrophages. Macrophages are abundantly present in vulnerable plaques, bordering the atheromatous core, and are located in the fibrous cap, especially near the shoulder regions of the cap (Falk 1995). Speculations have been made with regard to the processes that are involved in the heat generation, including the high metabolic activity of inflammatory cells, the presence of the uncoupling protein 2 (UCP-2) in the macrophages (Zarrabi 2002, Madjid 2002, Verheye 2002b), and lipid endocytosis and conversion by macrophages (Falk 1995). In addition, the action of matrix metalloproteinases (MMPs) secreted by macrophages (Falk 1995) might include exothermal processes.

#### MACROPHAGE METABOLISM

The turnover rate for the total ATP content of the macrophage in culture is about 10 times per minute, being an order of magnitude higher than a typical mammalian cell (Alberts 1989), which indicates that macrophages have a high metabolic rate (Newsholme 1989).

Oxygen consumption of the arterial wall increased up to a certain level with increasing degree of atherosclerotic involvement, and a supposed increase in foam cell density (Bjornheden 1987). This might be explained by an increased oxygen consumption of isolated foam cells, which was three times higher than that of isolated smooth muscle cells. However, with increasing intima thickness the available diffusion capacity for oxygen and nutrients, including glucose, to deeper parts of the lesion may become insufficient, which leads to a relative decrease in cellular oxygen consumption of the more diseased atherosclerotic tissue samples (Bjornheden 1987).

#### MECHANISMS RESPONSIBLE FOR INCREASED ENERGY CONSUMPTION

**Enzymatic extracellular matrix degradation** Microcalorimetric analysis of bacterial collagenase degradation of porcine pericardium tissues revealed that the heat released during degradation correlates well with the degree of tissue degraded (Sung 1997). Therefore, the MMP related breakdown of extracellular matrix in atherosclerotic plaques might also be an exothermal process. Toutouzas et al (Toutouzas 2001) have demonstrated that patients with acute coronary syndromes show increased MMP-9 concentration, which was well

correlated with temperature differences between the atherosclerotic plaque and the normal vessel wall.

**Lipid metabolism** After the uptake of modified lipids by macrophages through various routes of endocytosis, most of the lipids are finally transported into lysosomes, digested therein, and degraded into amino acids and free cholesterol, which is released into the cytosol and further into the extracellular space. In the cytosol, the free cholesterol is trapped in a continued cycle of esterification and hydrolysis, which is called the cholesterol ester cycle (Takahashi 2002) that wastes ATP (Brown 1980). The rate of cholesterol esterification is positively correlated with the cholesterol content of arterial segments from atherosclerotic animals (St Clair 1976).

**Uncoupling proteins** The uncoupling protein (UCP-1), also called thermogenin, is a protein that is found exclusively in brown adipose tissue (BAT) in mammals. Thermogenesis, or heat production, in BAT depends largely on UCP-1 activity (Palou 1998). Of the UCP-1 molecule, a number of homologues exist, of which UCP-2 has been speculated to cause the temperature increase in vulnerable plaques (Kockx 2000). Advanced complicated atherosclerotic plaques have shown a dense infiltration of macrophages of which a subpopulation strongly expressed UCP-2. The UCP-2 positive macrophages were associated with oxidized lipids, iNOS and nitrotyrosine and a fraction showed apoptosis. Whether UCP-2 acts thermogenic in any tissue is still under debate (Nedergaard 2003).

## MACROPHAGE HEAT PRODUCTION

Macrophage metabolism, and thus heat generation, can be measured in vitro using microcalorimetry. Heat production values of non-phagocytosing mouse macrophages were shown to be 300 to 2500  $\times 10^{-12}$  cal ( $0.072$  to  $10.5 \times 10^{-9}$  J) per cell per scan, its value decreasing upon increasing cell density (Loike 1981). This corresponds to 0.78 to 6.5 pW per cell. The generated heat was primarily due to glucose metabolism, and glycolysis was a major contributor to the produced heat.

Heat production values of alveolar rabbit macrophages grown in a monolayer were  $19.4 \pm 3.2$  pW per cell (Thóren 1990). Adding 20% homologous rabbit serum to the growth medium increased the heat production to  $27.0 \pm 2.0$  pW per cell.

Heat production values of phagocytosing peritoneal mouse macrophages were measured in different experimental conditions (Charlebois 2002). Mean

heat production values for resting cells were  $20.6 \pm 10.1$  and  $16.2 \pm 3.1$  pW per cell. When e.g. lipopolysaccharide bounded high-density polyethylene particles were phagocytosed, these values could rise up to 92 pW per cell, implying an increase of up to five times the basal value.

### 2.2.2 HEAT TRANSFER

Transfer of thermal energy, or heat transfer, between two objects occurs only when the objects are at different temperatures and its direction is from a region of higher temperature to a region of lower temperature. This occurs either by conduction, convection, radiation, or by a combination of these depending on the media involved.

#### CONDUCTION

Conduction, figure 2.2A, is the transfer of heat through a solid or fluid medium due to a temperature gradient by the exchange of molecular kinetic energy during collisions of molecules.

Thermal parameters governing this process are the specific heat capacity (how many Joules are needed to raise a certain amount of the material one °C) and the heat conductivity (the amount of Joules per second (Watts) that pass a certain distance of material driven by a temperature difference of one °C). Materials can be divided into conductors, for example metals, known for their ability to transfer heat fast, and insulators, for example air and most plastics, which have low heat conductivity values. Fatty tissue is also known for its insulating properties (Duck 1990), so lipid present in the lipid core of a vulnerable plaque is likely to behave as an insulating material and may obstruct the transfer of heat produced by macrophages to its neighborhood.

#### CONVECTION

Convection, figure 2.2B, is the transfer of heat due to bulk motion of the medium. Heat produced by the vulnerable plaque will be transferred through the wall by means of conduction as described above. Once arrived at the lumen wall it will be transported by the flow of blood. Distal from the heat source, the heat can be transferred back to the lumen wall by conduction.

Parameters influencing the blood flow profile, such as curvature of the vessel and presence of a catheter, will result into changes of temperature distribution. Increase of local flow velocity will decrease the temperatures at the lumen wall (ten Have 2004). In addition, pulsatility might effect the measurement,

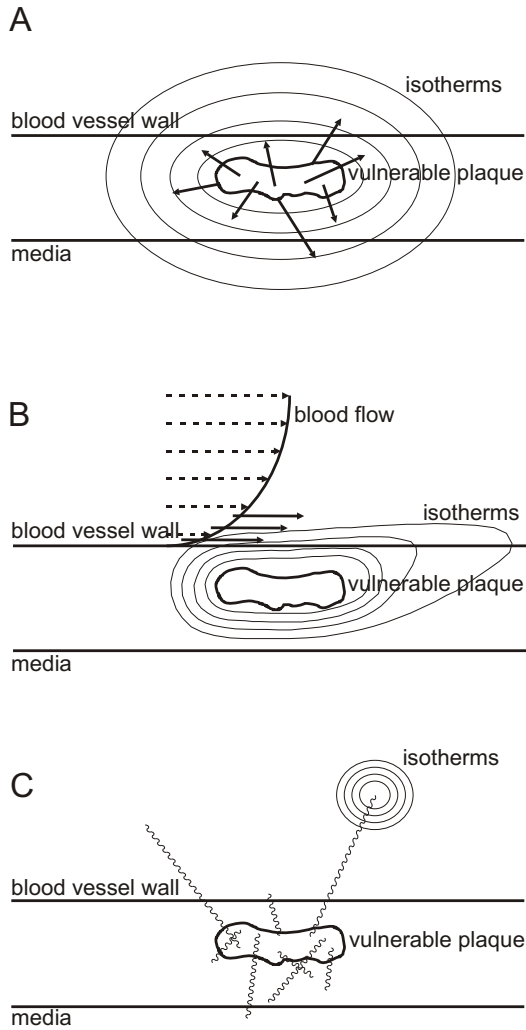


FIGURE 2.2: Different ways of heat transfer. A: conduction, B: conduction and convection, C: radiation and absorption.

since pulsating axial velocity produces a pulsating temperature distribution (Craciunescu 2001).

In a recently published review (Diamantopoulos 2003b) different ways of heat transfer are also identified. In the paper it is stated that convection is nonsignificant due to the strong blood flow. Clearly, just because of the strong blood flow in the lumen, convection cannot be neglected (ten Have 2004). This can be deduced from the Peclet number, that expresses the ratio of heat distributed by convection to the heat distributed by conduction, which has a value in the order  $1 \times 10^3$  for coronary arteries and normal physiological blood flow (ten Have 2004).

## RADIATION AND ABSORPTION

Heat transfer due to radiation, figure 2.2C, is energy transfer via electromagnetic waves. Every object radiates electromagnetic waves, the amount and the wavelength depending on the temperature and its emissivity (how well the object radiates compared to a perfectly radiating black body). Heat transfer by radiation does not require a medium. The radiation in its turn may again be absorbed in a medium, which results in local heating.

In the review (Diamantopoulos 2003b), the radiative heat transfer is considered negligible. It was calculated that an ideally radiating heat source area of  $1 \text{ mm}^2$ , and a temperature difference of  $3.3^\circ\text{C}$ , emits  $22 \times 10^{-6} \text{ W}$ , which is considered extremely small. However, a spherical volume having an area of  $1 \text{ mm}^2$  could contain  $93 \times 10^3$  macrophages of  $10 \times 10 \times 10 \text{ m}^3$ , which when generating each  $20 \text{ pW}$  would result in a radiation of  $1.4 \text{ } \mu\text{W}$ , which would make the  $22 \text{ } \mu\text{W}$  found in the review not negligible. For much smaller heat sources as described in another paper, having a surface area of  $0.05 \text{ mm}^2$  and heated to a temperature difference of  $3.13^\circ\text{C}$  the radiative power is  $1.08 \text{ } \mu\text{W}$ , which, indeed compared with the heat production value of  $5.0 \times 10^{-3} \text{ W}$ , is negligible. Apparently, whether it is correct to neglect radiation will depend on the dimensions of the heat source, with a tendency for larger sources to have a higher radiative emission.

### 2.2.3 HEAT DETECTION

Unfortunately, heat production cannot be measured *in vivo* using calorimetric methods, so other measuring techniques have to be used. One method is measuring temperature. By detecting a higher temperature among a range of so called background temperatures, one is able to locate a spot of higher heat production in the region.



Temperature can be measured by a variety of methods, using electrical, optical, magnetical or other types of sensors. Electrical methods include resistance, thermistor and thermocouple. Optical methods include infrared detection, liquid crystals (Ashforth 1996) and temperature dependent fluorescence techniques (Grattan 1995). Magnetic resonance thermography is a method using the magnetic properties of molecules (Wlodarczyk 1999). Another method is the use of quartz crystals or microwave thermography (Wang 2000). These methods can be divided into either contact or non-contact methods.

Contact thermography methods require contact between the thermosensitive material of the device and the lumen wall, whereas non-contact temperature methods can do without. Heat detection by a contact method occurs by conduction of heat from the luminal wall to the sensor. When the sensor does not approach the wall close enough, however, the sensor area is exposed to surrounding influences and this will influence the measurement. When designing a contact method, one should be extremely cautious since a vulnerable plaque is easily ruptured. The stress the sensor induces in the lumen wall cannot be too high in order to prevent adverse events.

Non-contact thermographic methods require an absorptive material, which will absorb the electromagnetic radiation emitted by the medium. The choice of this material is wavelength dependent. Many materials used for this purpose are sensitive for absorption in the infrared region. Blood is highly absorptive for most electromagnetic waves of these wavelengths, which makes *in vivo* detection difficult, since it requires flushing of the artery. Microwave detection could be a better option for *in vivo* temperature measurements, since microwaves have greater penetration depth for these wavelengths.

Catheter design will influence the temperature measurement, both by material choice as well as its geometric design (shape). As the presence of a catheter in an artery will change the flow profile, and the shape of the catheter is of influence on the profile, presence of a catheter will thus influence the temperature reading.

## **2.3 PREVIOUSLY USED CATHETERS AND REPORTED STUDIES**

The electrical sensors, thermistor and thermocouple, are well known and currently applied in intracoronary thermography catheters. These sensors are very sensitive to thermal changes of the object, but will also be affected by thermal changes of the surroundings of the object. Therefore, these sensors need to be well insulated to optimize the detection of local hot spots. A ther-

mistor needs a high current to achieve accurate readings. However, using a high current will heat the thermistor, which will influence the measurement and is thus unwanted. A compromise is thus needed.

The electrical signal is transported from the sensor to the measuring device using metal wires. Metals are known to be very good conductors, so the flow of heat from a hot spot through these wires may significantly lower read out. This is called thermal leakage and it should be minimized.

In vivo validation of intracoronary thermography, and of any other vulnerable plaque detection technique, encounters the fundamental problem that no golden standard to determine vulnerability of a plaque yet exists, although several IVUS based techniques are currently investigated. Currently, standard IVUS is used to determine presence of a plaque. Using this imaging technique, it is not possible to classify the plaque as vulnerable, though.

In this section, the main studies on intracoronary thermography are discussed. The studies are grouped together according to the temperature measuring devices that were applied. The results are discussed in light of the framework presented in the previous section.

### 2.3.1 NEEDLE THERMISTOR

The needle thermistor consists of a 0.6 mm diameter, 4 cm long needle in which a thermistor is embedded in the tip, figure 2.3. Its accuracy is  $0.1^{\circ}\text{C}$ , and it has a time constant of 0.15 s.

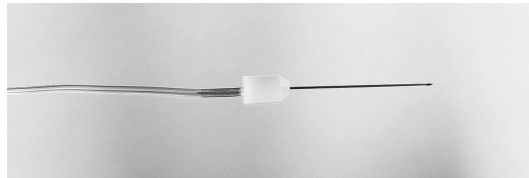


FIGURE 2.3: Needle thermistor, thermistor embedded in the tip of the needle (image from [www.coleparmer.com](http://www.coleparmer.com)).

Cascells et al (Cascells 1996) were the first to detect thermal heterogeneity in human atherosclerotic plaques using this needle thermistor. The measured temperature differences correlated positively with the density of underlying cells, of which most had characteristics of macrophages. Temperature differences of up to  $2.2^{\circ}\text{C}$  were reported.

The positive correlation between temperature measurement and macrophages makes it plausible that the heat source consisted of macrophages. If

absolute numbers had been given it would have been possible to approximate the heat generation values of macrophages in vulnerable plaques.

The arteries were studied at room temperature within 15 minutes after excision, which has an impact on the heat transfer. This implies that the arteries have had time to cool down. However, the different components of plaques will cool down at different rates due to their differing thermal parameters. In addition, hot spots, currently assumed to be embedded in lipid tissue, cannot transfer their heat easily to their surroundings, since both lipid and air are known for their insulating properties. And blood flow, acting as a cooling liquid *in vivo* thereby diminishing thermal heterogeneity, is absent in these *ex vivo* measurements. All these factors might have resulted into greater thermal heterogeneity in these *ex vivo* measurements than is present *in vivo*. Since the metal needle, being at room temperature, has a high heat conduction itself, temperature differences of layers deep in the tissue may have been masked by heat leakage through the needle to the environment.

### 2.3.2 HYDROFOIL THERMISTOR CATHETER

The hydrofoil thermistor catheter (Epiphany Coronary Thermography Catheter by Medispes SW AG) consists of a thermistor embedded in a so-called hydrofoil shaped polyurethane shaft, figure 2.4. The thermistor has an accuracy of  $0.05^{\circ}\text{C}$ , a time constant of 300 ms and is 0.5 mm in size (Stefanadis 2001). A more advanced design includes a balloon to enable occlusion of the vessel (Stefanadis 2003a).



FIGURE 2.4: Hydrofoil thermistor catheter. A: original design, B: modified balloon design (image from [www.medispes.com](http://www.medispes.com)).

Stefanadis et al and Toutouzas et al have published most of the intracoronary thermography data of human *in vivo* studies and were the first to do so (Stefanadis 1998), using the hydrofoil thermistor catheter. From their results it was concluded that temperature heterogeneity increases from stable angina patients to unstable angina patients to acute myocardial infarction patients (Stefanadis 1999). It was also concluded that increased temperature heterogeneity is a predictor for an unfavorable outcome after percutaneous coronary interventions (Stefanadis 2001), and that statin treatment reduces thermal het-

erogeneity in atherosclerotic plaques (Stefanadis 2002, Toutouzas 2004).

In 20, 40 and 67% of the stable angina patients, unstable angina patients and acute myocardial infarction patients thermal heterogeneity, and thus a focal heat source, was detected (Stefanadis 1999). The lesion of interest was selected using biplane angiography. Whether the artery was healthy or diseased was verified by standard IVUS. The study shows interesting temperature differences between different patient groups. Using standard IVUS one cannot determine whether a plaque is vulnerable or not, as was described previously. Some might be vulnerable, some not. This might explain why temperature heterogeneity was detected in only a subset of patients. Temperatures were obtained at five different locations at the plaque site. The data show that there was hardly any temperature variation within the plaque, which could mean that the heat producing cells are spread out over the plaque.

Because of the possible convection of heat due to the blood flow, it was suggested that thermal heterogeneity is underestimated in atherosclerotic plaques. Stefanadis et al studied the cooling effect of blood in effort angina patients (Stefanadis 2003b). Temperature differences of atherosclerotic plaques were measured both with blood flow and during full occlusion of the vessel. The vessel was occluded by a balloon filled with saline at 37.0°C. Whether this saline temperature was a good choice depends on the temperature of the healthy vessel wall. Temperature differences increased upon full occlusion of the coronary artery and went back to baseline levels after complete flow interruption.

The hydrofoil design of the catheter used to measure temperature was introduced to generate flow-induced forces that would direct the catheter towards the vessel wall. To test whether the sensor makes contact with the wall a 20 MHz ultrasound transducer was used, which allows to detect gaps between the catheter and the wall exceeding 100 to 200  $\mu\text{m}$ , depending on the spatial resolution of the ultrasound probe.

The thermistor is surrounded by polyurethane, which has a very low thermal conductivity (0.022 W/m °C). It thus acts as an insulator to the thermistor, which makes it a good material for this purpose.

Although the sensitivity of this device may be high, its practical utility may be somewhat restricted regarding the necessity of repeated pullbacks at different angular positions, due to the presence of only one thermistor in the catheter.

Temperature differences are defined as the difference between the maximum temperature measured at the lesion site and the body core (mouth) temperature (Stefanadis 2000). However, the group of control patients show quite large temperature differences, which might explain the relatively large temperature differences for the patient groups.

Of five temperature measurements at the site of healthy vessel wall, the most frequent temperature was used as background temperature and of five temperature measurements at the diseased vessel site, the maximum temperature was designated as the lesion temperature (Stefanadis 1999, Stefanadis 2001, Stefanadis 2002, Toutouzas 2004). Temperature differences were calculated by subtracting the background temperature from the diseased vessel temperature. This choice might have biased results towards optimistic temperature differences.

### 2.3.3 THERMISTOR CATHETER

The thermistor catheter (Thermography catheter, Thermocore UK Ltd.) consists of 4 thermistors attached to flexible nitinol strips, figure 2.5. The thermal accuracy of the thermistors is  $0.006^{\circ}\text{C}$  and the time constant less than 100 ms (Verheye 2004).

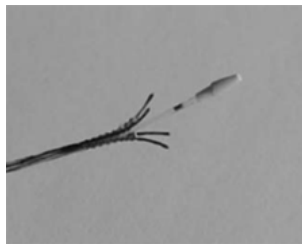


FIGURE 2.5: Thermistor catheter consisting of 4 thermistors attached to the ends of the flexible nitinol strips.

Both Verheye et al and Diamantopoulos et al have used the thermistor catheter for their studies. The former concluded that *in vivo* temperature heterogeneity of rabbit atherosclerotic plaques is determined by plaque composition (Verheye 2002a), and were thus the first to relate intracoronary temperature measurements to plaque composition. *Ex vivo* experiments in this study demonstrated the relation between local temperature and local total macrophage mass. Both groups reported on the influence of flow on intracoronary temperature measurements using this catheter (Verheye 2004, Diamantopoulos 2003a).

The *ex vivo* measurements on atherosclerotic aortas of 3 rabbits using this catheter were performed at room temperature (Verheye 2002a), which might have influenced heat transfer, and thus the results, in the same way as was described in section 2.3.1, describing the study by Casscells et al (Casscells

1996).

Diamantopoulos et al also concluded that coronary flow has an effect on the arterial wall temperature (Diamantopoulos 2003a). According to their results, this appears only below a critical threshold of average peak velocity and in a logarithmic fashion. A balloon was inflated with contrast agent at room temperature. This balloon was kept at least 10 mm from the sensor area to reduce influence on the temperature reading. Each flow restriction step lasted 30 s before the restoration of flow was allowed. This appears to be a long time span to be able to maintain a constant flow at which temperature can be measured, since an artery will adapt to flow occlusion by expansion and a hyperemic response. Full occlusion of an artery is manageable, but maintaining a certain constant flow in an artery could be quite troublesome.

Verheye et al (Verheye 2004) concluded that the temperature heterogeneity remained unchanged under normal physiologic flow conditions. In this study, too, it is extremely difficult to control the average flow velocity. When only a little blood stream passes the balloon, it will wipe away the collected heat. Their results confirm the findings by Diamantopoulos (Diamantopoulos 2003a) since also in this study the relationship between flow velocity and temperature difference was of logarithmic fashion up to a certain flow velocity. This means that temperature differences show a steep drop in the low flow range, whereas the temperature differences remain relatively constant in the high flow range. For velocities above this threshold value, the measured temperature differences remained relatively constant.

The thermistors of the thermistor catheters are brought in contact with the lumen wall after unsheathing the catheter. Nitinol is a nickel-titanium alloy and has a high thermal conductivity (around 10 W/m °C), which makes it an excellent heat conductor. This will reduce the sensitivity to detect temperature differences, since the blood flowing around the thermistor sensors will cool the nitinol strips on which the thermistors are mounted, and will thus indirectly cool the environment of the thermistors. The very high flexibility of the nitinol strips is needed to prevent vascular wall damage and adverse effects during or after the procedure. Verheye et al have tested this and reported that the intracoronary thermographic measurements using this catheter were safe and feasible with a similar degree of de-endothelialization as IVUS (Verheye 2004).

#### **2.3.4 BASKET THERMOCOUPLE CATHETER**

The controllable basket catheter (Intravascular Thermography Catheter by Volcano Therapeutics Inc.) is made from nitinol wires and contains 9 built in thermocouples, figure 2.6. At each bend, 2 thermocouples are placed 0.5 mm apart

and in the middle wire 1 thermocouple is located to measure blood temperature. Thermal resolution of the thermocouples is  $0.001^{\circ}\text{C}$  and the thermal accuracy is  $0.02^{\circ}\text{C}$  (Naghavi 2003).

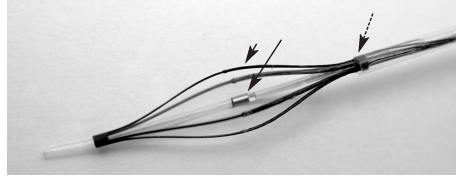


FIGURE 2.6: Basket thermocouple in which the thermocouples are embedded at the top of the nitinol wires (Schmermund 2003).

Both Naghavi et al and Schmermund et al have used the basket thermocouple catheter (Naghavi 2003, Schmermund 2003). Naghavi et al have found foci of warmth on the surface of atherosclerotic but not on disease-free regions of femoral arteries of cholesterol-fed dogs. In addition, marked thermal heterogeneity was observed in aortas of atherosclerotic Watanabe rabbits but not in normal rabbits. Schmermund et al have found temperature heterogeneity in both stable and unstable angina patients, however less pronounced than found by Stefanadis et al (Stefanadis 1999).

The study by Naghavi et al (Naghavi 2003) used both an in vitro and an in vivo model of atherosclerotic plaque. The in vitro model consisted of a tube around which coils of thermal-resistant wires were wrapped to simulate a heat source, placed in a newborn incubator which was kept at  $37^{\circ}\text{C}$ . The in vivo model were two animal models, one canine and one rabbit. The study by Schmermund et al (Schmermund 2003) was an in vivo patient study.

Both the influence of flow and the effect of luminal narrowing were studied by using the basket thermocouple catheter (Naghavi 2003) in the in vitro model. With respect to heat transfer, it was found that the cooling effect was proportional to blood flow.

### 2.3.5 THERMOCOUPLE GUIDEWIRE

A thermocouple is attached on a polymeric sphere covering the tip of a  $0.014''$  guidewire, figure 2.7 (ThermoCoil System by Imetrx Inc.). A localized bend near the tip of the guidewire causes the tip to contact the lumen wall. The thermocouple guidewire can detect changes in surface temperature with a precision of less than  $0.08^{\circ}\text{C}$  and has a time constant of 30 ms.

In a well designed in vitro study a relation between flow, or heat transfer

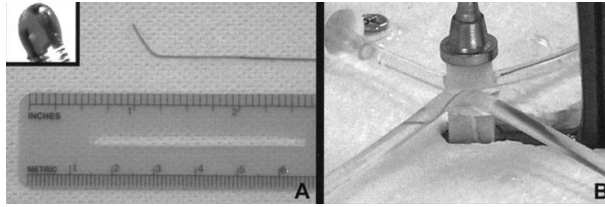


FIGURE 2.7: Thermocouple guidewire (Courtney 2004). A: detail of thermocouple guidewire, B: guidewire in in vitro set-up.

by convection, and maximal achievable temperature difference is found for this thermocouple guidewire system (Courtney 2004). Both the flow rates and the measured temperature ranges are realistic, based on the in vivo results that have been obtained so far. The in vitro set-up gives a good opportunity to test the catheter intensively and to prove and characterize its function before moving on to in vivo experiments.

The guidewire is connected to a motor driven system and is rotated along a helical path with an average pitch of 2 mm. Since heat sources may be smaller than 2 mm, this hampers the ability to detect all temperature elevations, even though local heat sources will cause a thermally diffuse pattern at the lumen wall (ten Have 2004). No experience is obtained in more complex geometries, yet, where nonuniform rotation might cause uncertainties in locating the heat source. In addition, rotation of the tip may be well controlled in straight segments, but will be more difficult to control in curved pieces of artery or in presence of pulsatile flow.

### 2.3.6 DETECTION OF TEMPERATURE DISTRIBUTIONS USING A MATHEMATICAL MODEL

Using a more fundamental approach, Matsui et al have determined temperature distribution of both a model vessel wall (Matsui 2001a) and swine aorta (Matsui 2001b) using thermocouple measurements at defined locations under pulsed laser irradiation and mathematical models. The mathematical model incorporated the temperature changes that occur due to pulsed laser irradiation.

In these articles it is assumed that heat generation is located in the atheromatous core. Currently it is assumed that heat production is related to macrophages, which are located at the shoulders of a vulnerable plaque or infiltrated in the cap or surrounding the lipid core. The location of macrophages is most



certainly related to the borders of the atheromatous core, but macrophages might also be present at other locations.

Flow was not considered in the model, so heat transfer from the source to the surroundings was due to conduction and radiation and absorption. Different temperature changes occurred due to the different thermal parameter values and emissivity of the tissues, and the wavelength of radiating light source.

The temperature change that occurs after the laser pulse is dependent on the thermal parameters of the tissue involved. These cannot be determined exactly. These parameter values are needed for the calculations to closely approximate the temperature of the atheromatous core.

## **2.4 CONCLUSIONS AND RECOMMENDATIONS**

This review has covered a selection of the results on intracoronary thermography that were published in the past. In addition, it has described the catheters that were used to obtain these results. Both were done from a physics point of view. Using this point of view, it opens new research opportunities in this area.

Previously published results are represented in figure 2.1. In this figure, it can clearly be seen that the temperature differences that were reported show a decrease over time. The first data points, labeled a, represent the variation in temperature differences that were found by Casscells et al (Casscells 1996) in their ex vivo study. Due to the lack of detailed knowledge on the difference between the ex vivo set-up of this study versus the in vivo set-up of the studies following this one, it is difficult to clarify these differences in temperatures. The studies labeled with the black squares were all performed using the hydrofoil thermistor catheter. Of these, the study labeled k was done proving the influence of flow, which shows higher temperature values at the lumen wall when the vessel was fully occluded, as expected. These values, though, are much lower than the values reported in studies labeled b through h, which suggests that catheter design or study design might have been of influence during measurements for these studies.

### **2.4.1 HEAT SOURCE**

Data from the studies labeled i and l are obtained using the basket thermocouple catheter and data labeled j are obtained using the thermistor catheter. The values of these data appear to be in agreement with each other, making it plausible that temperature differences of this magnitude, 0 to 0.3°C, are most realistically to be expected in vivo, however the temperature differences that

have been reported so far are hard to reconcile with the heat production values of macrophages that can be found in literature (ten Have 2004).

It is therefore necessary to quantify more accurately the heat generating processes in atherosclerotic plaques before continuing development of temperature measuring techniques. To determine the amount of heat that can be generated by atherosclerotic plaques, one would have to isolate fresh atherosclerotic plaque and study it using calorimetric methods. After this, one could isolate different cells, such as macrophages and foam cells, and/or other substances from the atherosclerotic plaque and subsequently study these selections calorimetrically to determine the exact origin of the heat generation. When a relationship between temperature increases in vulnerable plaques and plaque composition has been determined, then vulnerability of a plaque can be related to temperature measurements.

Some quantitative reasoning may aid to estimate the possible heat production of macrophages from another perspective. The nutritional value of fat equals 38 kJ/g. Considering a  $100 \times 100 \times 100 \mu\text{m}^3$  droplet of fat with a density of 0.900 kg/l, this equals an energy content of 34.2 mJ. This same volume corresponds to 1000 macrophage cells of  $10 \times 10 \times 10 \mu\text{m}^3$ . Assuming a heat production of 20 pW per cell, this equals a heat production 20 nW for this volume. If this heat is obtained from burning an amount of fat equal to their own volume, this will require, or last, 20 days. However, heat production values of 20 pW per macrophage appear too low to generate temperature differences that are reported in literature (ten Have 2004), implying that fat may be burned in a much shorter time span and that glucose metabolic activity and MMP tissue degradation must also be significant contributors.

## 2.4.2 HEAT TRANSFER

Given the fact that the temperature differences that have been reported most recently are small, it appears mandatory to exclude external thermal influences, such as those from heart muscle heat production and cooling of blood in lungs, or to compensate for them. Evidence for such mechanisms may be derived from several studies, since flow of blood influences the lumen wall temperature measurements (Stefanadis 2003b, Verheye 2004, Diamantopoulos 2003a). Furthermore the location and organization of heat sources are of influence (ten Have 2004). For these reasons it is recommended to combine intracoronary temperature measurements with both flow measurements and a vessel wall imaging modality. In this way, localization of a plaque and its morphology can be assessed (Nissen 2001, MacNeill 2004), flow can be measured separately (Lupotti 2003), and dedicated image and signal processing

techniques (Nair 2002, Schaar 2003) could even be added to obtain additional functional parameters that could be used to characterize the plaque.

### 2.4.3 HEAT DETECTION

The catheters that are currently used are based on electrical principles, and need to be insulated very well, as was described in sections 2.2.3 and 2.3. Other methods to measure temperature exist that may prove to be advantageous regarding this matter. Optical equipment, using fiber technology, might be a more appropriate choice for temperature measurement, since optical fibers are bad heat conductors. Combined with heat sensitive fluorescent coatings or liquid crystal coatings this might give a whole new direction to the field of intracoronary thermographic measurements. Another method to measure temperatures is using magnetic resonance (Wlodarczyk 1999), but so far its resolution is not sufficiently high. A great advantage is the non-invasiveness of this method.

All catheters that are currently used for intracoronary thermography, and that have been described in this review, only sparsely sample the vascular wall. The hydrofoil thermistor design measures temperature at one location, leaving most of the circumference of the vascular wall unexplored. The thermistor catheter and the thermocouple basket catheter measuring at 4 locations still leave over 2 mm of vascular wall in circumferential direction undetermined. The thermocouple guidewire covers the whole circumference, but leaves gaps of 2 mm in the longitudinal direction. If we assume that macrophage clusters are the heat sources, they may be focal and have sizes smaller than 1 mm. For that reason temperature increases on the vascular wall may be missed and a higher spatial resolution is needed, although the homogeneity of the temperature measurement in the second part of figure 1, labels (i) through (m), counteract this argument.

During the cardiac cycle the position of the catheter moves, so it is difficult to ensure contact at the same location during the full cardiac cycle. Measuring during diastole phase of cardiac cycle could be a solution, but then the measurement needs to be triggered and the thermal response time of the heat transducers must be accordingly short.

### 2.4.4 CLOSING REMARKS

Intracoronary thermography is, despite the number of publications that have already appeared in literature, still in development. Combined, a lot of research has already been done, but many questions are still unanswered. What

lacks is the answer to the question "What are we measuring?" Temperature differences exist in coronary arteries in vivo, but it is unclear what causes them. Is it really a temperature difference due to inflammation that has been measured? And what is the contribution of noise and artefacts? External thermal influences must be investigated. Influences of catheter design must be studied intensively. Changes in temperature due to source differences and flow must be known. All of these, and maybe even more, need to be studied before more firm conclusions can be drawn from thermographic data. This in order to more extensively validate intracoronary thermography and to be able to conclude on the usefulness of the method for vulnerable plaque detection.



## CHAPTER 3

# INFLUENCE OF PLAQUE GEOMETRY AND FLOW

To better understand the influence of flow and heat source parameters on thermographic measurements, numerical simulations have been performed on a model of a coronary artery segment containing a heat source. The results are described in this chapter, as well as their discussion. Maximal temperature differences at the lumen wall increased when the source volume increased and they differed with the source geometry. Blood flow decreased maximal temperatures depending on the source geometry, source volume and the maximal flow velocity. When cap thickness increased, maximal temperatures decreased and the influence of flow increased.

BASED ON: ten Have AG, Gijzen FJ, Wentzel JJ, Slager CJ, van der Steen AF. Temperature distribution in atherosclerotic coronary arteries: influence of plaque geometry and flow (a numerical study). *Physics in Medicine and Biology* 2004;49:4447-62.

### 3.1 INTRODUCTION

The macrophages of a thin cap fibroatheroma (TCFA) are situated at many possible locations, like in the fibrous cap or at the edge of the lipid-rich atheromatous core. Rupturing of human plaque caps is associated with increased macrophage accumulation (Lendon 1991). Macrophages are inflammatory cells and, when active, may produce heat that should be detectable using thermographic methods.

Casscells et al (Casscells 1996) used a 24 gauge needle thermistor for an ex vivo study, and showed that there exists a positive correlation between temperature increase of an atherosclerotic lesion and cell density. They stated that most of these cells were macrophages. This relation was later confirmed by Verheye et al (Verheye 2002a) whose ex vivo results from a rabbit study demonstrated that a relation exists between local temperature and local total macrophage mass using a thermography catheter based on four thermistors. A study by Stefanadis et al (Stefanadis 1999), in which an integrated hydrofoil thermistor catheter was applied, demonstrated that temperature differences could also be detected in humans in vivo. In addition, they showed that temperature heterogeneity was higher for patients suffering from unstable angina and acute myocardial infarction compared to patients suffering from effort angina (Stefanadis 2001).

Recently, Stefanadis et al (Stefanadis 2003b) showed that in vivo measured plaque temperature may have been underestimated by the cooling effect of flow. Diamantopoulos et al (Diamantopoulos 2003a) showed that this cooling effect exists but they concluded that arterial wall temperatures are affected by flow reduction only when the average peak velocity reaches a value below a critical threshold. In another study it was concluded that temperature heterogeneity reduced to 8 to 13% of the actual no-flow surface temperature when normal physiological flow conditions were present (Verheye 2004).

In these studies, all using lumen wall contact measurements, it is concluded that there exists temperature heterogeneity at the lumen wall and that the effects due to the flow of blood need to be taken into account. It is unknown, though, whether it are the macrophages that, when active, act as heat sources or whether there are other macrophage related processes that release heat. Macrophages secrete extracellular matrix degrading enzymes, which may cause heat releasing reactions in the plaque. Since macrophages, and thus heat production, can be located at many positions, the effect of flow could be different for different heat source configurations. To determine the influence of these effects, we have performed numerical simulations.

To study the influence of heat source geometry and of flow on the lumen

wall temperature, numerical simulations were performed on geometries representing the lumen of a coronary artery and the tissue surrounding the lumen. A heat source was embedded in the tissue. We have defined the Flow Influence Factor (FIF) to express the influence of flow on the lumen temperature when source parameters, such as source geometry and source volume, were varied.

## 3.2 METHODS

### 3.2.1 GEOMETRICAL MODEL

#### GENERAL

The geometry on which numerical simulations were performed, figure 3.1A, consisted of two fixed coaxial cylinders representing the blood vessel lumen and the tissue and plaque surrounding the lumen. The length of the cylinders was 5 mm. The radius of the lumen was 1.5 mm; the thickness of the tissue was 2.5 mm. This tissue represents the vessel wall as well as the tissue surrounding the vessel. The choice for the length of the vessel and the thickness of the tissue are further discussed in section 3.2.3 which deals with the boundary conditions. In the tissue a volume representing the heat producing source was embedded, figure 3.1B. We extended this heat source in circumferential, longitudinal, and radial directions resulting in heat sources of different geometries as well as different volumes. In figures 3.1C, D and E these different source geometries are depicted. The longitudinal center of the source was always located at half the length of the cylinder. Through the lumen a flow was modeled.

#### HEAT SOURCE

Of the circumferentially extended heat sources, figure 3.1C, both the radial and the longitudinal dimensions of the heat source were fixed at  $100\ \mu\text{m}$ . The sources were extended in the circumferential direction over angles of  $90^\circ$ ,  $45^\circ$ , and  $22.5^\circ$ . The largest volume therefore encompassed a quarter of the circumference of the artery. The resulting volumes were  $25.1 \times 10^{-3}$ ,  $12.6 \times 10^{-3}$ , and  $6.28 \times 10^{-3}\ \text{mm}^3$ , respectively. These volumes were used as reference values for varying the heat source dimensions in longitudinal and radial directions.

Of the radially extended sources, figure 3.1D, the longitudinal dimension of the source was fixed at  $100\ \mu\text{m}$ . The source was extended over  $3.58^\circ$  in the circumferential dimension, resulting to curvature lengths of approximately  $100\ \mu\text{m}$ . To obtain volumes equal to the reference volumes, the radial thickness was fixed at 1.68, 0.98 and 0.55 mm.

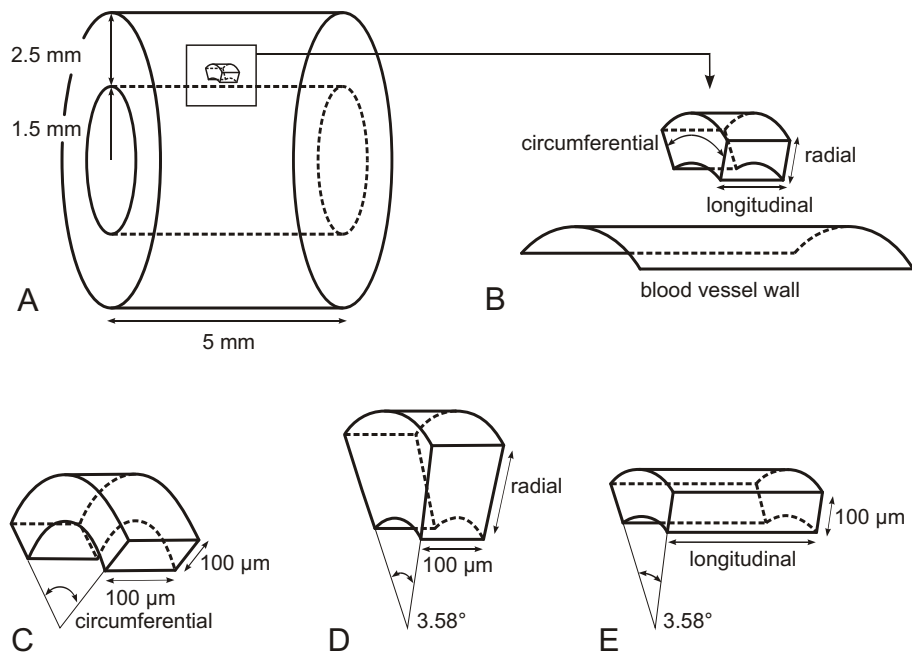


FIGURE 3.1: Geometry on which numerical simulations were performed. A: object geometry, B: close-up of heat source, C: heat source extended circumferentially, D: heat source extended radially, E: heat source extended longitudinally.



For the longitudinally extended heat sources, figure 3.1E, the radial dimension of the source was fixed at 100  $\mu\text{m}$ , and the circumferential dimension was extended over 3.58°. To obtain volumes equal to the reference volumes the lengths of the sources were fixed at 2.51, 1.26 and 0.63 mm in longitudinal direction.

### CAP THICKNESS

The cap thickness, which is the distance between the blood vessel wall and the nearest face of the heat source, was varied. The cap thickness was fixed to either 50, 100 or 150  $\mu\text{m}$ . The influence of increasing cap thickness was studied for the largest heat source volume of  $25.1 \times 10^{-3} \text{ mm}^3$ , for all three source geometries.

### 3.2.2 EQUATIONS

On the whole geometry the heat equation, in which both conductive and convective heat transfer are taken into account, was solved. Radiative heat transfer was neglected (Welch 1995). To obtain the velocity needed for the convective heat transfer in the lumen, the Navier-Stokes equations were solved on the lumen.

The heat equation can be expressed as

$$\rho c_p \left( \frac{\partial T}{\partial t} + \vec{u} \cdot \nabla T \right) - \text{div} (k \nabla T) = H \quad (3.1)$$

in which  $T$  is the temperature ( $^{\circ}\text{C}$ ),  $\rho$  is the density ( $\text{kg m}^{-3}$ ),  $t$  the time (s),  $c_p$  the specific heat capacity at constant pressure ( $\text{J kg}^{-1} \text{ }^{\circ}\text{C}^{-1}$ ),  $\vec{u}$  the velocity ( $\text{m s}^{-1}$ ),  $k$  the heat conductivity ( $\text{W }^{\circ}\text{C}^{-1} \text{ m}^{-1}$ ), and  $H$  the heat production per unit volume ( $\text{W m}^{-3}$ ). The first term on the left represents the total rate of stored thermal energy, the second term represents the heat transfer due to convection, and the third term represents the heat transfer due to conduction.

The Navier-Stokes equations for an incompressible, Newtonian medium can be expressed as

$$\rho \left( \frac{\partial \vec{u}}{\partial t} + (\vec{u} \cdot \nabla) \vec{u} \right) = \rho \vec{f} - \nabla p + \eta \nabla^2 \vec{u} \quad (3.2)$$

$$\nabla \cdot \vec{u} = 0 \quad (3.3)$$

in which  $\vec{f}$  represents the body forces ( $\text{N kg}^{-1}$ ),  $p$  the pressure ( $\text{N m}^{-2}$ ) and  $\eta$  the viscosity ( $\text{Pa s}$ ). Equation 3.2 represents the conservation of momentum

and equation 3.3 represents the conservation of mass. To keep the solution procedure as general as possible, we have chosen to solve the full Navier-Stokes equations.

### 3.2.3 BOUNDARY CONDITIONS

At all the outer boundaries of the geometry, except for the nodal points comprising the outlet of the lumen, a temperature equal to the assumed body core temperature of 37.0°C was applied. At the outlet, the boundary condition  $\partial T/\partial n = 0$  was applied. The body core temperature remains relatively constant due to the tissue perfusion. Similarly, the vasa vasorum, the tissue surrounding the vessel wall and the plaque, is well perfused. This effect was taken into account in the simulations by fixing the temperature at 37.0°C a certain distance away from the heat source, which clarifies the choice of the tissue thickness. Since blood is able to remove heat from the lumen wall by convection, we did not fix the temperature at the lumen outlet.

Temperature differences between the plaque temperature and the background temperature of up to 2.2° have been reported (Casscells 1996). Using a background temperature of 37.0°C, this results to plaque temperatures of around 39.0°C. When cell temperatures exceed 41.0°C for a period of time, cells could lose their functionality or die. Therefore it is unnecessary to consider lumen wall temperatures above 41.0°C, which was taken as the upper limit in determining the heat source production values. The heat source production values that we used in this study are 0.4, 0.2 and 0.1 W mm<sup>-3</sup>.

We used stationary parabolic flow profiles forced upon the inlet, with different maximal velocities  $V_{max}$ , which were 0, 25, 40 and 55 cm s<sup>-1</sup>. These flow velocities equal flows of 0, 53.0, 84.8, and 117 cc min<sup>-1</sup>, which are representative flow values for human coronary arteries (Doriot 2000). Varying the maximal velocity induces a proportional change in shear rate at the lumen wall, so a dependence on  $V_{max}$  can be translated to an identical dependence on shear rate at the lumen wall.

At the outlet a zero stress boundary condition was applied.

Dimensionless numbers defining this problem are the Reynolds number  $Re$ , equation 3.4, and the Peclet number  $Pe$ , equation 3.5.

$$Re = \frac{D\bar{u}\rho}{\eta} \quad (3.4)$$

$$Pe = \frac{\bar{u}Dc_p\rho}{k} \quad (3.5)$$

TABLE 3.1: Tissue parameters for the different types of tissue that were used in this model.

	Blood	Arterial tissue	Fatty plaque
Heat conductivity (W °C <sup>-1</sup> m <sup>-1</sup> )	0.49	0.476	0.484
Specific heat capacity (x 10 <sup>3</sup> J kg <sup>-1</sup> °C <sup>-1</sup> )	3.66	3.72	3.30
Density (kg m <sup>-3</sup> )	1064	1075	920
Viscosity (Pa s)	0.003		

in which  $D$  is the diameter of the lumen (m) and  $\bar{u}$  the average velocity of the flow (m s<sup>-1</sup>). The Reynolds number represents the ratio of inertia forces to the viscous forces. For our study the Reynolds number ranges between 125 for  $V_{max}=25$  cm s<sup>-1</sup> and 275 for  $V_{max}=55$  cm s<sup>-1</sup>, meaning that we are in the laminar flow regime. The Peclet number is the ratio of heat distributed by convection to the heat distributed by conduction. In our study the Peclet number varies between  $3.0 \times 10^3$  for  $V_{max}=25$  cm s<sup>-1</sup> and  $6.6 \times 10^3$  for  $V_{max}=55$  cm s<sup>-1</sup>, meaning that convection is dominant.

### 3.2.4 TISSUE PARAMETERS

The values for the tissue parameters used in this study were found in literature and can be found in table 3.1 (Duck 1990, Welch 1995). The thermal parameter values that were used for the tissue surrounding the heat source were assumed to equal the values found for healthy arterial tissue. The heat conductivity value for the heat source were assumed equal to the values found for fatty tissue. We assumed the density and the specific heat capacity of the heat source to equal those of fatty plaque. The viscosity and density were considered to be independent of temperature. The blood was modeled as a Newtonian fluid.

### 3.2.5 SOLUTION PROCEDURE

The geometry was converted to a hybrid mesh containing mainly linear tetrahedral mesh elements using the mesh generator Gambit 2.0.4 (Fluent Inc.,

Lebanon NH, USA). The mesh also contained other element types like hexahedral, pyramidal and wedge shaped elements. Because large temperature gradients were expected in the region surrounding the heat source, we refined the mesh around the heat source. Mesh independence was tested by changing the length of the cylinders and varying the mesh density around the heat source.

The problem was defined as a 3 dimensional symmetrical problem, so the equations could be solved on only one half of the mesh. The full Navier-Stokes equations were solved to obtain the velocity field needed for calculation of the convection terms. The convective terms were included in the heat equation and the problem was considered to be weakly coupled so temperature dependence of the momentum equation was not considered. The equations were solved using the Finite Element Method provided by the widely used package Fidap 8.7.0 (Fluent Inc., Lebanon NH, USA). We used the segregated solver to solve the equations. Convergence was obtained when the relative errors between two iterations were less than  $1 \times 10^{-4}$  for the temperature and the velocity solutions. Solutions were stabilized using standard techniques.

The number of elements varied between 20,766 and 47,852, depending on the geometry and size of the heat source. The number of iterations needed to obtain convergence depended on whether a flow existed in the lumen, i.e. whether the full Navier-Stokes equations had to be solved. The number of iterations was about 10 when no flow existed, and about 30 when there existed a flow in the lumen.

Visualization was done using FieldView (Intelligent Light, Lyndhurst NJ, USA). Processing the numerical output was done using Matlab 6.1 (The Math-Works Inc., Natick MA, USA).

### 3.2.6 FLOW INFLUENCE FACTOR

To express the influence of flow on the temperature distribution at the lumen wall, the Flow Influence Factor (FIF) is defined. All temperatures are expressed as maximal temperature differences from the background temperatures of 37.0°C. The FIF is the ratio of the maximal temperature difference at the lumen wall when no flow exists in the lumen to the maximal temperature difference at the lumen wall when there exists a flow.

$$FIF = \frac{\Delta T_{no\ flow}}{\Delta T_{flow}} \quad (3.6)$$

The FIF indicates how much the measured temperature differences are underestimated due to flow. The temperature difference that would have been mea-

sured when the vessel were occluded is FIF times higher.

## 3.3 RESULTS

### 3.3.1 MESH INDEPENDENCE AND BOUNDARY CONDITIONS

The object used for testing mesh independence contained the largest circumferentially extended heat source volume of  $25.1 \times 10^{-3} \text{ mm}^3$ , the highest heat source production of  $0.4 \text{ W mm}^{-3}$ , and the smallest cap thickness of  $50 \text{ }\mu\text{m}$ .

The optimal element size around the heat source was selected to be  $50 \text{ }\mu\text{m}$ , since the last step of decreasing the element size, from  $100 \text{ }\mu\text{m}$  to  $50 \text{ }\mu\text{m}$ , resulted in changes of  $\Delta T$  of only 1.8% when the flow was  $25 \text{ cm s}^{-1}$  and 1.3% when no flow existed in the lumen. Due to the tetrahedral element type used for meshing the object, the element size of  $50 \text{ }\mu\text{m}$  resulted in nodal points between the source and the lumen, even for the smallest cap thickness.

When extending the source longitudinally, the distance between the edge of the source and the boundaries near the inlet and outlet, which were fixed at  $37.0^\circ\text{C}$ , became relatively small. To check the influence of this small distance we increased the lengths of the cylinders from 5.0 to 7.48 mm, thus doubling the smallest distance from the end of the source to the outer boundary from 1.24 mm to 2.48 mm. Performing simulations on these longer objects resulted in less than 3.5% change of maximal temperature differences at the lumen wall and the absolute error of  $\Delta T$  then was  $0.11^\circ\text{C}$ . The FIF was influenced by less than 1.0%. These errors were considered acceptable.

### 3.3.2 DEPENDENCE OF $\Delta T_{flow}$ AND $\Delta T_{noflow}$

Examples of temperature distributions at the lumen wall are shown in figure 3.2. The influence of the source geometry on the temperature distribution is shown for the largest source volumes and a flow with lowest  $V_{max}$ . In case of a circumferentially extended source, figure 3.2A, the distribution was wider in the circumferential direction, whereas the distribution coming from a longitudinally extended source, figure 3.2C, was extended in the longitudinal direction. For a radially extended source, figure 3.2B, the distribution resembled a spot-like temperature profile, small in both longitudinal and circumferential directions.

In all three of the examples given in figure 3.2, the influence of the flow can clearly be appreciated. Due to the flow, the temperature profile is smeared out in the direction of the flow and a longitudinal shift of the location of  $\Delta T_{flow}$  occurs which is most pronounced for the longitudinally extended source.

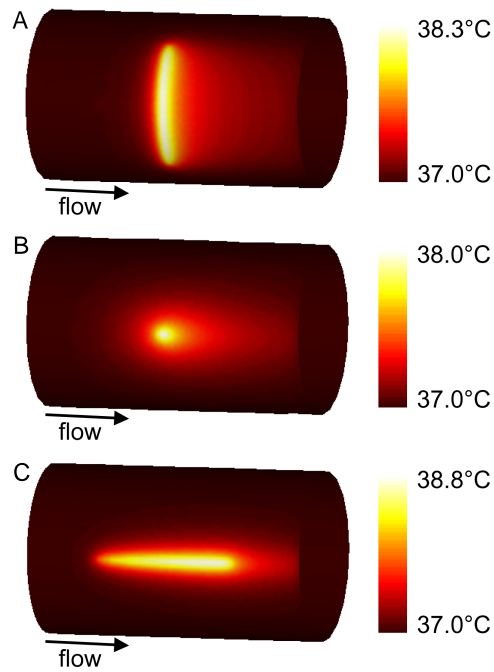


FIGURE 3.2: Temperature distributions at the lumen wall for A: circumferentially, B: radially, and C: longitudinally extended sources. Heat source volume =  $25.1 \times 10^{-3} \text{ mm}^3$ , heat source production =  $0.4 \text{ W mm}^{-3}$ , cap thickness =  $50 \text{ }\mu\text{m}$ ,  $V_{max} = 25 \text{ cm s}^{-1}$ . Note the different temperature scales.

In figures 3.3A, 3.3B and 3.3C the values of  $\Delta T_{flow}$  and  $\Delta T_{noflow}$  are shown resulting from the numerical simulations on circumferentially, radially and longitudinally extended heat sources, respectively. In these figures the values are depicted for either a flow with  $V_{max}=25 \text{ cm s}^{-1}$  or no flow in the lumen. Values of both  $\Delta T_{flow}$  and  $\Delta T_{noflow}$  are higher when the heat source production is higher for all source geometries. Maximal temperature differences were linearly dependent on the heat source production, keeping the heat source volume constant. This holds for both with and without a flow in the lumen. As was expected, the values of  $\Delta T_{flow}$  are always lower than the values of  $\Delta T_{noflow}$  for identical source parameters.

Values for  $\Delta T_{noflow}$  are highest for circumferentially extended sources, and lowest for radially extended sources. The differences between  $\Delta T_{noflow}$  for circumferentially extended sources and for longitudinally extended sources are almost negligible;  $0.01^\circ\text{C}$  for the smallest heat source volumes and  $0.09^\circ\text{C}$  for the largest heat source volumes, compared for the highest heat source production. Values for  $\Delta T_{flow}$  are highest for longitudinally extended sources, and lowest for radially extended sources. The differences between  $\Delta T_{flow}$  for longitudinally extended sources and circumferentially extended sources are clearly present, in contrast to their values of  $\Delta T_{noflow}$ .

All the lines in the graphs of figure 3.3 have a positive slope. That is, the maximal temperature difference at the lumen wall increases when the source volume increases, irrespective of its geometry and of the presence of flow. The slope is steepest for smaller heat source volumes extended either circumferentially or longitudinally when no flow exists in the lumen. The slope is flattest when a flow exists in the lumen and when the heat source is extended circumferentially or radially.

How the maximal temperatures at the lumen wall vary with cap thickness can be seen in figure 3.4. Both  $\Delta T_{noflow}$  and  $\Delta T_{flow}$  decrease when the cap thickness increases. The relative decrease of  $\Delta T_{flow}$  is larger than the relative decrease of  $\Delta T_{noflow}$ .

### 3.3.3 FLOW INFLUENCE FACTOR

Figure 3.5 shows a representative temperature distribution along a straight line on the lumen wall from inlet to outlet right underneath the heat source. In this figure, the influence of flow can be appreciated. The maximal lumen wall temperature when no flow exists lies in the middle of this line, right beneath the source. If a flow is present, the maximal temperature shifts longitudinally towards the outlet. For this situation,  $\Delta T_{noflow}=3.75^\circ\text{C}$  and  $\Delta T_{flow}=1.83^\circ\text{C}$ . This results in a FIF value of 2.05, meaning that the temper-

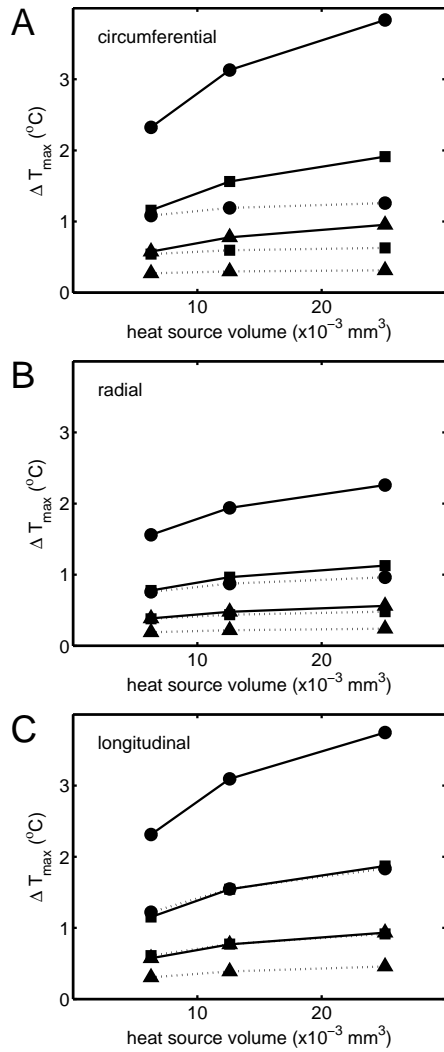


FIGURE 3.3: Maximal temperature differences at lumen wall ( $\Delta T_{max}$ ) for A: circumferentially, B: radially, and C: longitudinally extended heat sources. Cap thickness =  $50\mu\text{m}$ . Heat source production  $0.4 \text{ W mm}^{-3}$  (circle),  $0.2 \text{ W mm}^{-3}$  (square),  $0.1 \text{ W mm}^{-3}$  (triangle). Solid line: no flow, dotted line:  $V_{max} = 0.25 \text{ m s}^{-1}$ .



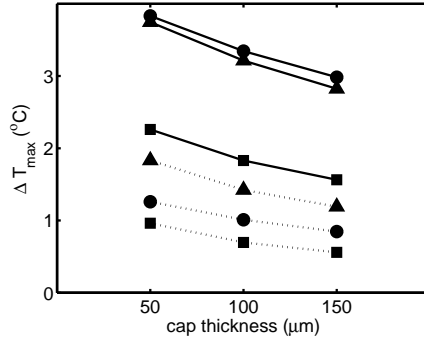


FIGURE 3.4: Maximal temperature differences at lumen wall ( $\Delta T_{max}$ ) for different source geometries and different cap thicknesses.  $V_{max} = 25 \text{ cm s}^{-1}$ , heat source volume =  $25.1 \times 10^{-3} \text{ mm}^3$ , heat source production =  $0.4 \text{ W mm}^{-3}$ . Heat source geometry circumferential (circle), longitudinal (triangle), radial (square).

ature measured at the lumen wall when this specific flow exists in the lumen is underestimated by a factor of 2.05.

The FIF was independent of the heat source production. Due to small round off errors inherent to numerical simulations, FIF values varied less than 2% for different heat source production values. The FIF values mentioned result from averaging the FIF values that were obtained for the different heat source production values. In figures 3.6A, 3.6B and 3.6C the dependence of FIF on the source volume, the source geometry and maximal flow velocity is displayed. FIF values were highest for circumferentially extended sources and lowest for longitudinally extended sources, irrespective of  $V_{max}$ . FIF values were larger when the maximal velocity  $V_{max}$  of the flow was higher. FIF values also increase when the heat source volume increases.

Figure 3.7 depicts how the FIF values increase when cap thickness increases.

### 3.4 DISCUSSION

To study the influence of heat source parameters and flow on the temperature distribution on the lumen wall generated by heat production in an atherosclerotic plaque, we have performed numerical simulations on geometries representing a straight part of a coronary artery. Surrounding the lumen, arterial

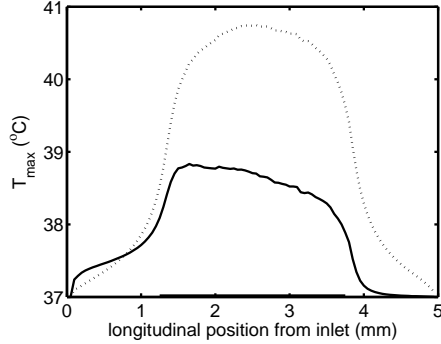


FIGURE 3.5: Temperature distribution along a line on the lumen wall passing directly below the longitudinally extended heat source (source length and position are denoted by a thickened part on the x-axis). Heat source volume =  $25.1 \times 10^{-3} \text{ mm}^3$ ,  $V_{max} = 25 \text{ cm s}^{-1}$ , cap thickness =  $50 \text{ }\mu\text{m}$ , heat source production =  $0.4 \text{ W mm}^{-3}$ .  $\Delta T_{no\text{flow}} = 3.75^\circ\text{C}$ ,  $\Delta T_{flow} = 1.83^\circ\text{C}$ , FIF = 2.05

tissue was assumed in which a relatively small heat producing source was embedded. We have used the Flow Influence Factor (FIF) to express the influence of flow on the maximal wall temperature. The heat source parameters, such as source geometry, source size, and heat source production were varied and were shown to be of influence on the temperature distribution at the lumen wall. Maximal temperature differences at the wall and FIF values differ when source volumes and source geometries differ. FIF values are independent of heat source production, but increase when the cap thickness increases.

### 3.4.1 DEPENDENCE OF $\Delta T_{flow}$ AND $\Delta T_{no\text{flow}}$

The maximal temperature differences at the lumen wall when a flow exists,  $\Delta T_{flow}$ , are always lower than the values of the maximal temperature difference at the lumen wall when no flow exists,  $\Delta T_{no\text{flow}}$ , for identical heat source parameters, which signifies that flowing blood acts as a coolant on the lumen. The positive slopes in the graphs in figure 3.3 are the result of the increase in total heat source production. This results in higher temperatures at the lumen wall.

Values for  $\Delta T_{no\text{flow}}$  are highest for circumferentially extended sources and lowest for radially extended sources. When extending the source circumferentially, the location of the center of the heat source shifts slightly towards the lumen wall. When extending the source radially, the location of the center of

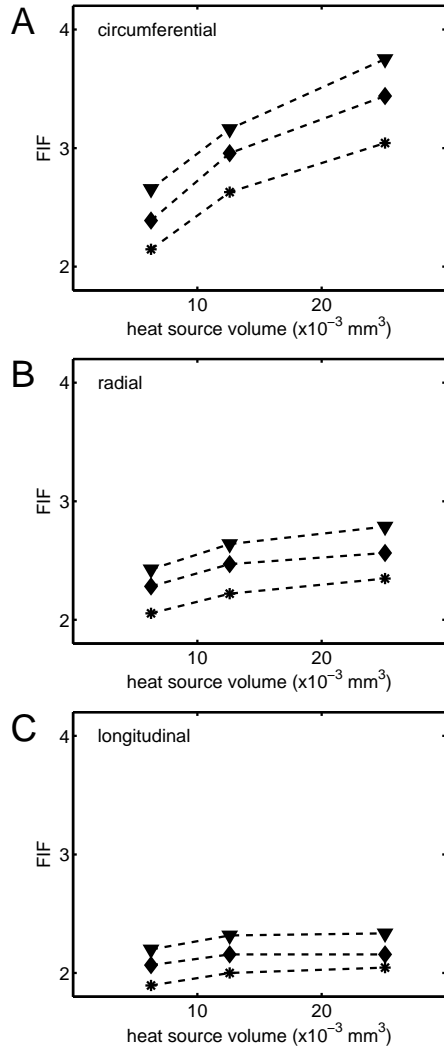


FIGURE 3.6: FIF values for A: circumferentially, B: radially, and C: longitudinally extended heat sources. Cap thickness= $50 \mu\text{m}$ . Flow:  $V_{max} = 25 \text{ cm s}^{-1}$  (star),  $V_{max} = 40 \text{ cm s}^{-1}$  (diamond),  $V_{max} = 55 \text{ cm s}^{-1}$  (downward triangle).

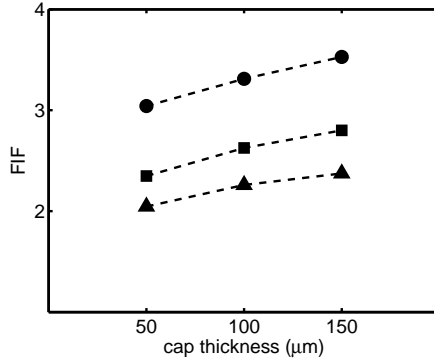


FIGURE 3.7: FIF for different heat source geometries and different cap thicknesses.  $V_{max} = 25 \text{ cm s}^{-1}$ , heat source volume =  $25.1 \times 10^{-3} \text{ mm}^3$ . Heat source geometry circumferential (circle), longitudinal (triangle), radial (square).

the heat source shifts away from the lumen. In case of the longitudinally extended sources, the location of the center of the source remains unchanged. These differences explain the difference in the heat distributions around the source and the corresponding  $\Delta T_{no\text{flow}}$  values. The closer the center of gravity of the source is to the lumen wall, the higher  $\Delta T_{no\text{flow}}$ .

Values for  $\Delta T_{flow}$  are highest for longitudinally extended sources, and lowest for radially extended sources. For longitudinally extended sources, the blood has a longer distance at its disposal to be heated, compared to circumferentially or radially extended sources, and thus less potential to cool the lumen wall, because the source is oriented in the direction of the flow. The dimension of the heat source in the flow direction is  $100 \mu\text{m}$  for the circumferentially and radially extended sources, whereas for longitudinally extended sources this dimension is  $0.63 \text{ mm}$  for the smallest heat source volume, already being more than six times larger. This longer distance results in higher values of  $\Delta T_{flow}$ . The differences between  $\Delta T_{flow}$  for circumferentially and those for radially extended sources are due to the area of the source face closest to the lumen. In case of a circumferentially extended source, this area increases when the source volume increases, whereas for a radially extended source this area remains constant. More heat will be directed towards the lumen wall in the case of a circumferentially extended source compared to a radially extended source, which results in a higher  $\Delta T_{flow}$ . The radially extended sources best resemble point sources, and thus have one more dimension available to release the produced heat to. This results in less heat directed towards the lumen wall

and thus a lower  $\Delta T_{flow}$  value.

The values for  $\Delta T_{flow}$  resulting from our simulations reach from a minimum of  $0.16^{\circ}\text{C}$  to a maximum of  $1.8^{\circ}\text{C}$ . For  $\Delta T_{noflow}$  this interval ranges from  $0.39^{\circ}\text{C}$  to  $3.8^{\circ}\text{C}$ . These values coincide with values for  $\Delta T_{flow}$  and  $\Delta T_{noflow}$  reported in literature. Casscells et al (Casscells 1996) reported ex vivo values for  $\Delta T_{noflow}$  of  $0.2^{\circ}\text{C}$  to a maximum of  $2.2^{\circ}\text{C}$ . In vivo results of Stefanadis et al (Stefanadis 1999) showed temperature differences from  $0.106\pm 0.110^{\circ}\text{C}$  for stable angina patients to  $1.472\pm 0.691^{\circ}\text{C}$  for patients suffering from acute myocardial infarction. In contrast, Diamantopoulos et al (Diamantopoulos 2003a) recently reported much smaller  $\Delta T_{noflow}$  values, from  $0.015\pm 0.005^{\circ}\text{C}$  for partial vessel occlusion to  $0.188\pm 0.023^{\circ}\text{C}$  for total vessel occlusion. These values are outside the range of maximal temperature differences we found.

Casscells et al (Casscells 1996) found that temperature decreases when cap thickness increases. This is in accordance with our findings which are depicted in figure 3.4. The majority of cap thicknesses in their study were thicker than  $150\ \mu\text{m}$ , though. In addition, in their study they considered pieces of arterial tissue. So the inverse correlation they noted might also be due to lower macrophage cell activity, which was not considered in our study in which we did not vary source activity when considering changes in cap thickness.

Temperature distributions at the lumen wall depend on a number of parameters, including source size, source geometry and heat source production. Circumferentially extended sources cause the highest temperature differences when no flow is present. When a flow runs through the lumen, longitudinally extended sources cause the highest temperature differences. The influence of flow increases with the velocity of the flow. In addition, the influence of flow also differs when certain source characteristics such as source size and source geometry differ. The influence of flow is highest for circumferentially extended heat sources and lowest for longitudinally extended heat sources. Decreasing cap thickness increased maximal lumen wall temperature differences, but decreased sensitivity for flow.

From the results presented in this study it can be concluded that a certain measured temperature difference can be associated with a number of different combinations of heat source size, source geometry, cap thickness, flow and heat source production. From these simulations a maximal temperature difference of, for example  $0.8^{\circ}\text{C}$ , can result from many different combinations of parameters. These include a circumferentially extended heat source of  $25.1\times 10^{-3}\ \text{mm}^3$ , heat source production  $0.4\ \text{W}\ \text{mm}^{-3}$ , separated from the lumen by a cap thickness of  $150\ \mu\text{m}$  and a flow with a maximal flow velocity of  $25\ \text{cm}\ \text{s}^{-1}$ , but also a radially extended heat source of  $6.28\times 10^{-3}\ \text{mm}^3$ , heat source production  $0.2\ \text{W}\ \text{mm}^{-3}$ , separated from the lumen by a cap thickness of  $50\ \mu\text{m}$  and a

flow with a maximal flow velocity of  $55 \text{ cm s}^{-1}$ . The variety in source characteristics combined with the variety in flow might partially explain the different maximum temperatures and temperature intervals reported by others.

### 3.4.2 FLOW INFLUENCE FACTOR

The influence of flow is highest for circumferentially extended sources. This can be appreciated when one compares the area of the source closest to the lumen, and therefore being influenced most by the flow. This area is smallest in the case of radially extended sources. This type of source delivers the least amount of energy towards the lumen wall than do circumferentially and longitudinally extended sources. Therefore, the influence of the flow is low, but not as low as for the longitudinal source. For longitudinally extended sources the blood has a longer distance at its disposal to be heated, compared to the other source geometries, as was mentioned previously. The heated blood has less capacity to take up more heat, meaning that the flow is of less influence. The circumferentially extended sources have an area closest to the lumen comparable to that of the longitudinally extended sources. Since the direction of flow is perpendicular to the direction of the source geometry, the blood cannot be heated as much as is the case for longitudinally extended sources. This means that the blood is able to take up most heat for a circumferential geometry, and blood flow therefore has the largest impact on wall temperatures for this type of source geometry.

Values of FIF are higher when  $V_{max}$  is higher. When the maximum blood flow velocity increases, the velocity of the blood close to the lumen wall will increase. Blood is therefore able to remove heat faster by convection from the lumen wall, so the influence of blood flow is higher for higher  $V_{max}$ .

FIF values increase when source volume increases. Previously, we have discussed that both  $\Delta T_{noflow}$  and  $\Delta T_{flow}$  increase when source volume increases. In figure 3.3 it can be seen that  $\Delta T_{noflow}$  values increase more rapidly than  $\Delta T_{flow}$  values, resulting in increasing FIF values for increasing heat source volumes.

FIF values are independent of heat source production. Since both  $\Delta T_{noflow}$  and  $\Delta T_{flow}$  were found to be linearly dependent on the heat source production, this was to be expected.

In the study by Stefanadis et al (Stefanadis 2003b), temperature differences are also considered. The temperature difference in this study is the difference between the maximal temperature measured at the atherosclerotic plaque and the temperature measured at disease free proximal vessel wall both with and without flow. From the reported temperature differences with and without a

flow running through the lumen, a FIF value of 2.25 can be deduced, which is within the range of FIF values that were calculated in this study.

In the study of Diamantopoulos et al (Diamantopoulos 2003a) temperature measurements were done at one location, but no temperature difference was detected above average peak velocities of  $9 \text{ cm s}^{-1}$ , so a FIF value cannot be deduced from this study.

Verheye et al (Verheye 2004) reported in vivo temperature data for various flows and for the highest, the median and the lowest temperature difference. From these data we have derived six FIF values, namely 1.4, 2.6 and 4.2 for  $V_{max}=20 \text{ cm s}^{-1}$  and 1.4, 3.4 and 8.4 for  $V_{max}=40 \text{ cm s}^{-1}$ . No information on the source was given. With exception of the highest value, these FIF values are all within the range of FIF values that were calculated in this numerical study. Another similarity between the study of Verheye and ours is that FIF values increased when  $V_{max}$  values increased.

FIF values increase when cap thickness increases, which can be interpreted that the influence of flow increases when the source is removed further from the lumen. The FIF is calculated on the lumen wall, and thus combines the influence that the flow has on the lumen wall on the one hand and the influence that the source has on the lumen wall on the other hand. When the source is at further distance from the location at which the FIF is calculated, the influence of the source on that location becomes less. The relative influence of the flow thus increases, resulting in increasing FIF values. The flow thus becomes of more influence when the source is thermally "less connected" to the lumen.

The influence of flow clearly is not negligible. Lumen wall temperatures are significantly influenced by the flow running through the vessel. Therefore, in a clinical setting, it might be advantageous to occlude the section of coronary artery where presence of a vulnerable plaque is suspected before performing temperature measurements, thus improving repeatability and enabling comparison with other studies.

### 3.4.3 REMARKS

For the model we have used a straight tube, suggesting that the lumen is unobstructed by the plaque. This is a reasonable approximation, since in reality most vulnerable plaques are barely protruding into the lumen due to adaptive remodelling of the lumen, which makes them undetectable using conventional angiography. Data on the size of heat sources have not been reported, so the heat source dimensions were chosen rather arbitrarily. The source was given finite dimensions and was considered homogeneous. In reality boundaries of macrophage clusters in atherosclerotic plaques may not be that clear and ma-

crophages may be distributed over a much larger area.

The material parameters in this model are considered isotropic and homogeneous, and were those reported for pathologically acquired tissues, so the influence of normal perfusion on the parameter values was not taken into account. The heat conductivity of the tissue surrounding a vulnerable plaque might show some anisotropy due to the perfusion of the vasa vasorum. Data on this subject has not been reported, though. The heat source was given thermal parameter values found for fatty plaque. This resulted in a heat conductivity of  $0.484 \text{ W } ^\circ\text{C}^{-1} \text{ m}^{-1}$  (Welch 1995), which paradoxically appears slightly higher than the value used for healthy arterial tissue,  $0.476 \text{ W } ^\circ\text{C}^{-1} \text{ m}^{-1}$  (Welch 1995) and much higher than that of fatty tissue, which is around  $0.200 \text{ W } ^\circ\text{C}^{-1} \text{ m}^{-1}$  (Duck 1990). However, since the source is small compared to the tissue surrounding it, simulations have shown that the effect of using this possibly overestimated heat conductivity value results to maximal temperature differences at the lumen wall that differ by less than 0.1% compared to using a heat conductivity value of  $0.200 \text{ W } ^\circ\text{C}^{-1} \text{ m}^{-1}$ . In reality, differences in heat conductivity may have influenced the ex vivo temperature measurements presented by Casscells et al (Casscells 1996) and by Verheye et al (Verheye 2002a). Due to the differences in heat conductivities, there may exist differences in cooling rate of fatty spots and regions of healthy arterial tissue. Fatty spots, more likely having a lower heat conductivity value compared to normal arterial regions, may cool down slower. This might possibly have contributed to the higher temperature values of the fatty spots in ex vivo temperature measurements of excised tissue exposed to room temperature.

In our study we assumed the heat source production to have values of 0.4, 0.2 and  $0.1 \text{ W mm}^{-3}$ . No data has been reported on heat production of macrophages in vulnerable plaques, so it is not possible to independently validate these assumptions. Some data on heat production of other macrophage types have been reported (Charlebois 2002, Thóren 1990). These studies report heat production values of approximately 20 pW per cell. These values are much lower than the values needed to produce the temperature differences reported in this study. Assuming a macrophage volume of  $10 \times 10 \times 10 \text{ } \mu\text{m}$ , this implies a heat production of  $0.02 \text{ mW mm}^{-3}$ , being a factor 5000 smaller than the lowest heat production that was used in the simulations for the largest heat source volume. It might be that our selected heat source volume of  $25.1 \times 10^{-3} \text{ mm}^3$  underestimates the real volume occupied by macrophages since in reality the plaque is more diffuse and the macrophages might be spread out over a larger volume. In addition, the macrophages in vulnerable plaques may be metabolically more active, and other enzymatic heat releasing processes are also likely to be present.



Another difference between the simulations and a clinical setting is that in these simulations no measuring device inserted in the lumen is taken into account. Presence of such a device will change the velocity profile, change the maximal velocities, and therefore also change the thermal boundary layer. This changes the temperature profile at the lumen wall which then becomes heavily dependent on the catheter position with respect to the wall. If the catheter contacts the wall, and if the contact area is sufficiently large, the flow in this region is halted and locally the no flow situation may be approximated. Uncertainties as these might also influence the FIF values presented in this study.

### **3.5 CONCLUSIONS**

Results from this study show that thermographic measurements do not always correlate one-to-one with the amount of heat produced by a vulnerable plaque. Measuring higher lumen wall temperature differences does not necessarily mean that one deals with larger or more intense heat sources. Flow clearly influences the measurements, and the influence of flow depends on vulnerable plaque geometry.

Therefore, sole thermographic measurements should be interpreted with great care. For a more accurate interpretation of thermographic measurements, one should combine measuring temperature with an imaging modality to obtain more information on the geometry of the vulnerable, atherosclerotic plaque and a flow measuring device to define the flow.





## CHAPTER 4

# INFLUENCE OF VULNERABLE PLAQUE COMPOSITION

In this chapter the influence of vulnerable plaque composition on lumen wall temperatures was studied numerically. The heat source location was the main determinant of the lumen wall temperature distribution. The strongest effect was noticed when the heat producing macrophages were located in the shoulder region, leading to focal spots of higher temperature. The maximal lumen wall temperature was mainly determined by the heat production of the macrophages and the cooling effect of blood. The insulating properties of the lipid core increased lumen wall temperatures when the heat source was located in the cap and the presence of vasa vasorum lowered the temperatures.

**BASED ON:** ten Have AG, Gijzen FJH, Wentzel JJ, Slager CJ, Serruys PW, van der Steen AFW. A numerical study on the influence of vulnerable plaque composition on intravascular thermography measurements. Submitted for publication in *Physics in Medicine and Biology*.

## 4.1 INTRODUCTION

The many temperature readings that have been reported up to now vary greatly, even when the same thermographic catheter type was used (Stefanadis 1998, Stefanadis 2000, Toutouzas 2004). Even though vulnerable plaques are characterized by distinct features, they too can show great variation with respect to their composition. These variations include the location of the macrophages, the lipid density of the lipid core, and the location of the vasa vasorum with respect to the plaque. These differences in composition may influence the temperatures at the lumen wall.

In this paper we will describe the numerical simulations we have performed to study how variation in plaque composition influences the lumen wall temperatures. The simulations were performed on a schematic representation of the lumen wall in which a realistically shaped plaque was embedded. The location of the heat source in the plaque was varied, as were the thermal parameters of the lipid core. Also, the influence of the location of the vasa vasorum was studied. The results from this study will allow further optimization of intracoronary thermography for vulnerable plaque detection.

A vulnerable plaque of the TCFA type consists of a lipid core separated from the lumen by a thin fibrous cap and macrophage infiltration. The macrophages can be located at different locations, but were shown to be most pronounced in the cap and the shoulder regions of the plaque (Pasterkamp 1999), see also figure 4.1C. Since it is generally assumed that the lipid scavenging activities of macrophages, and thus an increased metabolism, cause an increased plaque temperature, it could imply that heat producing macrophages are also located in a thin shell surrounding the lipid core. It is unknown how much heat is produced by macrophages in vulnerable plaques. Studying the influence of heat production can be done by studying the effects of either a constant heat production per unit volume or a constant total heat production. These options imply an optimal, dense amount of macrophages present in the volume or identical numbers of macrophages present in the volume, irrespective of the volume, respectively.

With respect to heat transfer it has already been shown that blood flow strongly influences the thermographic measurements in vivo (Stefanadis 2003b, Diamantopoulos 2003a, Verheye 2004, ten Have 2004). Blood flow is not only present at the lumen side of the vulnerable plaques, since these plaques are also well perfused by the surrounding vasa vasorum (Kwon 1998, Galili 2004). This perfusion might influence the temperature distribution at the lumen wall, when the temperature of the perfusing blood is lower than the temperature of the plaque.

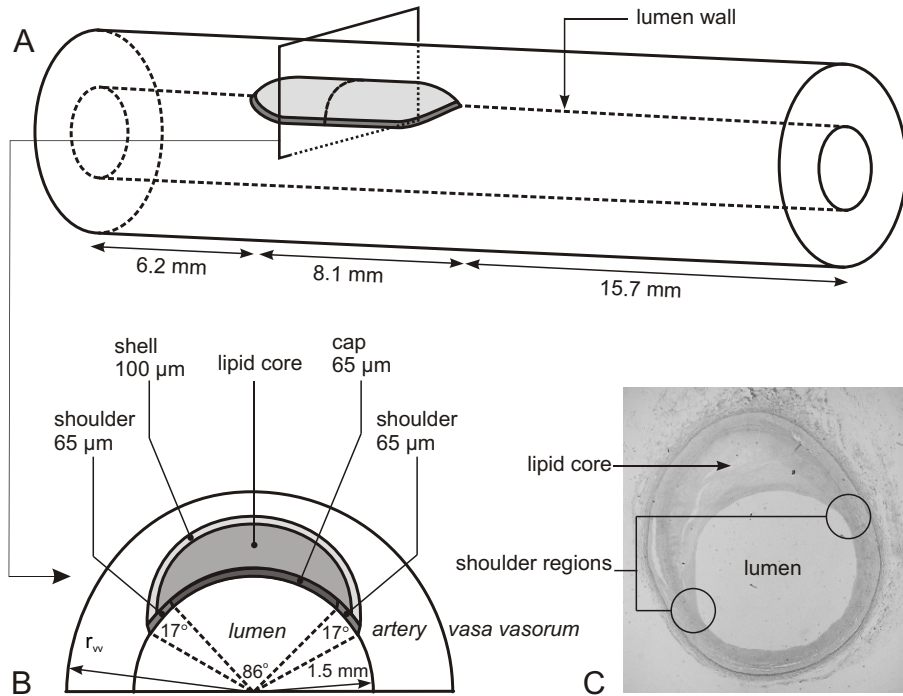


FIGURE 4.1: Schematic of the geometrical model. A: full view, B: cross section, C: a histological cross-section of a coronary vessel with atherosclerotic plaque.

Heat transfer from the vulnerable plaque to its surroundings can also take place by conduction. This manner of transfer might be influenced by the insulating properties of the lipid core, which may affect the lumen wall temperature. This effect could be different when the heat source is located either in front of the lipid core or behind it.

## 4.2 METHODS

### 4.2.1 GEOMETRICAL MODEL

A geometrical model, depicted in figure 4.1A, was created using two coaxial cylinders, which represented the lumen and the tissue surrounding the lumen. A plaque was embedded in the tissue following data presented by Kolodgie

et al (Kolodgie 2004). The length of the plaque was 8.1 mm. The necrotic core area, in our case the area that the lipid pool comprised in a cross-section, was 1.7 mm<sup>2</sup> and extended in circumferential direction over 120°. The thickness of the cap, separating the lipid core from the blood flow, was 65 μm. The outer part of the cap was separated from the inner part and it was designated as the shoulder region. In a cross sectional perspective, the shoulder regions were of 17° circumference and the inner cap part of 86° (ratio 1:5:1). The outer part of the lipidic, necrotic core was designated shell, and its thickness was 100 μm. The resulting volumes were 3.95 mm<sup>3</sup> for the lipid core, 1.42 mm<sup>3</sup> for the shell, 0.48 mm<sup>3</sup> for the cap and 0.26 mm<sup>3</sup> for the shoulder region.

The radius of outer cylinder,  $r_{vv}$ , which represented the location of the vasa vasorum, varied between 3.5 mm, 3.0 mm and 2.5 mm. The vasa vasorum was thus located at 2.0, 1.5 and 1.0 mm distance from the lumen wall, respectively.

#### 4.2.2 EQUATIONS

The heat equation was solved for the whole geometry, such that both conductive and convective heat transfer were taken into account. The heat equation can be expressed as

$$\rho c_p \left( \frac{\partial T}{\partial t} + \vec{u} \cdot \nabla T \right) - \text{div} (k \nabla T) = H \quad (4.1)$$

in which  $T$  is the temperature (°C),  $\rho$  is the density (kg m<sup>-3</sup>),  $t$  the time (s),  $c_p$  the specific heat capacity at constant pressure (J kg<sup>-1</sup> °C<sup>-1</sup>),  $\vec{u}$  the velocity (m s<sup>-1</sup>),  $k$  the heat conductivity (W °C<sup>-1</sup> m<sup>-1</sup>), and  $H$  the heat production per unit volume (W m<sup>-3</sup>).

The velocity field in the lumen was obtained by solving the Navier-Stokes equations for the lumen. The Navier-Stokes equations for an incompressible, Newtonian medium can be expressed as

$$\rho \left( \frac{\partial \vec{u}}{\partial t} + (\vec{u} \cdot \nabla) \vec{u} \right) = \rho \vec{f} - \nabla p + \eta \nabla^2 \vec{u} \quad (4.2)$$

$$\nabla \cdot \vec{u} = 0 \quad (4.3)$$

in which  $\vec{f}$  represents the body forces (N kg<sup>-1</sup>),  $p$  the pressure (N m<sup>-2</sup>) and  $\eta$  the viscosity (Pa s). The conservation of momentum and equation is represented by equation 4.2, whereas equation 4.3 represents the conservation of mass.

TABLE 4.1: Tissue parameters for the different types of tissue that were used in this model.

	Blood	Arterial tissue	Fatty plaque
Heat conductivity ( $\text{W } ^\circ\text{C}^{-1} \text{ m}^{-1}$ )	0.49	0.476	0.200
Specific heat capacity ( $\times 10^3 \text{ J kg}^{-1} \text{ } ^\circ\text{C}^{-1}$ )	3.66	3.72	2.3
Density ( $\text{kg m}^{-3}$ )	1064	1075	920
Viscosity (Pa s)	0.003		

### 4.2.3 BOUNDARY CONDITIONS AND MATERIAL PROPERTIES

The material properties that were assigned to the different materials composing the geometry can be found in table 4.1 (Duck 1990, Welch 1995). All material properties were considered to be temperature independent, since the expected temperature differences are small. The lipid core and the shell regions were assigned the thermal properties of fatty plaque. The other regions, together with the remaining vessel wall were assigned those of arterial tissue.

The heat source production was assigned to different regions, to study the influence of different locations at which the heat could be generated. Since macrophages are expected to be found in the cap, the shoulder and a thin shell surrounding the lipid core, we assigned the heat source to these regions, see figure 4.1B. We also studied the effect when all three of these regions were assigned to act as the heat source simultaneously. We will refer to this combination as mixed region, or mixed heat source. The heat source production values were chosen such that the resulting temperature differences resembled those that were reported recently (ten Have 2005). Firstly, we assigned a constant heat production per unit volume,  $H_{volume}$ , of  $5 \text{ mW mm}^{-3}$  to the different regions. Secondly, we studied the effect of a constant total heat production,  $H_{total}$ . For this, the total heat production was calculated when a  $H_{volume}$  of  $5 \text{ mW mm}^{-3}$  was applied to the cap region. This resulted to a  $H_{total}$  value of  $2.4 \text{ mW}$ , which was then applied to the other regions.

To study the influence of the insulating properties of fatty tissue, we also performed simulations in which the parameters of the lipid core and the shell regions were equal to those of arterial tissue, table 4.1.

All outer walls of the geometry, except that of the outlet and the nodes comprising the outlet, were assigned a temperature of 37.0°C, representing body core temperature. These walls include the interface between the plaque and the vasa vasorum. At the inlet of the lumen, a parabolic inflow of 75 ml min<sup>-1</sup> was assigned (Doriot 2000). At the outlet a zero stress boundary condition was applied.

#### 4.2.4 SOLUTION PROCEDURE

The geometry was meshed using mesh generator Gambit 2.2.30 (Fluent Inc., Lebanon NH, USA). The mesh consisted of tetrahedral elements. The smallest mesh element size was 30 μm in the cap and shoulder elements. The mesh elements increased to 500 μm at the outer boundaries of the geometry. The mesh was tested for mesh independency. The symmetry of the geometrical model was used, such that the solution had to be calculated for only one half of the geometry. The number of elements was around 740,000.

The equations were solved using the finite element method. The segregated solver of Fidap 8.7.2 (Fluent Inc., Lebanon NH, USA) was used. Convergence criteria were set to 1x10<sup>-4</sup> for both the velocity and the temperature solutions. Streamline upwinding was performed for the temperature solution. The number of iterations needed to obtain convergence was around 13 when no flow existed in the lumen, and around 32 when a flow was present.

Processing the numerical output was done using FieldView (Intelligent Light, Lyndhurst NJ, USA).

#### 4.2.5 ANALYSIS OF RESULTS

The results of the simulations will be described along the lines of variations in plaque composition that affect heat generation and those that affect heat transfer. The results were analyzed using the maximal temperatures at the lumen wall,  $T_{max}$ , and the maximal temperature differences at the lumen wall,  $\Delta T_{max}$ , with respect to the background temperature of 37.0°C.

Regarding heat generation, the lumen wall temperature profiles were studied for the different regions where the macrophages were located. This was done for both the flow and no flow situation. Furthermore, we have commented on the difference between assigning a constant heat production per unit volume,  $H_{volume}$ , and a constant total heat production,  $H_{total}$ , to the heat source regions.

Regarding heat transfer, both the influence of lipid core composition and vasa vasorum location were described. The influence of convection at the lumen side of the plaque has been described previously. This paper focuses on



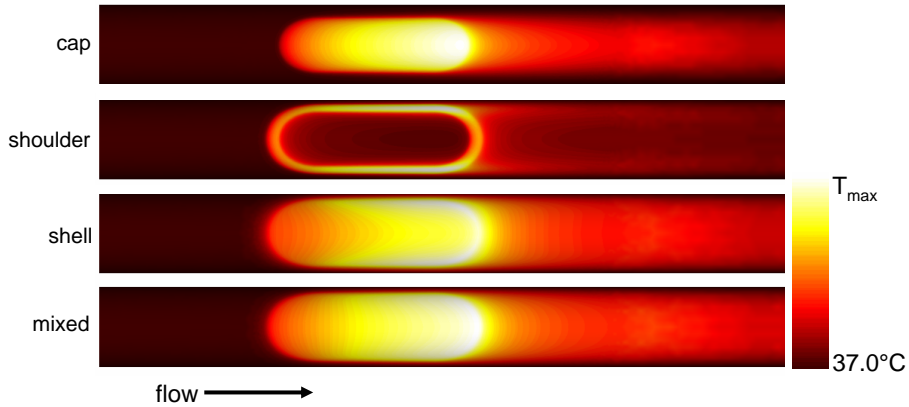


FIGURE 4.2: Temperature profiles at the lumen wall when a flow was simulated in the lumen. Assigned regions from top to bottom: cap, shoulders, shell and mixed region.

the heat exchange at the vasa vasorum side of the plaque. The results regarding the vasa vasorum location were studied using the flow influence factor (ten Have 2004). This factor was calculated as

$$FIF = \frac{\Delta T_{no\ flow}}{\Delta T_{flow}} \quad (4.4)$$

in which  $\Delta T_{no\ flow}$  represents the maximal temperature difference at the lumen wall when no flow exists in the lumen, and  $\Delta T_{flow}$  the maximal temperature difference at the lumen wall when a flow does exist in the lumen. The FIF indicates how much the measured temperature differences are changed by the blood flow in the lumen.

## 4.3 RESULTS

### 4.3.1 HEAT GENERATION

In figure 4.2 temperature distributions at the lumen wall are given when the heat source was assigned to the different regions and when a flow was present in the lumen, since this is the physiological default situation, and the one preferred by interventional cardiologists. From top to bottom, the heat source was assigned to the cap, the shoulders, the shell and the mixed region. The results are depicted for the situation when a flow was simulated in the lumen. The

scales belonging to the individual profiles range from 37.0°C to the maximal temperature at the lumen wall, which differed for the different heat source regions. These maximal lumen wall temperatures can be found in table 4.2. The resulting profile of the simulation in which the shoulder region was assigned to be the heat source clearly showed the shape of the shoulder region of the plaque. The profiles belonging to the shell and mixed region were longest in both the direction of the blood flow and the circumferential direction.

In table 4.2, the maximal lumen wall temperature differences are given for both the flow and no flow situations. In the two columns on the left, the heat production per unit volume,  $H_{volume}$ , was kept constant at  $5 \text{ mW mm}^{-3}$  for all the heat source regions. The two columns on the right represent the maximal lumen wall temperature differences when the total heat production,  $H_{total}$ , was kept constant at 2.4 mW for all the heat source regions.

TABLE 4.2: Maximal temperature differences at the lumen wall in °C. Vasa vasorum at 2 mm from lumen wall.

	$H_{volume} =$ 5 mW mm <sup>-3</sup>		$H_{total} =$ 2.4 mW	
	flow	no flow	flow	no flow
cap	0.12	0.56	0.12	0.56
shoulders	0.08	0.19	0.14	0.37
shell	0.12	0.61	0.04	0.19
mix	0.24	1.30	0.05	0.27

For the constant  $H_{volume}$ , one can see that for both the flow and the no flow situation the maximal temperature difference existed when the mixed region was assigned to be the heat source, followed by the shell region. The lowest maximal temperature difference was found for the shoulder region. For a constant  $H_{total}$  and a flow situation, the highest temperature differences existed when the shoulder region was assigned to be the heat source, followed by the cap region. For a constant  $H_{total}$  and a no flow situation, the highest temperature differences existed for the cap region, followed by the shoulder region. The lowest temperature difference for both flow and no flow was found when the shell region was assigned to be the heat source.

The temperature profiles at the centerline, the line of symmetry in the direction of blood flow, of the profiles in figure 4.2 are given in figure 4.3, when a  $H_{volume}$  of  $5 \text{ mW mm}^{-3}$  was assigned to the regions acting as the heat source. These centerlines represent pullbacks along these lines that could have been

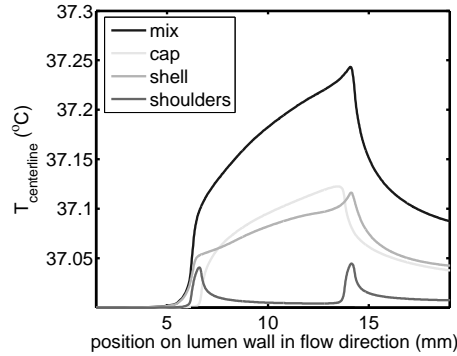


FIGURE 4.3: Temperature profiles along the center line when a flow was simulated in the lumen. Vasa vasorum at 2 mm from lumen wall. Constant heat production per unit volume =  $5 \text{ mW mm}^{-3}$ .

obtained with a catheter used for intracoronary thermography. The pullbacks obtained when the cap, shell and mixed regions were assigned to be the heat source were of identical appearance, with the mixed region showing the highest  $T_{max}$ , whereas the pullback for the shoulder region differed strongly. In the pullback for the shoulder region two peaks could clearly be distinguished, representing the proximal and distal shoulder regions. In addition, the centerline pullback of the shoulder region did not reveal the maximal lumen temperature, which is  $37.08^\circ$ . This maximal temperature was located at the parts of the shoulder region that were parallel to the blood flow direction.

### 4.3.2 INFLUENCE OF THERMAL PROPERTIES OF THE LIPID CORE

In table 4.3 the maximal temperature differences at the lumen wall are given, which are used to study the influence of the insulating properties of the lipid core. The results are given for when the cap and shell regions were assigned to be the heat source. These were the regions to be influenced most by this parameter variation since they were located in front of the lipid core and behind it. In the table the maximal lumen wall temperature differences are given when the lipid core was assigned to have thermal parameters of healthy arterial tissue and of fatty plaque.

The results in the table show that more lipid-rich tissue in the lipid core resulted in higher temperature differences at the lumen wall when the cap region was assigned to be the heat source, whereas for the shell region it resulted

TABLE 4.3: Maximal temperature differences at the lumen wall. Constant total heat production = 2.4 mW. Vasa vasorum at 2 mm from lumen wall.

	cap		shell	
	flow	no flow	flow	no flow
healthy	0.11	0.43	0.05	0.21
lipid	0.12	0.56	0.04	0.19

in lower temperature differences. These statements hold for both the flow and the no flow situation. For a flow situation these changes are smaller than for a no flow situation. The shape of the pullback curves did not change much by the parameter variation.

### 4.3.3 HEAT EXCHANGE BY THE VASA VASORUM

In figure 4.4 the influence of the location of the vasa vasorum on the maximal temperature differences at the lumen wall are depicted. A constant  $H_{total}$  of 2.4 mW was assigned to the heat source regions. In the left panel, a flow was simulated, and in the right panel no flow existed in the lumen. Note the different scale on the y-axes.

When the vasa vasorum approached the plaque, the lumen wall temperatures decreased, for both the flow and the no flow situations, but not largely. When a flow was present, the highest temperatures were found when the shoulder region was assigned to be the heat source, followed by the cap region. The lowest temperature differences were found for the shell region. When no flow existed, the highest maximal temperature differences were found when the cap region was assigned to be the heat source, followed by the shoulder region. The lowest temperature differences in a no flow situation were found for the shell region. These orders did not change for different locations of the vasa vasorum.

In figure 4.5 the flow influence factors, FIF values, resulting from the temperatures in figure 4.4 are given. The FIF values, and thus the influence of the lumen blood flow, were highest for the mixed region and a distance of 2.0 mm between the vasa vasorum and the lumen wall. The FIF was lowest for the shoulder region, independent of the location of the vasa vasorum.

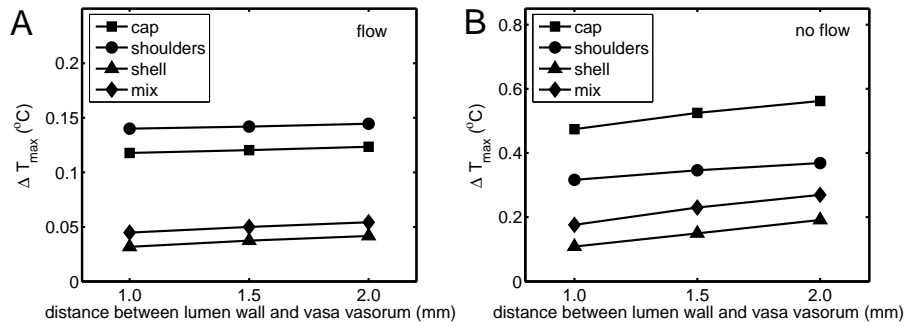


FIGURE 4.4: Maximal temperature differences at lumen wall for varying heat source regions and varying locations of vasa vasorum. Constant total heat production = 2.4 mW, A: flow, B: no flow. Note the different scale on the y-axes.

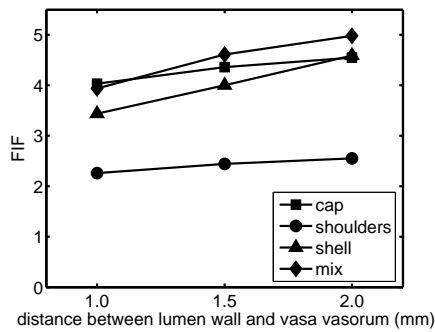


FIGURE 4.5: Flow influence factor for varying heat source regions and varying locations of vasa vasorum. Constant total heat production = 2.4 mW.

## 4.4 DISCUSSION

In this study, numerical simulations were performed to study the effect of differences in plaque composition on the temperature profile at the lumen wall. Firstly, the effect of the location of the heat source and its production was described, which concern the heat generation of the plaque. Secondly, the effects of both the lipid core composition and the location of the vasa vasorum were studied, both concerning the heat transfer from the vulnerable plaque to the lumen wall.

### 4.4.1 HEAT GENERATION

The first results described in this paper were obtained using a constant heat production per unit volume,  $H_{volume}$ , representing an optimal, dense macrophage infiltration. After this, a constant total heat production,  $H_{total}$ , was assigned to the regions, representing identical numbers of macrophages irrespective of the volume. This resulted in identical temperatures when the cap region was assigned to act as heat source, since this region was considered the default. Changing from  $H_{volume}$  to  $H_{total}$  resulted in higher temperatures when the shoulder region was assigned to be the heat source, since this region has a smaller volume than the cap region. For the shell and the mixed regions this resulted in lower lumen wall temperatures, due to the larger heat source volumes compared to that of the cap. When a constant  $H_{total}$  was used, the cap region showed higher lumen wall temperatures than the shell region. This means that, even though the macrophages may produce equal amounts of heat, the macrophages that lie further from the lumen wall contribute less to the temperature profile at the lumen wall (ten Have 2004). Macrophages that have scavenged lipids and have thereby migrated deeper into the plaque might thus contribute less to the temperature profile than macrophages that lie close to the lumen.

From the figures representing the lumen wall temperature profiles and the pullbacks, figures 4.2 and 4.3, it becomes clear that the location of the macrophages strongly influences the resulting temperature profile. This determines the requirements regarding the spatial resolution that a measuring method should fulfill. When the macrophages are clustered together in the cap region, this resulted in a shorter temperature profile, both in the direction of the blood flow and the circumferential direction, than when the macrophages are clustered together in the shell region. The effect was even stronger when the shoulder region was assigned to be the heat source, since the profile is of small circumferential dimensions, which requires a high spatial resolution of a thermography catheter to enable its detection. With the current methods

used for in vivo intracoronary thermography, not allowing full circumferential scanning, vulnerable plaques with macrophages located only in the shoulder regions might be left undetected.

Except for when the shoulder region was assigned to be the heat source, the maximal temperatures of the temperature profile are all located at the center-lines, which were depicted in figure 4.3. The maximal temperatures of the shoulder region lie on the regions of the profile parallel to the blood flow. In other publications, thermography pullbacks were depicted which showed multiple hot spots, which were attributed to a single vulnerable, atherosclerotic plaque (Verheye 2002a, Krams 2005). The shape of the temperature profile resulting from the heat producing macrophages located in the shoulder region could clarify these reported profiles.

From figures 4.2 and 4.3 it becomes clear that the location at which the temperature is measured is of influence on the results. As can be seen in figures 4.2 and 4.3, the temperatures upstream of the plaque differ from the temperatures downstream of the plaque. The locations where the temperature measurements were performed, have previously been determined using angiographic images and/or IVUS images (Stefanadis 1999, Stefanadis 2001, Toutouzas 2006), and were based on the degree of stenosis. This location, though, is not necessarily the location at which the macrophages are located, since vulnerable plaques are, in general, not stenotic due to expansive remodelling (Schaar 2004a). In addition, when the macrophages are clustered together, this need not be the location at which the degree of stenosis is highest. These arguments might explain the variation in the results obtained with catheters of identical design (Stefanadis 1998, Stefanadis 2000, Toutouzas 2004). They could also explain why not every patient that was inspected showed thermal heterogeneity (Stefanadis 1999).

#### **4.4.2 INFLUENCE OF INSULATING PROPERTIES OF LIPID CORE**

The thermal properties assigned to the lipid core influenced the lumen wall temperatures, but the effects were opposite for when the heat source was assigned to the shell and cap regions. When the lipid core tissue is more lipid-rich, the thermal conductivity decreases. This causes the lumen wall temperatures to increase when the cap region acted as heat source, whereas for the shell region they decreased. This can be attributed to the location of the heat source with respect to the lipid core, of which the thermal properties were changed. The lipid core lies in front of the shell region. When the thermal conductivity decreases, this means that the core will conduct the heat produced by the shell less well to the lumen wall. Less thermal energy will arrive at the lumen wall,

resulting in lower lumen wall temperatures. In case of the cap region, the lipid core lies behind the heat source. With decreasing thermal conductivity of the lipid core, more of the heat will thus flow to the lumen wall, resulting in higher lumen wall temperatures.

In vivo measurements need to be interpreted with great care due to the influence of the lipid core. When the location of a plaque is determined by angiography and/or IVUS images, the thermal properties of the surrounding tissue remain unknown. Heat producing macrophages surrounded by a less lipid-rich core might result to lumen wall temperatures identical to those found for heat producing values surrounded by a highly lipid-rich core, depending on their location with respect to the core. The latter case is considered to be more vulnerable, but this might not be deduced from the temperatures that were measured. The implication of the lumen wall temperature measurements could thus be misinterpreted. When different tissues have different thermal properties, this means that they also have different cooling rates. Ex vivo measurements (Casscells 1996, Verheye 2002a), generally performed at room temperature, are influenced by these differences and they thus need to be interpreted with care. The presence or absence of a lipid core, or more generally the composition of the plaque, might have attributed to the variety in temperature differences that have previously been reported (ten Have 2005).

#### **4.4.3 INFLUENCE OF LOCATION OF VASA VASORUM**

In figure 4.5 the FIF values were given, representing the influence of the blood flow on the lumen wall temperatures. This value can be interpreted as the factor by which measured temperatures increase when the flow is halted. For the results depicted in the figure, it means that the temperatures increase by a factor between 2 and 5 when the vessel is occluded. This is large when it is compared to the influence that the location of the vasa vasorum has on the lumen wall temperatures, which can be observed in figure 4.4, since these temperatures were not strongly influenced by the location of the vasa vasorum. The FIF decreases with decreasing distance between the lumen wall and the vasa vasorum, but not largely.

Vasa vasorum density has been related to plaque rupture (Moreno 2004) and plaque progression (Langheinrich 2006). From our results it can be seen that the closer the vasa vasorum lies to the lumen, the lower lumen temperatures are. The thermographic measurements that were reported by others might thus have underestimated the vulnerability of the plaque when they concerned advanced lesions.



#### 4.4.4 LIMITATIONS

In this study it was assumed that macrophages act as the heat source due to their increase metabolic activity, which has not yet been proven, though. Other exothermal processes might be present in the vulnerable plaque and the vessel wall surrounding the plaque (ten Have 2005). The heat production values of exothermal processes in the vulnerable plaque and its surroundings are unknown. Heat production values of macrophages in other environments, different from that of the vulnerable plaque, have been reported previously (Charlebois 2002, Thóren 1990). Based on numerical simulations, it was concluded that these reported values were not sufficiently high to generate temperature differences equal to those reported in literature (ten Have 2004).

The geometry that was used for these simulations consisted of straight tubes, and a stationary parabolic blood flow profile was used. A more realistic geometry and a pulsatile flow are both expected to influence the velocity profile near the wall, which will change the results in this paper only by a geometry or time-dependent scaling factor. The influence of a catheter in the lumen was studied in a separate paper (ten Have 2006).

The impact of the vasa vasorum might have been underestimated in this study, since in this geometrical model the vasa vasorum covered only the upper side of the plaque and not the proximal and distal regions. In addition, perfusion of the plaque was not included in the simulations.

#### 4.5 CONCLUSIONS

In conclusion, the lumen wall temperature distribution is influenced by vulnerable plaque composition. The results from this numerical study have important implications for in vivo vulnerable plaque detection using thermographic methods.

The design of the thermographic device that measures lumen wall temperatures in vivo should fulfill a number of requirements which can be deduced from this study. Firstly, the method needs high a spatial resolution. Since thermal heterogeneity can be caused by small macrophage clusters with high metabolic activity, thus acting as focal heat source, this heterogeneity might not be detected when the spatial resolution of the method not high enough. So for optimal vulnerable plaque detection by intracoronary thermography, the spatial resolution of the existing contact measurement techniques needs to be improved.

Secondly, the variety in plaque composition requires combining intracoronary thermography with an imaging technique that is able to image

macrophage clusters, the location of lipid regions, and, when possible, the location of the vasa vasorum. Intracoronary thermography can then be responsible for determining the inflammatory activity of a plaque and the imaging technique provides the essential information required for correct interpretation of the thermographic measurements.



## CHAPTER 5

# INFLUENCE OF CATHETER DESIGN

We studied how catheter design and catheter location influence the temperature readings, and thus its capacity to detect vulnerable plaques. Numerical simulations were performed on geometries representing the coronary artery, the vulnerable plaque and the catheter. Catheter material, diameter and location with respect to the plaque were varied. Both flow and no flow situations were studied. The location at which a thermosensitive element should be placed for most optimal temperature readings differed for polyurethane and nitinol catheters. Catheter design can contribute to enhanced temperature readings and can thus enable more optimal vulnerable plaque detection.

BASED ON: ten Have AG, Draaijers EBGT, Gijzen FJH, Wentzel JJ, Slager CJ, Serruys PW, van der Steen AFW. Influence of catheter design on lumen wall temperature distribution in intracoronary thermography. Accepted for publication in *Journal of Biomechanics*, 2006.

## 5.1 INTRODUCTION

Different catheters have been developed and were used for thermographic studies (Stefanadis 1999, Verheye 2002a, Naghavi 2003, Courtney 2004). These catheters differ in their dimensions, from 0.1 mm to 1.3 mm diameter; the material of which they are made, nitinol and polyurethane; and the thermosensitive elements that are used, thermocouple and thermistor. The thermographic readings were shown to be influenced by flow (Diamantopoulos 2003a, Stefanadis 2003b, ten Have 2004, Verheye 2004).

Since the presence of a catheter changes the velocity profile, its presence might influence the temperature readings. These influences are not only due to the changes in the velocity profile, but also due to its thermal properties and its location with respect to the heat source. To study the influence of catheter presence and its design on temperature readings, we have performed numerical simulations on a geometrical model of a coronary artery in which a vulnerable plaque and a catheter were modeled.

## 5.2 METHODS

### 5.2.1 GEOMETRICAL MODEL

The geometrical model, depicted in figure 5.1, consisted of a straight cylinder of 3 mm diameter which represented the coronary artery lumen. Around this cylinder, a second co-axial cylinder was created, which represented the vessel wall and the tissue surrounding the coronary artery. The heat source and the lipid core were modelled as homogenous entities in 90° circumferential direction. The dimensions of the plaque fall within the ranges that were reported for fibrous cap atheromas, thin cap fibroatheromas and plaques that caused acute plaque rupture (Kolodgie 2004).

The modelled catheters had diameters of 1, 0.5 and 0.2 mm. The contact surface of the catheter to the lumen wall was created such that the catheter radius at that site was flattened and had a curvature identical to the lumen curvature. When the diameter of the catheter was smaller, the contact surface area was smaller. The contact surface areas were 1.407, 0.594 and 0.218 mm<sup>2</sup>, respectively.

The location of the catheter was varied in longitudinal, circumferential and radial directions, which is shown in figure 5.2. For the longitudinal variation, which represented a pullback that was used for determining the optimal sensor location, the catheter tip was positioned at 5 locations with respect to the heat source, causing various degrees of overlap. Full overlap was created when

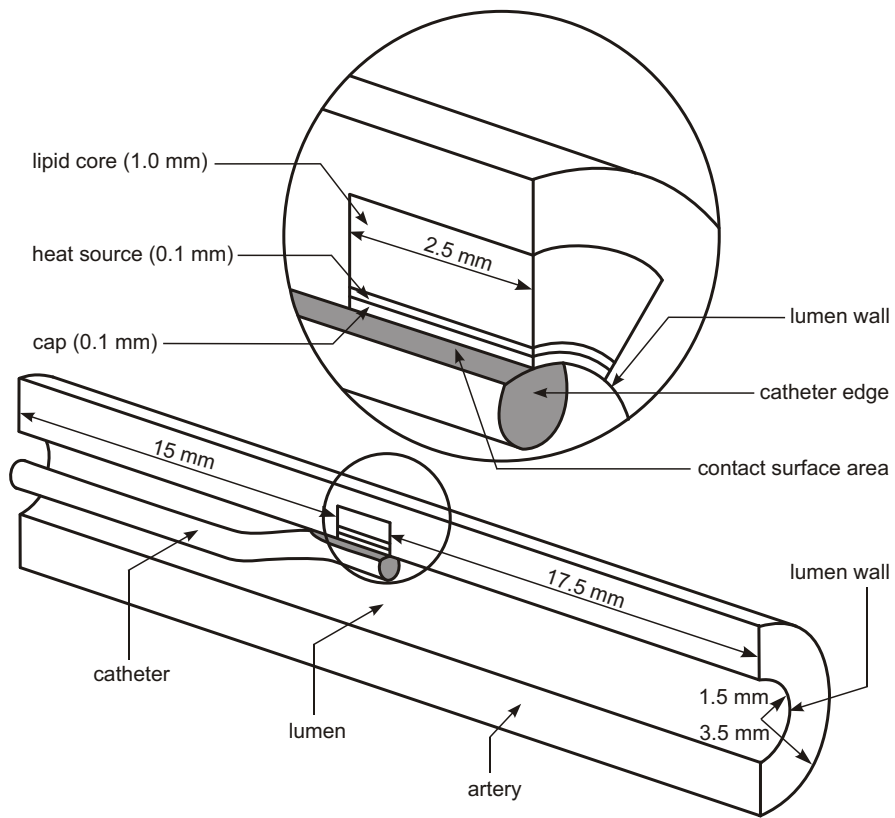


FIGURE 5.1: Geometrical model of the artery and the catheter. In the artery a lipid core, heat source and cap are embedded.

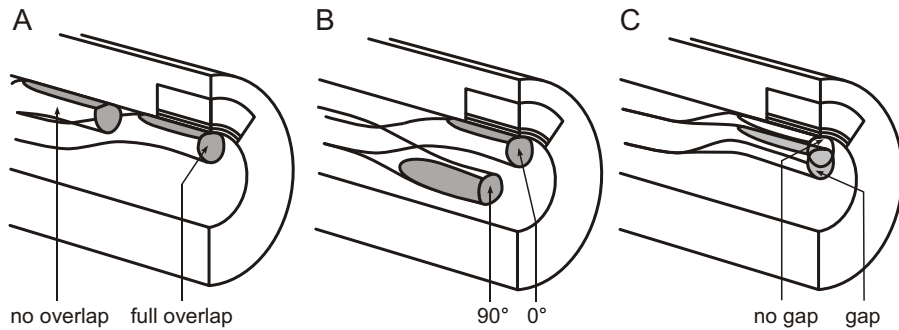


FIGURE 5.2: Variation in catheter location. A: longitudinal, B: circumferential, and C: radial variation.

the catheter edge was positioned at the end of the heat source, partial overlap when the catheter was positioned such that half of the heat source was covered by the contact surface, both upstream and downstream, and no overlap existed when the catheter edge was positioned 1 cm from the heat source, both upstream and downstream. The variation in catheter location in the circumferential direction was created when the catheter was positioned at  $0^\circ$ ,  $45^\circ$  and  $90^\circ$ . These positions thus caused full, partial and no overlap at all, respectively, between the catheter and the heat source. Radially, the position was varied between full contact, and a gap size of 200 and 300  $\mu\text{m}$  between the contact surface and the lumen wall.

## 5.2.2 BOUNDARY CONDITIONS

The body core temperature remains relatively constant due to the tissue perfusion. Similarly, the vessel wall and the plaque borders are perfused by microvessels called the vasa vasorum. This effect was taken into account in the simulations by application of a temperature of  $37.0^\circ\text{C}$  at all the outer boundaries. Since blood is able to remove heat from the lumen wall by convection, we did not fix the temperature at the lumen outlet.

Temperature differences between warmer and cooler regions of a plaque up to  $2.2^\circ\text{C}$  have been reported (Casscells 1996), yet the most recently published results have converged to values around  $0.2^\circ\text{C}$  (ten Have 2005). The heat source production value that we used in this study was  $5 \text{ mW mm}^{-3}$ , which resulted in temperatures in this latter range. We used stationary uniform velocity profiles forced upon the inlet resulting in a flow of  $75 \text{ cc min}^{-1}$ ,

TABLE 5.1: Parameter values for the different types of tissue and catheter materials that were used in this model.

	Blood	Arterial tissue	Fatty tissue	Nitinol	Polyurethane
Heat conductivity ( $W \text{ } ^\circ C^{-1} \text{ m}^{-1}$ )	0.49	0.476	0.2	18	0.251
Specific heat capacity ( $\times 10^3 \text{ J kg}^{-1} \text{ } ^\circ C^{-1}$ )	3.66	3.72	2.30	0.49	2.2
Density ( $\text{kg m}^{-3}$ )	1064	1075	900	6450	1220
Viscosity (Pa s)	0.003				

which is a representative value for blood flow in human coronary arteries (Doriot 2000). At the outlet a zero stress boundary condition was applied.

### 5.2.3 MATERIAL PARAMETERS

Material parameter values, including thermal parameters, that were assigned to both the tissues and the catheter can be found in table 5.1 (Duck 1990, Welch 1995). The parameter values for nitinol and polyurethane were provided by vendors of these materials.

The thermal parameter values that were used for the vessel wall and the tissue surrounding the coronary artery were assumed to be equal to the values that were found for healthy arterial tissue. The thermal parameters for the lipid core and the heat source were assumed to be equal to the values of fatty tissue. All parameters were considered to be independent of temperature. The blood was modelled as a Newtonian fluid.

### 5.2.4 NUMERICAL SOLUTION PROCEDURE

The geometrical models were created and meshed in Gambit 2.1.6 and 2.2.30 (Fluent Inc., Lebanon NH, USA). The mesh contained linear tetrahedral mesh elements and we increased mesh density where large thermal gradients were expected. The mesh was refined such that the results were mesh independent. The mesh element size increased from  $50 \mu\text{m}$  in the cap and heat source volumes to a maximum element size of  $200 \mu\text{m}$  at the edges of the geometry. The number of elements was typically around  $150 \times 10^3$ .

The steady heat equation and the steady Navier-Stokes equations were solved for a Newtonian fluid (ten Have 2004). The calculations were performed with the widely used package Fidap 8.7.2 (Fluent Inc., Lebanon NH, USA). The problem was considered weakly coupled, so temperature dependence of the momentum equation was not considered. The segregated solver method was used to solve the equations. Convergence was obtained when the relative errors between two iterations were less than  $1 \times 10^{-4}$  for the temperature and the velocity solutions. Where possible, symmetry of the geometrical model was used to reduce calculation time. Streamline upwinding was used for stabilization of the temperature solution.

Visualization and processing of the numerical output was done using Field-View 10F (Intelligent Light, Lyndhurst NJ, USA).

## 5.2.5 ANALYSIS OF RESULTS

The results are expressed as temperature differences,  $\Delta T$ , with respect to the background temperature of  $37.0^\circ\text{C}$ .

The location at which a thermosensitive element, such as a thermistor or a thermocouple, should be placed on the contact surface for most the optimal temperature readings, and thus for most optimal vulnerable plaque detection, needs to be determined. Using the data for the pullback under flow conditions, as was described in section 5.2.1, this optimal sensor location was defined as the point on the symmetry axis of the the contact surface where  $\Delta T$  is maximal. The temperature differences at this optimal sensor location are referred to as  $\Delta T_{sens}$ .

## 5.3 RESULTS

### 5.3.1 GENERAL OBSERVATIONS

The temperature profile at the lumen wall when a flow was present with no catheter, is depicted in the top two panels of figure 5.3 representing the temperature distributions at the lumen wall. The maximal  $\Delta T$  at the lumen wall for the reference situation was  $0.12^\circ\text{C}$ . In the bottom panels the temperature distributions at the lumen wall are given when a 1 mm nitinol, left, or a 1 mm polyurethane, right, catheter contacted the lumen wall. The maximal  $\Delta T$  at the lumen wall for these situations were  $0.14$  and  $0.51^\circ\text{C}$ , respectively. For the 1 mm polyurethane catheter, the maximal  $\Delta T$  was found on the contact surface, whereas for the 1 mm nitinol catheter, it was found beside the contact surface



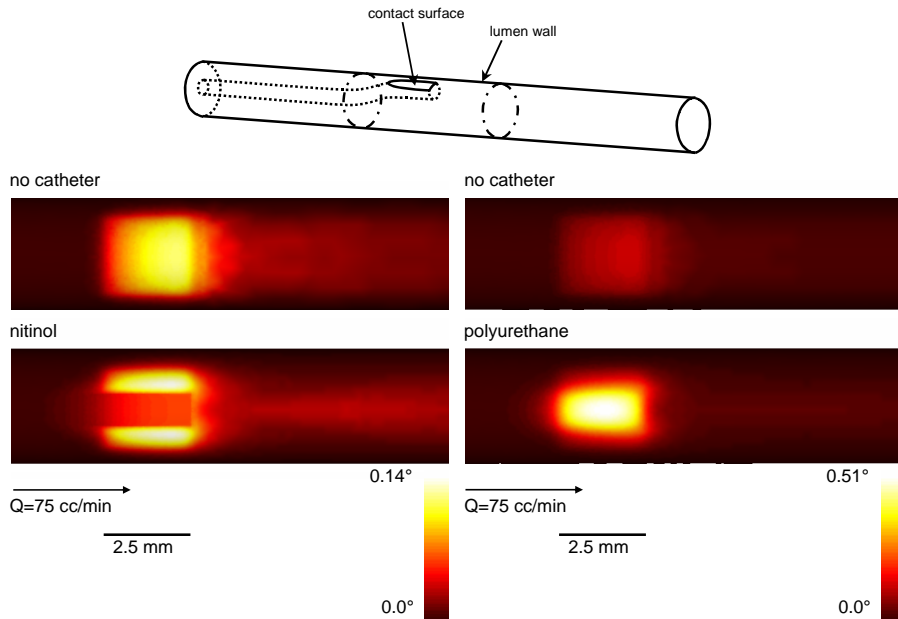


FIGURE 5.3: Temperature distributions at the lumen wall. The distributions are shown for the area between the dash-dotted lines depicted on the lumen wall. The area where the contact surface of the catheter contacts the lumen wall is shown with solid lines. The catheter was located right under the heat source. A flow,  $75 \text{ cc min}^{-1}$ , was present. Left: Temperature distribution at the lumen wall without catheter (top) and with 1 mm nitinol catheter (bottom). Right: Temperature distribution at the lumen wall without catheter (top) and with 1 mm polyurethane catheter (bottom). Note the different temperature scales.

on the lumen wall. The maximal temperature at the contact surface of the 1 mm nitinol catheter was  $0.06^\circ\text{C}$ .

One can appreciate the effect of the thermal properties of the catheter; the highly conductive nitinol reduced the maximal  $\Delta T$  at the contact surface and the insulating polyurethane enhanced the maximal  $\Delta T$ .

The uniform velocity profile at the inlet of the lumen developed to a parabolic profile in the absence of a catheter. When a catheter was present, the profile developed to an annular tube velocity profile. The effect the catheter had on the velocity profile right behind the catheter can be seen in figure 5.4. A horseshoe vortex and a recirculation zone can be appreciated in the left

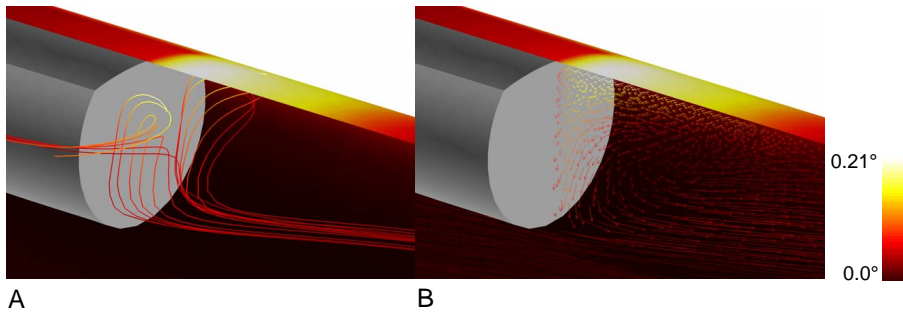


FIGURE 5.4: Effect of a 1 mm nitinol catheter on the velocity profile and on the blood temperature. The catheter was positioned such that it partially overlapped the heat source upstream. A: streamlines show a horseshoe vortex, B: vectors represent the velocity in the symmetry plane and show a recirculation zone.

and right panel, respectively. Further downstream, the profile recovered to a parabolic velocity profile.

### 5.3.2 PULLBACK AND OPTIMAL SENSOR LOCATION

In figure 5.5 the temperature profiles on the contact surface are given for the various longitudinal positions for a 1 mm nitinol, left, and a 1 mm polyurethane, right, catheter. The maximal  $\Delta T$  on the symmetry line of the contact surface is indicated with an arrow in both panels. For the nitinol catheter the maximal temperature difference, and thus the optimal sensor location, was found on the catheter edge of the contact surface; for the polyurethane catheter it was found at 1.1 mm from the edge. These optimal sensor locations were maintained for all catheters that were modelled.

### 5.3.3 INFLUENCE OF CATHETER LOCATION

In figure 5.6 temperature differences at the sensor location,  $\Delta T_{sens}$ , are given for different catheter positions.  $\Delta T_{sens}$  was almost always higher for the polyurethane catheters.  $\Delta T_{sens}$  decreased when the catheter was moved away from the source, but did so faster for the polyurethane catheter. In addition,  $\Delta T_{sens}$  was always higher for no flow than for flow. The catheter positions can be divided into positions in which overlap, either full, denoted with encircled times symbol, or partial, denoted with an asterisk, existed between the heat

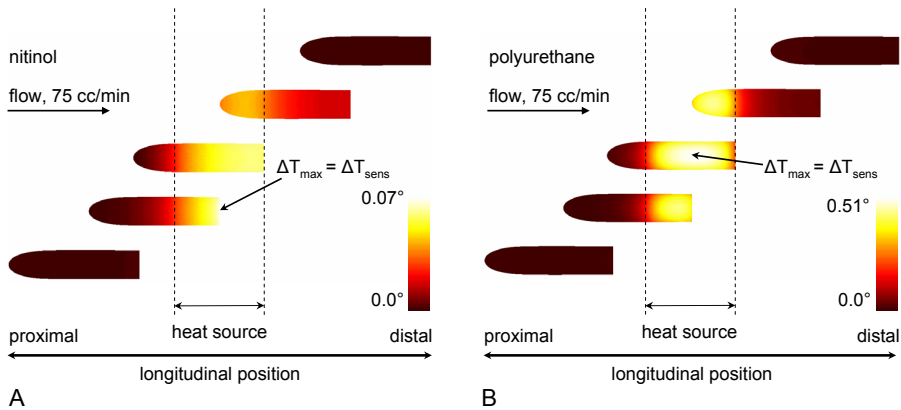


FIGURE 5.5: Temperature profiles on contact surface of the catheter of 1 mm diameter made from A: nitinol and B: polyurethane, under flow conditions. The position of the contact surface with respect to heat source (from top to bottom): no overlap, upstream (top); partial overlap, upstream; full overlap (middle); partial overlap, downstream; no overlap, downstream (bottom). Note the different temperature scales.

source and the contact surface, and positions for which there existed no overlap.

In the top two panels of 5.6 the results of the variation in longitudinal position of the catheters are given. The location of the heat source is marked with a bold line on the x-axis. For the nitinol catheter the source appeared flattened when a pullback was performed, whereas for the polyurethane catheter an explicit peak existed. When there was overlap and flow,  $\Delta T_{sens}$  was on average 5.4 times higher for the polyurethane catheter compared to the nitinol catheter. For a nitinol catheter, when there was overlap,  $\Delta T_{sens}$  values were on average 5.5 times higher for no flow compared to flow. For a polyurethane catheter, this factor was only 1.7 times.

The results for the circumferential variation in catheter position are given in the middle two panels of figure 5.6.  $\Delta T_{sens}$  values were similar for the no overlap positions of the nitinol and polyurethane catheters, but showed great variation when there was overlap. When there was overlap and flow,  $\Delta T_{sens}$  was on average 8.1 times higher for the polyurethane catheter compared to the nitinol catheter. For a nitinol catheter, when there was overlap,  $\Delta T_{sens}$  values were on average 6.1 times higher for no flow compared to flow. For a polyurethane catheter, this factor was only 1.8.

In the bottom two panels of figure 5.6 the results for the variation in gap

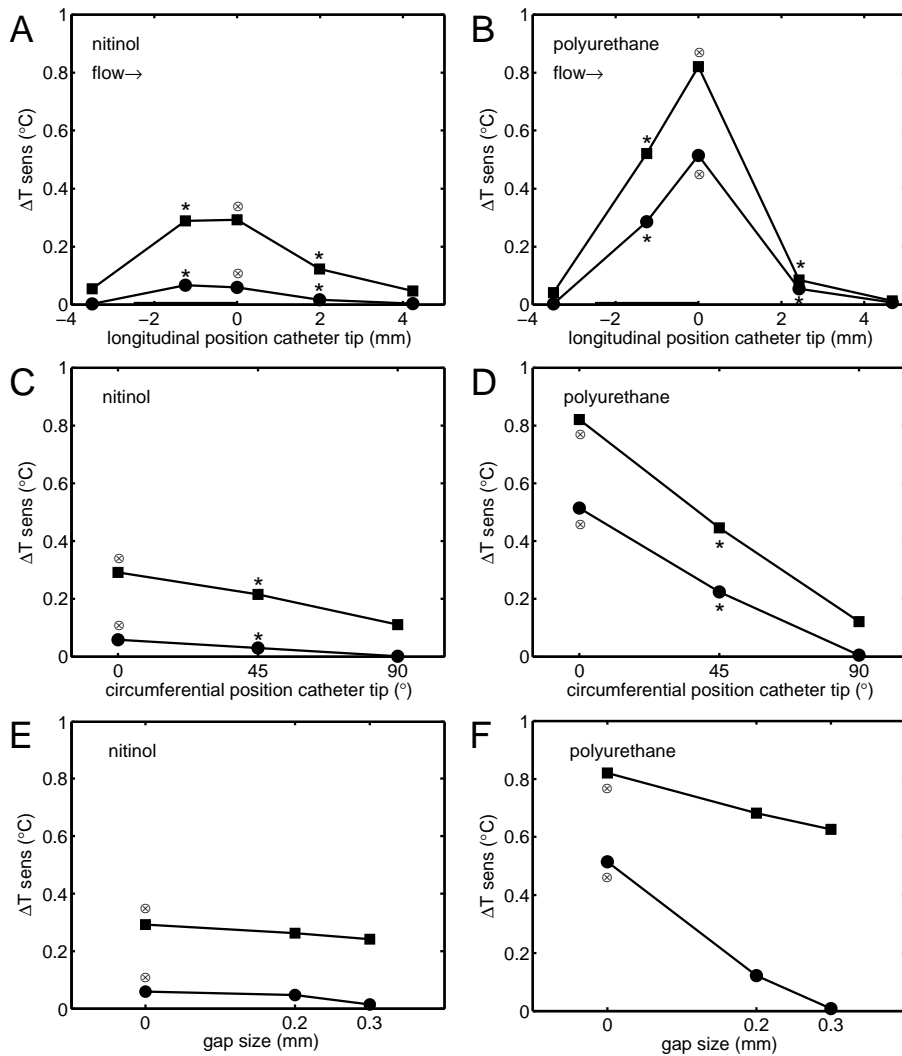


FIGURE 5.6:  $\Delta T_{sens}$  values for nitinol (A, C, E) and polyurethane (B, D, F) catheters of 1 mm diameter, at different longitudinal (A, B, position measured from the downstream edge of the heat source), circumferential (C, D) and radial (E, F) locations. For both flow (circle) and no flow (square) conditions. Full and partial overlap between heat source and catheter contact surface are indicated by encircled times symbols and asterisks, respectively.

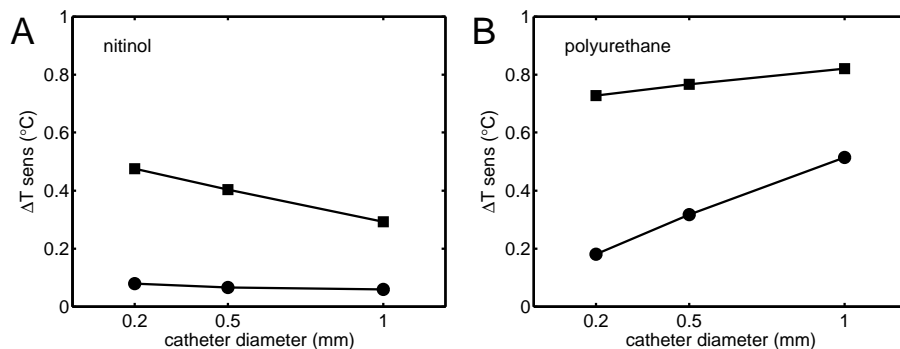


FIGURE 5.7:  $\Delta T_{sens}$  values for A: nitinol and B: polyurethane catheters of varying diameters positioned right under the heat source. For both flow (circle) and no flow (square).

size are given. For no flow,  $\Delta T_{sens}$  values for the polyurethane catheter were on average 2.7 times higher than those of the nitinol catheter. This value was relatively constant for the three different gap sizes. For flow, when the gap size increased from 0 to 0.3 mm, this factor strongly decreased from 8.7 to 0.71. For the nitinol catheter, and gap sizes 0 and 0.2, the  $\Delta T_{sens}$  values were 5.0 and 6.3 times higher for no flow compared to flow, respectively. For a polyurethane catheter these values were 1.6 and 5.3, respectively, showing a great increase.

### 5.3.4 INFLUENCE OF CATHETER DIAMETER

In figure 5.7 it can be seen that for nitinol catheters  $\Delta T_{sens}$  decreased when catheter diameter increased; for polyurethane these values increased. The influence of flow decreased when catheter diameter increased. For a 0.2 mm nitinol catheter,  $\Delta T_{sens}$  was 6.5 times higher for no flow compared to flow. For a 1.0 mm nitinol catheter, this number was 5.0. For polyurethane catheters this number reduced from 3.7 to 1.6.

## 5.4 DISCUSSION

Presence of a catheter in the artery changed the lumen wall temperature profile and the maximal temperature values, as could be seen in figure 5.3. It was previously demonstrated that reducing blood flow increased the temperature readings (Stefanadis 2003b, Verheye 2004) and changed the temperature profile

(ten Have 2004). Presence of a catheter changed the velocity distribution, and thus the convective heat transfer, compared to when no catheter was present. Conductive heat transfer changed due to the differences in thermal parameters between catheter material and those of blood and arterial tissue. Therefore, the changes in temperature were the result of both catheter presence and catheter design parameters.

The optimal sensor location was chosen under flow conditions because this is favored by interventional cardiologists. Fully occluding a vessel can cause chest pain and an uncomfortable feeling for the patient under treatment, and is therefore avoided. The optimal sensor location of the nitinol catheter was found at the catheter edge, whereas for the polyurethane catheter it was found upstream at 1.1 mm from the edge. For the nitinol catheter, the part of the lumen wall beside the contact surface of the catheter, was of higher temperature than the contact surface. Thus when the blood flowed beside the catheter it was heated. When entering the recirculation zone it was able to heat the catheter. For the polyurethane catheter, the lumen wall was of lower temperature than the contact surface, so when the blood entered the recirculation zone it cooled the catheter.

The heat source could be detected by the nitinol catheter when the contact surface overlapped the heat source, but temperatures were higher when there was full overlap. When the nitinol catheter approximated the heat source, the temperatures did not differ much from the background temperature. Using a polyurethane catheter, though, the temperature differed from the background temperature even when there existed partial overlap. This meant that the exact location of a heat source could not be exactly determined. A small gap between the contact surface and the lumen wall caused convective heat transfer by the small layer of blood flowing through this gap. Therefore, for optimal vulnerable plaque detection, it is necessary to ensure wall contact.

Temperatures measured with polyurethane catheters that were reported in literature were higher than those reported for nitinol catheters (Stefanadis 1999, Verhey 2002a, Schmermund 2003). Presence of a polyurethane catheter enhanced the temperature readings. This is due to its lower heat conductivity compared to that of blood, which makes it a very good choice for heat source detection, and thus for vulnerable plaque detection. The polyurethane catheter used for in vivo measurements has a diameter of about 1 mm (Stefanadis 1999), whereas the nitinol catheters that were used are of smaller diameter (Verhey 2002a, Diamantopoulos 2003b, Naghavi 2003). In our study, we have used the catheter with 1 mm diameter for the variation in catheter position. In figure 5.7 it can be seen that the results for nitinol catheter in presence of flow were more or less independent of catheter diameter. For smaller catheter diameters, the

$\Delta T_{sens}$  values of polyurethane catheter were higher both for flow and no flow conditions.

In this study a schematic representation of the artery and the catheter were used so that changes in temperature could be ascribed to changes in one specific parameter. In reality, vulnerable plaques are less homogenous and coronary arteries are not straight tubes. Also, when the heat source would appear more like a point source, the spatial resolution becomes more important. Both the pulsatility of the blood flow and the non-Newtonian viscosity of blood need further evaluation. The heat source production value used in this study resulted in temperature differences that approximate the values that have been reported in literature most recently. This value,  $5 \text{ mW mm}^{-3}$ , is higher than macrophage heat production values that have been reported in literature (Thóren 1990, Charlebois 2002). In addition, the catheter geometry was simplified, whereas in reality it can be more complex.

## 5.5 RECOMMENDATIONS FOR CATHETER DESIGN

Presence of a catheter in the lumen and its design influence the temperature measurements, and these effects cannot be neglected when interpreting in vivo temperature readings for vulnerable plaque detection.

To optimize vulnerable plaque detection by intracoronary thermography, one should take into account the aforementioned parameters. In addition, the choice for the thermosensitive device to be placed on the catheter should be made carefully. Enhancing temperature readings can be done by using an insulating material, ensuring full lumen wall contact and optimally positioning the sensor with respect to the heat source. Insulating materials can be used for the whole catheter, but also for coating catheters made from conductive materials. For optimal positioning of the catheter it is recommended to combine the thermographic system with an imaging device, or to optimize spatial sampling of the thermographic readings. Reducing convective heat transfer by occluding flow, preferably locally such that the patient will not suffer from it, will also contribute to more optimal vulnerable plaque detection.







## CHAPTER 6

# TEMPERATURE MEASUREMENT OF ADVANCED MURINE ATHEROSCLEROTIC PLAQUES

Obtaining a one-to-one relationship between macrophages and temperature was the objective of the study described in this chapter. Excised murine aortic arches, showing advanced atherosclerotic plaques, were studied with an infrared camera. Macrophage and lipid content of these aortas were obtained with histological staining, and these were matched to the observed temperature distributions. The results were described per mouse, per plaque and per histological cross-section. The results showed no clear, unambiguous relationship between macrophages and temperature increase. It was recommended that additional staining is performed to distinguish active macrophages from non-active ones.

## 6.1 INTRODUCTION

In the previous chapters, a number of studies are described in which parameters that possibly influence intracoronary thermographic measurements were identified and studied numerically. These studies have given us insights in how these different parameters, related to the vulnerable plaque and its thermographic detection, are of influence on the temperature distribution at the lumen wall and how these insights could be used to optimize thermographic detection methods and the measurements. The parameters that were studied include the blood flow through the lumen, the geometry and size of the heat source and its heat production value, the design of the catheter and the composition of the plaque. From the results described in the previous chapters, it could be concluded that knowledge of the parameters regarding the heat source, such as its location and its heat production, is of great importance in designing an intracoronary thermography system to enable optimal vulnerable plaque detection by thermographic means.

Casscells et al. have measured surface temperatures on excised human carotid arterial tissue at room temperature (Casscells 1996). Their plaques showed temperatures that varied reproducibly by 0.2 to 0.3°C, but 37% of their plaques had substantially warmer regions of 0.4 to 2.2°C. The thermal heterogeneity that was found after re-equilibration at 37°C was even greater and also reproducible. The temperatures correlated with cell density, and inversely with the distance of the cell clusters from the luminal surface. Most cells were macrophages, but a relation between increased temperatures and macrophages was not given. Infrared images, though not shown, were said to also reveal thermal heterogeneity.

Verheye et al. compared temperature pullbacks that were measured in rabbit aortas that had received a cholesterol-rich diet for 6 months with the pullbacks of rabbits that had received normal diet (Verheye 2002a). The temperature heterogeneity was markedly elevated and increased with plaque thickness. After 3 months of cholesterol lowering, plaque thickness remained unchanged, but temperature heterogeneity was significantly decreased. This paralleled plaque histology, which showed a marked loss of macrophages. Ex vivo experiments, performed at room temperature on 3 additional rabbits, demonstrated the positive relation between local temperature and local total macrophage mass.

Krams et al. have studied temperature pullbacks in rabbits presenting atherosclerotic plaques in vivo and compared selected hot and cold regions to histology (Krams 2005). The hot regions showed an average temperature of  $0.40 \pm 0.03^\circ\text{C}$  and the cold regions  $0.07 \pm 0.03^\circ\text{C}$ . Higher macrophage densities,

173%, and increased MMP-9 activity, 673%, were noted in the hot regions. A regression analysis revealed that MMP-9 predicted hot regions better than macrophages accumulation alone. No relationship was inferred between thermal heterogeneity and lipid content. Since the individual location of the four thermistors on the catheter that was used remained unknown, local temperatures could not be related to local macrophage nor MMP-9 content.

The previously discussed studies all imply that macrophages act as the heat source in a vulnerable plaque. A one-to-one relationship between macrophages and temperature increase has not yet been shown to exist, though. We hypothesize that macrophages produce enough heat to generate thermal heterogeneity at the lumen surface of advanced atherosclerotic plaques. In order to obtain a one-to-one relationship between temperature and macrophage content, we have studied excised aortic arches of apolipoprotein E deficient (ApoE -/-) mice, re-equilibrated at body temperature in an incubator. The aortas were imaged with an infrared (IR) camera, resulting to thermal maps of the surface of the aorta. The aortas showed plaques containing both macrophages and lipid-rich regions by histology, which were quantified. Matching of these data sets allows us to study the one-to-one relationship between macrophages and temperature.

## 6.2 METHODS

### 6.2.1 MICE

For the experiments, 7 male ApoE -/- mice, 30-34 weeks of age, were used. The last 9-11 weeks, the mice were fed a Western diet containing 15% (w/v) cocoa butter and 0.25 % (w/v) cholesterol (diet W, Hope Farms, Woerden, the Netherlands). The mice were euthanized by exposing them to an overdose of isofluorane, after which the vasculature was flushed using a MOPS solution (145 mM NaCl, 4.7 mM KCl, 2 mM CaCl<sub>2</sub>·2H<sub>2</sub>O, 1.17 mM MgSO<sub>4</sub>·7H<sub>2</sub>O, 1.2 mM NaH<sub>2</sub>PO<sub>4</sub>·H<sub>2</sub>O, 5 mM glucose-D, 2 mM pyruvate, 0.02 mM EDTA, 3 mM MOPS) heated to 37°C. The aortic arch was clipped above the renal sidebranch and removed, the tissue up to the adventitial layer surrounding the arch was removed, and the arch was clipped open at the outer curve. The aortic arch was pinned on to a silicone rubber pad. An illustration can be found in figure 6.1. On the silicone rubber pad, two rulers were placed which were also visible in the IR image. MOPS solution at 37.0°C was applied to the tissue to prevent dehydration. All experiments were performed in accordance with the institutional (Erasmus MC, Rotterdam, the Netherlands) and national guidelines.

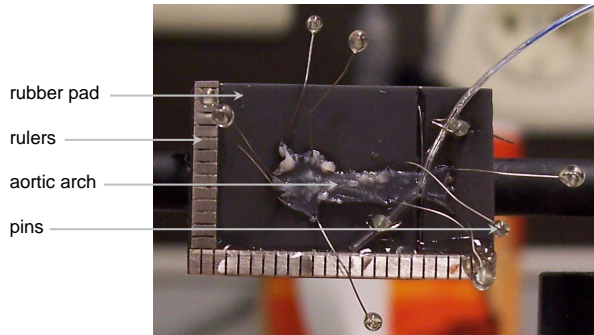


FIGURE 6.1: An aortic arch removed from an ApoE  $-/-$  mouse pinned onto a silicone pad. Scale of rulers is mm.

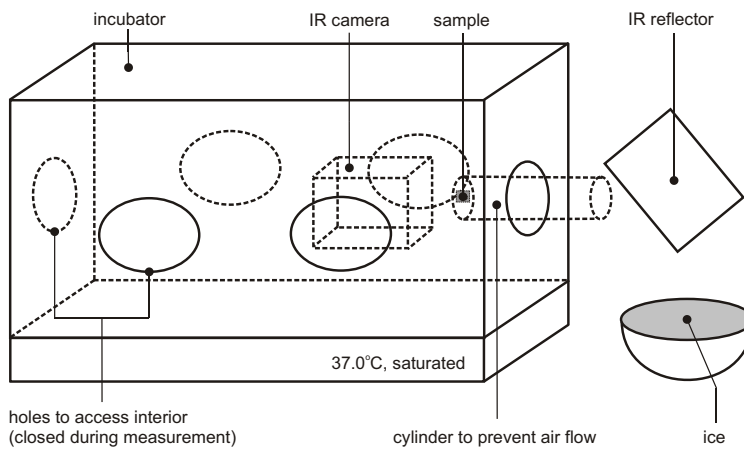


FIGURE 6.2: Schematic representation of experimental set-up, including an infrared camera located in an incubator.



FIGURE 6.3: Reference image, image from digital camera, with contours of aortic arch (purple) and plaque regions (yellow).

## 6.2.2 EXPERIMENTAL SET-UP AND PROTOCOL

A schematic of the experimental set-up can be found in figure 6.2. After the aortic arch was removed and pinned on to the rubber pad, a digital picture (Kodak, DX7630) was taken from the sample before it was placed in the experimental set-up in the incubator (Dräger, Incubator 8000 SC). The temperature of the incubator was fixed to  $37.0^{\circ}\text{C}$  and the relative humidity of the air in the incubator was nearly saturated. This enabled re-equilibration of the sample to body temperature and minimized the cooling effect of evaporation. The infrared camera (ThermaCAM®SC 3000, FLIR Systems AB, Sweden, thermal sensitivity  $0.02^{\circ}\text{C}$  at  $30^{\circ}\text{C}$ , thermal accuracy  $\pm 1\%$ , spatial resolution  $106\ \mu\text{m}$  using a close-up lens) was placed in the incubator and aligned with the sample. A uniform background temperature was realized by reflecting the infrared radiation of ice such that it fully surrounded the sample in the IR image.

After placing the sample in the experimental setup capturing the IR images was started at a rate of one per second. After the sample had reached thermal equilibrium, based on real-time evaluation of the IR images, at least 30 IR images were captured. IR images were captured up to the point at which point the sample was removed from the incubator. A ligature was then attached to the distal end of the sample. One of the sides was dyed (Davidson Marking System, Bradley Products, Bloomington MN, USA) so that it could be used as an orientation marker and the sample was embedded in TissueTek (Finetek Sakura, Zoeterwoude, the Netherlands) and snap-frozen in liquid nitrogen. The samples were stored at  $-80^{\circ}\text{C}$ .

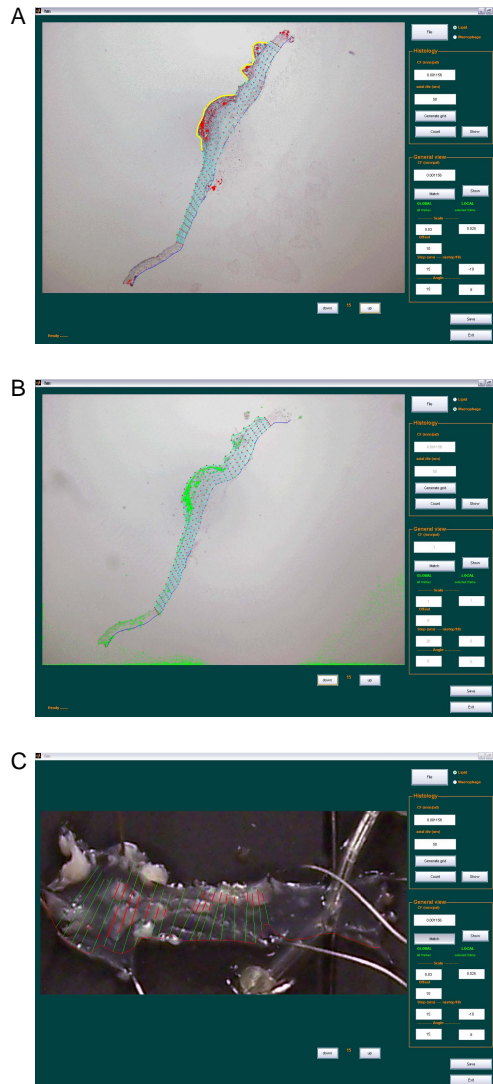


FIGURE 6.4: Snapshots of software developed in-house used for the matching procedure. A: histology cross-section showing lipid counts in red (yellow contours represent assigned plaque regions) and grid, B: histology cross-section showing macrophage counts in green and grid, C: matching of the lines resulting from histology cross-sections on to the reference image (red: plaque regions, green: non-plaque regions).

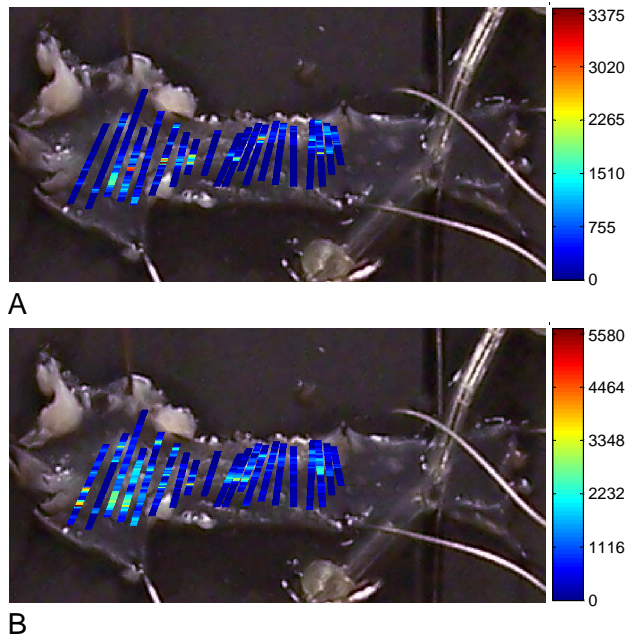


FIGURE 6.5: Reference images showing A: lipid counts and B: macrophage counts. Note that scales are in arbitrary units and differ between images.

### 6.2.3 HISTOLOGY

On the aortic arches, histologic staining was performed. Aortic arch cryosections of  $7\ \mu\text{m}$  at  $250\ \mu\text{m}$  intervals, sliced in axial direction, were mounted on Superfrostplus glass slides (Menzel-Gläser, Braunschweig, Germany). The sections were immunostained with anti-CD68 (1:200, rat antimouse, Serotec) for macrophage detection and Oil-Red-O for the identification of lipid depositions. The sections were counterstained using nuclear fast red and Mayer's hematoxylin, respectively. The stained cross-sections were captured digitally and analyzed with a microscope image analysis system (Clemex Vison PE, Clemex Technologies, Quebec, Canada).

### 6.2.4 ANALYSIS

The data that were obtained from the experiments with the IR camera had to be matched to the data obtained from histology in order to obtain a one-to-one relationship between macrophages and temperature measurement. The

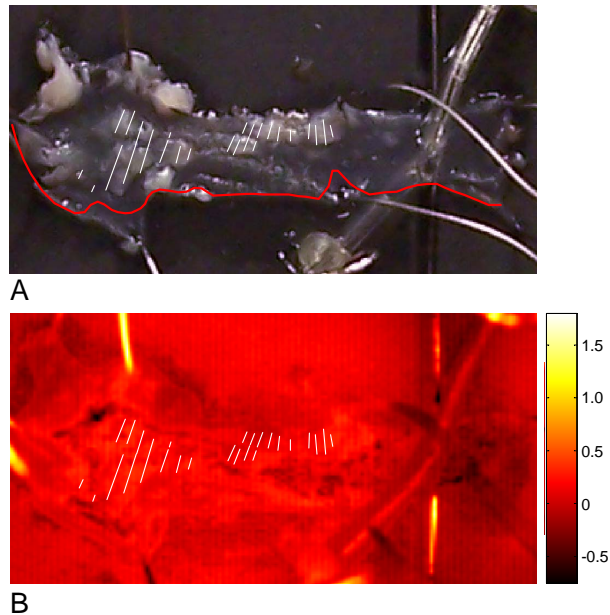


FIGURE 6.6: A: reference image in which the red line represents location of marker dye, B: temperature difference image. In both images, the white lines represent plaquelines at which histological information was available.

procedure that was followed for all mice is described in this section. Software that was used for this procedure was developed in-house and programmed in MATLAB (The MathWorks Inc., Natick MA, USA).

Since the images from the IR camera and the images showing the quantified histology results cannot be mapped directly on to each other, the former showing no landmarks such as fatty regions and the latter showing only a cross-section, the digital camera image was used as a reference image. In the digital camera image, contours were drawn, see figure 6.3, thereby selecting the aortic arch tissue and the plaque regions. The plaque regions were selected based on the lipid-rich, visible as white, tissue.

In the images showing the quantified histology results for the lipid staining, figure 6.4A, contours were drawn for the adventitial side of the section (blue), the luminal side of the section (green), and for the plaque region (yellow). The plaque regions were identified based on the lipid-rich, visible as red, staining. In these images, a grid was created. The resolution of this discretizing grid was  $50 \mu\text{m}$  in circumferential direction and in radial direction the thickness of



the tissue was divided into 5 sections. Using this grid, the spatial information on the histological counts could be retained and it also allowed separating the histological counts for plaque and non-plaque regions. In the images showing the quantified histology results for the macrophage staining, figure 6.4B, contours were also drawn for the adventitial side of the section (blue) and the luminal side of the section (green). Based on the lengths and the locations of these contours, the grid created in the images of the lipid histology was copied to the images of the macrophage histology. In this copy procedure, the grid was allowed to transform since the images were not identical.

These histological images were then mapped onto the reference image, the digital camera image, using the plaque contours that were drawn in the histology images for the lipid staining, figure 6.4C. The contours for the adventitial side of the lumen were stretched and laid on the digital camera image, their orientation based on the ligature and marker dye that was added to the sample after the IR camera experiments. The software allowed relocating the stretched contours by changing the position and angle, such that lipid regions denoted in the histology images coincided with the lipid regions seen in the digital camera image. In figure 6.4C image, the green parts of the lines represent the non-plaque regions of the adventitial contours, the red parts represent the plaque-regions. The histological results of this line were shown in figures 6.4A and B. The spatial coordinates of the results of the histological counts at the grid locations were then transformed to the spatial coordinates of the digital camera image. In figures 6.5A and B, the counts of the lipid staining and macrophage staining, respectively, are depicted on the digital camera image.

In order to match the IR camera images to the reference image, the digital camera image, they were studied to check when thermal equilibrium of the sample had been reached. Of the IR camera images after this time point, 16 consecutive images were exported and averaged using MATLAB, resulting to one mean image. The IR data was converted to temperatures assuming an emissivity of 0.95 (ThermaCAM Researcher 2000, FLIR Systems AB, Sweden). On this mean temperature image, a trend in temperature could clearly be visualized on the sections of the rubber pad that did not contain the aortic arch tissue. The temperature data at those sections were fitted with a plane. This plane, considered to be the background temperature, was subtracted from the mean temperature image, resulting to a temperature difference image. Studying the rubber pad with the IR camera outside the experimental set-up revealed no such trend in temperature. It could thus be attributed to factors related to the experimental set-up, and thus justified subtraction. On the resulting temperature difference image, points on the rulers that were both visible in the IR camera image and the digital camera image were assigned as

landmarks. Using the spatial coordinates of these landmarks, the temperature difference image was transformed to the digital camera image, such that the spatial coordinates of the landmarks, and thus also the other parts of the images, coincided.

In figure 6.6A an example of a digital camera image including the lines representing the plaque regions, based on the histology results, can be seen. The gray line represents the marker dye. In figure 6.6B, the matching IR image is given, also including the plaque lines. Using the data of these images, and those in figure 6.5, temperatures and macrophage counts can be matched.

The results, described in the next sections are stated as mean  $\pm$  SD, unless mentioned otherwise. Statistics were performed using the package SPSS 11.0 (SPSS Inc., Chicago IL, USA). To test the difference between averaged temperatures and differences between the 95th and 5th percentile of the temperature ranges, a paired t-test was used. Linear regression analysis was used to test whether slopes were different from zero. To test a positive sign of the relationship between macrophages and temperatures, the sign test was used. To test whether differences existed between results after categorization of macrophages, lipids and temperature in high and low, ANOVA was used. Results were considered to be statistically significant when  $p < 0.05$ .

## 6.3 RESULTS

### 6.3.1 GENERAL

The experiments were completed according to the protocol. The time between sacrifice of the mouse and the start of infrared imaging was  $28 \pm 8.0$  minutes. All mice showed one or more visibly lipid rich atherosclerotic lesions. The plaques were generally located at the inner curve of the aortic arch, but plaques could also be observed at bifurcations.

A total of 72 histological cross-sections were successfully matched and quantified. These cross-sections contained 89 plaque lines, the white lines as in the left panel of figure 6.6A. These plaque lines could be matched to 28 plaques by visual inspection of the matching results and the digital camera image.

### 6.3.2 TEMPERATURE

The average temperature difference for the plaque regions was  $0.21 \pm 0.26^\circ\text{C}$  and for the non-plaque region it was  $0.19 \pm 0.24^\circ\text{C}$  ( $p=0.09$ ). We observed that all plaque regions showed thermal heterogeneity. The difference between the 5th percentile and 95th percentile plaque temperature difference was 0.27

$\pm 0.04^{\circ}\text{C}$  for the plaque regions. Outside the plaque regions, the aortic arch also showed thermal heterogeneity. The difference between the 5th percentile and the 95th percentile temperature difference was  $0.37 \pm 0.07^{\circ}\text{C}$  for the non-plaque region ( $p=0.03$ ). This difference for the non-plaque regions was always higher than that for the plaque regions, though sometimes only slightly.

### 6.3.3 HISTOLOGY

Each cross-section was discretized and macrophages and lipid counts were obtained for each grid point. The total average macrophage count was on average 5 times higher for plaque regions than for non-plaque regions. The locations with high macrophage counts frequently colocalized with regions of high lipid count. The top layer, the two layers of the grid closest to the intimal side of the lumen, contained on average 83% of the total macrophage count (range 73-93%).

The plaques all contained lipid rich regions. This is not surprising, since the lipid rich regions were used to identify the plaque and for matching the histological results to the digital camera image. Some parts of the plaque regions, though, did not reveal high lipid counts.

### 6.3.4 TEMPERATURE VS. HISTOLOGY

**Per mouse** For all mice ( $n=7$ ), the relationship between macrophage counts and temperature differences at the plaque locations was studied using linear regression analysis. An example of this type of data set can be seen in figure 6.7, where the results are shown for the same mouse that was used to clarify the analysis in section 6.2.4, including the regression line. It was tested whether the slopes resulting from linear regression analysis differed from zero. Three of the seven slopes were negative ( $p=0.7$ ), of which two statistically significant. Four of the seven slopes were positive ( $p=0.7$ ), of which three statistically significant.

Linear regression analysis on the relationship between the macrophage counts in the top layer and the temperature differences was also performed. Of these slopes, three of the seven were negative ( $p=0.7$ ), of which one statistically significant. Four of the seven slopes were positive ( $p=0.7$ ), of which three statistically significant.

When comparing the statistical results of the slopes of the full macrophage counts and those of the top layer, the resulting p-values improved slightly. Two of the negative slopes had a higher p-value when only the top layer is considered, and one of the positive slopes had a lower p-value. Three of the p-values remained the same.

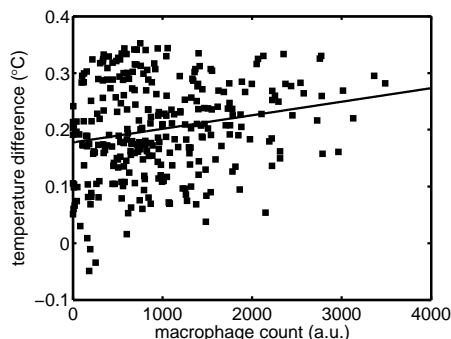


FIGURE 6.7: Example of analysis per mouse. Regression line shows the relationship between macrophage counts (on x-axis, in arbitrary units) and temperature difference (on y-axis).

**Per plaque** The data points as shown in figure 6.7 were grouped per plaque, based on visual inspection of the digital camera image and the matching results. An example of this division of the data set and the resulting slopes can be seen in figure 6.8. For all the plaques ( $n=28$ ), the slopes were calculated using linear regression analysis. Of the total of 28 slopes, 14 were positive ( $p=1.0$ ).

When only the macrophage counts in the top layer were considered and studied in this way, also 14 slopes were positive ( $p=1.0$ ).

**Per plaqueline** The data points were also considered per plaque line, of which an example can be seen in figure 6.9. These plaque lines coincide with the white lines in figure 6.6. For all the plaque lines ( $n=89$ ), the slopes were calculated using linear regression analysis. Of these slopes, 55 were positive ( $p=0.03$ ).

When only the top layer was considered, also 55 of the slopes, relating the macrophage counts in the top layer to the temperature, were positive ( $p=0.03$ ).

**Histology and temperature categorized** The relationship between macrophage counts and temperature differences could be influenced, either positively or negatively, by the presence of lipids. Positively when it is assumed that lipids are needed to stimulate the macrophages scavenging activities, thereby causing increased temperatures. Negatively when one assumes the lipids to act as an insulator, depending on the relative position

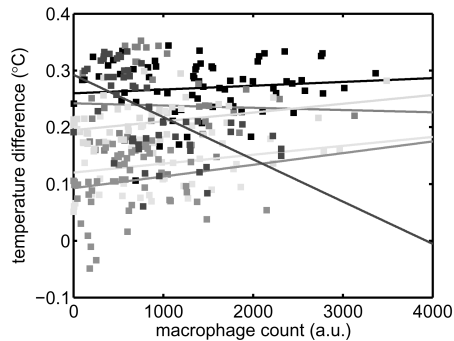


FIGURE 6.8: Example of analysis per plaque. Different shades of gray show different plaques. Regression lines show the relationships between macrophage counts (on x-axis, in arbitrary units) and temperature difference (on y-axis) for 6 plaques.

of macrophages, thereby diminishing the effect of the heat production by macrophages.

To study this influence the macrophage counts and the lipid counts on identical locations on the plaque lines were categorized into high and low. To see whether the presence of lipids influenced the results, the relationship between categorized macrophage counts and categorized temperature differences was compared to the relationship between both categorized macrophage and lipid counts and categorized temperature differences. The median values of the macrophage and lipid counts per mouse were used for this categorization into high and low. The temperature differences at these location, too, were categorized into high and low, also based on the median value.

In table 6.1 can be seen which percentage of data show a low and high temperature difference for low and high macrophage counts, only. For example for mouse 1, for low macrophage counts, thus macrophage counts below the median value, 41% of data show a low temperature difference, a temperature below the median temperature difference, and 59% show a high temperature. When the macrophage counts are higher than the median macrophage count, 57% of data show a low temperature difference and 43% a high temperature difference. A high macrophage count together with a high temperature difference, and a low macrophage count together with a low temperature difference value would suggest a positive relationship between macrophages and temperature difference.

In the last column, the sign of the relationship is given. When the p-value,

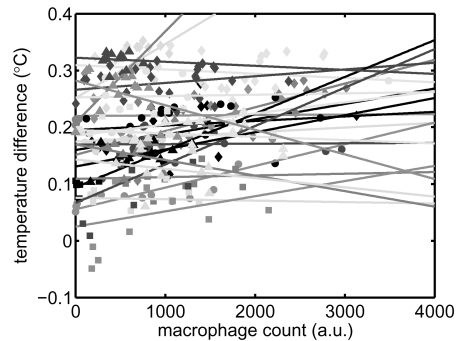


FIGURE 6.9: Example of analysis per plaqueline. Different shades of gray and different symbols show different plaquelines. Regression lines show the relationships between macrophage counts (on x-axis, in arbitrary units) and temperature difference (on y-axis) for 24 plaquelines.

resulting from a paired t-test, was  $<0.05$ , either positive or negative, the relationship was assigned + or -. When the p-value did not show a statistically significant relationship, it was assigned a 0. It was thus found that three of the seven relationships between macrophages and temperature difference were of positive sign and one negative. Three relationships were found to be statistically not significant.

The same was done for the data sets in which the macrophage and lipid counts on the plaque lines are combined. In table 6.2 these results are given. In these columns the percentages are given that show a low or high temperature difference when both macrophage and lipid counts are either low or high. For example, for mouse 1, when both macrophage and lipid counts are low, below their respective median values, 23% of the data points show a temperature difference lower than the median value and 77% show a higher temperature difference. When both macrophage and lipid counts are higher than their respective median values, 55% of the data show a temperature difference lower than the median value and 45% show a higher temperature difference.

The last column in this table also shows the sign of the relationship. Like in the previous table, the sign is + or - when the p-value showed a statistically significant relationship, and 0 when that was not the case. For the combined categorized data analysis, four relationships showed statistical significance, of which two were positive. Three relationships did not show statistical significance.

TABLE 6.1: Percentages of categorized macrophage data, high/low, that show high/low categorized temperature differences. First column: mouse number. Sixth column: p-value. Last column: sign of relationship when  $p < 0.05$ .

Mouse no.	Macrophages low		Macrophages high		p	+ / 0 / -
	T low	T high	T low	T high		
1	41	59	57	43	0.12	0
2	59	41	41	59	0.001	+
3	35	65	65	35	<0.001	-
4	66	34	35	65	0.01	+
5	58	42	42	58	0.01	+
6	57	43	36	64	0.42	0
7	45	55	55	45	0.23	0

TABLE 6.2: Percentages of categorized macrophage and lipid data, high/low, that show high/low categorized temperature differences. First column: mouse number. Sixth column: p-value. Last column: sign of relationship when  $p < 0.05$ .

Mouse no.	Macrophages and lipids low		Macrophages and lipids high		p	+ / 0 / -
	T low	T high	T low	T high		
1	23	77	55	45	0.01	-
2	62	38	37	63	0.001	+
3	35	65	63	37	0.001	-
4	73	27	33	67	<0.001	+
5	55	45	43	57	0.14	0
6	60	40	50	50	0.75	0
7	56	44	51	49	0.61	0

## 6.4 DISCUSSION

The results of studying thermal heterogeneity on excised murine aortic arches with an infrared camera, in order to obtain a one-to-one relationship between macrophages and temperature, were described in this chapter.

For a number of cases, our results showed a clear, positive, and, depending on how the data was evaluated statistically significant, relationship between macrophage counts and temperature difference. When considering all data points per mouse, 3 mice (43%) showed a positive, statistically significant relationship between macrophage counts and temperature difference. When considering these data points per plaque, 14 plaques (50%) showed a positive relationship. When considering the data per plaque line, 55 plaque lines showed a positive relationship (62%).

The presence of only high macrophage counts could not explain the observed thermal heterogeneity. Some locations with a high macrophage count did show increased temperature differences, while others did not. Furthermore, higher temperature differences were observed at locations showing low macrophage counts. The positive relationship between temperatures and macrophage content found by others (Casscells 1996, Verheye 2002a, Krams 2005) could not be affirmed by our data. Our findings could imply that not all macrophages present in a plaque contribute to increased temperatures, which may have to do with macrophages being in an active state or not. To distinguish between active macrophages and non-active macrophages, an enzymatic staining could be introduced. In this way, active macrophages and their locations could be identified, and a relationship between active macrophages and temperature could be established.

The relationship between categorized macrophage data and temperature differences showed 3 positive, statistically significant relationships. When combining categorized macrophage and lipid data, the number of positive, statistically significant relationships reduced to 2, and one relationship that was not statistically significant became negative. This might indicate that lipids, needed to stimulate the scavenging activity by macrophages, act as an insulator. This effect was also described in chapter 4. To ascertain this effect, more experiments are needed.

Thermal heterogeneity could be observed for all the mice that were studied. This heterogeneity did not exist only in the plaque regions, but also in regions of the aortic arch outside the plaque. Thermal heterogeneity is caused by differences in heat production and differences in cooling rates, both related to tissue composition. Different cell types might show different heat production values. Since in this study thermal equilibrium was assured before images



were selected, differences in cooling rates could be excluded. Plaques are commonly known to show differences in tissue composition depending on the location within the plaque (van der Wal 1994), which could explain the thermal heterogeneity within the plaque. Thermal heterogeneity outside the plaque could imply that also at those locations differences exist in tissue composition, resulting to differences in heat production, and thus explaining the thermal heterogeneity at these locations.

The observation that not all plaques show equal thermal heterogeneity was previously found by others. Cascells et al in their study on excised human carotid arteries found that only 37% of the plaques had substantial warmer regions (Cascells 1996). Thermal heterogeneity of plaques measured in vivo in coronary arteries was present only in 20, 40 and 67% of patients suffering from stable angina, unstable angina and acute myocardial infarction, respectively (Stefanadis 1999).

Using an IR camera, only the IR radiation emitted by the top layer of the tissue to be studied is imaged. Focal heat sources lying deeper within the tissue cannot be seen unless the produced heat results to a focal hot-spot on the top layer. Heat production of this top layer, resulting in temperature differences on the surface, should be detectable using an IR camera when it results in temperature differences that are larger than the accuracy of the camera. The results that were found for macrophage counts in the top layer were identical to the results that were found for the whole grid. This can be explained by the fact that most of the macrophage count was located in the top layer.

One of the difficulties in interpreting the data from an IR measurement is the influence of the emissivity of the material. The emissivity value represents how well a body irradiates IR radiation compared to a black body, of which the emissivity is 1. The human body approximates this value rather well, having an emissivity of 0.95. In our study we have assumed equal emissivity values for both the plaque and the non-plaque regions, thereby not discriminating between lipid-rich and lipid-poor tissue. Including emissivity differences, however small, between lipid-rich and lipid-poor tissue might influence the results.

The quantification of the histology results is of a qualitative approach, based on visual inspection of the histology images. Exact nor approximate cell counts were possible using this way of analysis, thus making it impossible to estimate heat production values of macrophages. Macrophage and lipid counts between mice could not be compared, since their histology was performed in different batches. Plaques were assigned based only on increased lipid counts, assuming lipid to be an exclusive prerequisite for presence of plaque. In addition, the matching procedure also is of a qualitative nature,

based on visual inspection of the digital camera image. The way the histology quantification and the matching were performed could influence the results found describing the relationship between macrophages and temperature. To prevent the influence of matching, a consensus meeting with four observers was organized. Nevertheless, when performed by other observers, differences in quantification of the histology images and differences in the matching might occur.

The time between the excision of the aortic arch and the IR measurement was on average 28 minutes, which is longer than the 15 minutes that Casscells et al have used (Casscells 1996). Even though dehydration and dying of the tissue was prevented by applying MOPS buffer, we cannot be certain that the cells were still metabolically active. To check whether cells were still alive and active, vital stains and staining for e.g. MMP's could be applied.

## **6.5 CONCLUSIONS AND RECOMMENDATIONS**

From our results we can conclude that sometimes there exists a positive relationship between macrophage content and increased temperature difference. In our experiments, we have used only 7 mice, which might not have been enough. More experiments are needed, thereby including the remarks that were made in the previous section. These include an additional staining to discriminate between active and non-active macrophages, somehow overcome the qualitative nature of the histology quantification and reduce the time between excision and IR imaging.

## **6.6 ACKNOWLEDGEMENTS**

The infrared camera used in this study was borrowed from the department of Mechatronics, biostatistics and sensors (MeBioS) of the University of Leuven. Support during the measurements was generously provided by Cédric Bravo, Jeroen De Temmerman, Carmen Wallays and Philippe Billet. Rob Krams, Rini de Crom, Caroline Cheng, Dennie Tempel and Dolf Segers provided the mice and histology. Hans Schuurbiens wrote the software that allowed matching of the histology to the digital camera images. Miranda Harteveld, Jan Honkoop and Wim van Alphen are acknowledged for their substantial technical support.



## CHAPTER 7

# CONCLUSIONS: HEAT GENERATION, TRANSFER AND DETECTION

In this chapter, the results from the previous chapters are summarized and discussed. The parameters that are discussed are divided into parameters regarding heat generation, heat transfer and heat detection. The main issue to be addressed is whether intracoronary thermography can be used for vulnerable plaque detection. The parameters regarding the heat generation include the dimensions of the heat source, the heat production and the location of the heat source. Heat transfer is influenced by the flow of blood through the lumen and the location of the heat source regarding the lipid pool. Catheter design is discussed as main parameters involved in heat detection. From this discussion, conclusions and a future perspective are given.

## 7.1 INTRODUCTION

The studies reported in this thesis were performed to answer the central question: can intracoronary thermography be used for vulnerable plaque detection? To answer this question, we have identified parameters that influence intracoronary thermography measurements, and have studied to what extent they do so. The parameters that we have studied and discussed were identified in chapter 2, in which we combined a review of existing publications on intracoronary thermography with related biological and physical aspects. These parameters were studied, and the results of these studies are described in chapters 3 through 6. In this final chapter we will summarize the results from these chapters and discuss them regarding the aspects of heat generation, heat transfer and heat detection. Finally, we will conclude with a future perspective for intracoronary thermography.

## 7.2 SUMMARY

The results of parameter studies described in chapters 3 through 5, have been obtained using computational fluid dynamics. In these studies, we used a schematic representation of a coronary artery in which we embedded a plaque containing a heat source. We solved the heat and flow equations on the geometrical model by applying the finite element method.

In chapter 3 both the the geometry of the heat source and the influence of blood flow on the temperature distribution at the lumen wall were discussed. The maximal temperature differences at the lumen wall increased when the heat source volume increased. These maximal temperature differences varied for different heat source geometries, being highest for circumferentially extended heat sources and heat sources extended in the direction of blood flow. The blood flow was shown to act as a coolant to the lumen wall, and its influence differed for different heat source geometries. This influence was highest for circumferentially extended heat sources and lowest when the heat source was extended in the direction of blood flow. When the cap thickness increased, the maximal lumen wall temperatures decreased and the influence of flow increased.

The results discussed in chapter 4 related to the influence of plaque composition on the temperature distribution at the lumen wall. These results showed the heat source location to be the main determinant of the shape of the lumen wall temperature distribution. The impact of the location of the heat source was most notable when the heat source was located in the shoulder region of the plaque, leading to focal spots of higher temperature. It was shown that

the maximal lumen wall temperature was mainly determined by the heat production of the heat source and the cooling effect of blood flow. The insulating properties of the lipid core increased lumen wall temperatures when the heat source was located in the cap and the presence of vasa vasorum lowered these temperatures.

Chapter 5 dealt with the influence of the presence and design of an intracoronary thermography catheter. Presence of a polyurethane catheter, an insulating material, contacting the lumen wall at the heat source location increased temperatures, whereas a nitinol catheter, a conducting material, decreased the temperatures. The location at which a thermosensitive element should be placed on the intracoronary catheter for maximal temperature readings during a pullback differed for these two catheters. It was shown to lie at the catheter edge for the nitinol catheter and at a certain distance from the edge for the polyurethane catheter. The temperature readings reduced to background temperatures when the catheter was in close proximity but not overlapping the plaque. It also reduced to nearly background temperatures when a gap existed between the catheter and the lumen wall. Occlusion of the vessel increased temperatures, but most pronounced for the nitinol catheter.

From the results in the studies mentioned above, it was clear that more information on the heat production in vulnerable plaque is necessary. Therefore, we have performed experiments in a first attempt to identify the heat source in advanced, atherosclerotic plaques. In previous studies it was concluded that macrophages act as the heat source causing the increased temperatures in vulnerable plaques (Casscells 1996, Verheye 2002a, Krams 2005), yet a one-to-one relationship between temperature and macrophages has not yet been established. Having such a relationship, one could draw conclusions on the heat production of macrophage cells in vulnerable plaques. In chapter 6 we have tested this hypothesis and have matched macrophage counts from histology to temperature measurements with an infrared camera on a one-to-one basis. This matching showed no evident relationship between macrophages and temperature differences, though it was present and statistically significant in some of the mice, plaques and histological cross-sections that were studied. This could imply that macrophages only sometimes act as the heat source in a vulnerable plaque. Due to the way of quantification of the histologic results it was not possible to relate heat generation by macrophages to resulting temperatures, and thus to heat production values.

## 7.3 DISCUSSION

The vulnerable plaque is a developmental stage in atherosclerosis, which is known to be a disease with an important inflammatory component (Libby 2002). Inflammation is associated with increased temperatures (Rocha e Silva 1978), so vulnerable plaque could possibly be detected with thermographic methods. Thermal heterogeneity in vulnerable plaques was shown to exist (Casscells 1996), and thus the promising possibility of vulnerable plaque detection using thermographic methods.

### 7.3.1 HEAT GENERATION

Regarding the heat generation, a number of aspects influence the lumen wall temperature increase. These include the geometry of the heat source, the location of the heat source and the amount of heat that is produced. Translating these aspects to vulnerable plaque detection, this signifies that the dimensions of the plaque, the cap thickness and the metabolic cell activity, or the amount of heat generated by certain chemical processes in the vulnerable plaque, are of importance.

In chapter 6 we have studied the thermal profile of advanced atherosclerotic plaques of mice, using an infrared camera. This camera detects the radiation emitted by the tissue. When the mice were studied individually, we observed that some mice did and some did not show a relationship between macrophages and increased temperature. The same holds when the plaques were studied. This could imply that if we assume that macrophages are the heat producing elements, some macrophages do generate heat and some do not. The combination of macrophage content with lipid content did not lead to a relationship between regions of high macrophage content and high lipid content with increased temperature. This might indicate that scavenging of lipid might not be an incentive for macrophages to produce heat.

Maximal lumen wall temperatures increase with heat source volume. The larger the plaque, the higher the temperatures. When plaques were larger in the circumferential dimension or in the direction of the blood flow, this resulted to higher lumen wall temperatures than for plaques of equal volume extended into the lumen wall. Heat produced at locations further away from the lumen, will be of lower influence on the lumen wall temperature than heat produced closer to the lumen wall. This is also the reason for the decreasing lumen wall temperature with increasing cap thickness. The shape of the lumen wall temperature distribution is mainly determined by the shape of the heat source. When the heat source is located in the shoulder region of the plaque, this will result to a temperature profile resembling the shape of the plaque's shoulder

region. The lumen wall temperatures are mainly determined by the amount of heat that is produced by the heat source, and its volume.

The processes by which heat is generated in the vulnerable plaques, and the location at which it is generated, are unknown. From literature we know that certain plaque components, like macrophages, can produce heat above basal metabolic levels. Macrophages, though not those associated with vulnerable plaques, produce around 20 pW per cell at basal metabolic level (Thóren 1990), but this amount can increase up to 92 pW per cell (Charlebois 2002). In addition, certain processes that take place in vulnerable plaques, like extracellular matrix breakdown and the cholesterol ester cycle, might be exothermal and contribute to vulnerable plaque heat generation.

A human body of 75 kg produces around 100 W of heat when moderately active. This results to a heat production of  $1.3 \text{ kW m}^{-3}$ . This body of  $0.075 \text{ m}^3$  fits  $7.5 \times 10^{13}$  cells of  $10 \times 10 \times 10 \text{ }\mu\text{m}^3$ . When all these cells are considered to have a basal metabolic level of 20 pW, this results to a heat production of  $1.5 \text{ kW m}^{-3}$ , closely resembling the  $1.3 \text{ kW m}^{-3}$  obtained before. So, normal body core temperatures exist when cells produce 20 pW on average. This implies that, when macrophages indeed act as the heat source in a vulnerable plaque, their heat production must be higher than this basal metabolic level of 20 pW per cell, which would result to a mere body core temperatures. Macrophages occupy only  $14 \pm 10 \%$  of the TCFA's cross section (Kolodgie 2004), which implies that macrophages need not only produce more heat than at basal metabolic level to be thermally detectable, but much more.

For the numerical simulations we have performed, we adjusted the heat production values such that the lumen wall temperatures coincided with those that were reported in literature. We have used heat production values of  $5 \text{ mW mm}^{-3}$  (equal to  $5 \text{ MW m}^3$ ) to obtain lumen wall temperatures of around  $0.2^\circ\text{C}$ . When assuming a cell volume of  $10 \times 10 \times 10 \text{ }\mu\text{m}^3$ , this results to a heat production of 5 nW per cell, which is 250 times higher than the heat production of macrophages at basal metabolic level found in literature (Thóren 1990), but only 50 times higher than those found for metabolically active macrophages (Charlebois 2002). The results of our infrared study on excised murine aortic arches, described in chapter 6, could not be used to verify these values.

### 7.3.2 HEAT TRANSFER

Since the intracoronary thermography techniques that are currently employed rely on registration of temperatures at the lumen wall, it is necessary to know how heat is transferred from the source to the lumen wall. Heat can be transferred by conduction, convection and by a combination of radiation and ab-

sorption. Conduction is the transfer of heat through a medium due to a temperature gradient by the exchange of molecular kinetic energy during collisions of molecules. Transfer by convection requires a moving medium, such as blood. Radiation and absorption involve the transfer of energy by electromagnetic waves, which every object irradiates.

Regarding the results on heat transfer by convection, we found that flow past the lumen wall influences the lumen wall temperatures. The influence of flow is represented by the flow influence factor (FIF), as was defined in chapter 3. This factor increases with increasing flow, and is highest for plaques with a large circumferential dimension. Its value is lowest for plaques that are extended in the direction of the blood flow. The blood can transfer heat only from the plaque in case of a circumferentially extended plaque, whereas it can transfer the heat back to the plaque in case of a plaque extended in the direction of the flow. When the cap thickness increases, the influence of the blood flow, and thus the amount of convection, increases. This appears counter-intuitive, since the heat source is removed further away from the blood flow. The FIF, though, combines the influence of both the location at which the heat is generated and the blood flow on the lumen wall. Increasing FIF values with increasing cap thickness thus signifies that the blood flow is of increasing influence when the plaque is thermally less connected to the lumen wall. From the results by others, FIF values between 1.4 and 8.4 can be calculated, which are well within the range we have found (Stefanadis 2003b, Verheye 2004).

Results on conduction showed us that lumen wall temperatures differ when heat is produced in front of a lipid-rich core compared to when it is produced behind it. Heat produced in front of the core results to higher lumen wall temperatures than when it is produced behind the core. The higher the lipid-richness of the core, the stronger its insulating properties, and thus its influence on the heat transfer. The categorized results from chapter 6 showed that when lipid counts were included in the analysis, the number of positive relationships between macrophage counts and temperature differences decreased, though slightly, which might indeed confirm our numerical results.

### 7.3.3 HEAT DETECTION

If the heat is generated in a plaque, at a level higher than the basal metabolic level, and transferred to the lumen wall, an increased lumen wall temperature will result. Lumen wall temperatures are currently measured with catheters in which an electrical thermosensitive elements, like a thermistor or a thermocouple, is embedded (Stefanadis 1999, Verheye 2002a, Naghavi 2003). These elements are embedded into either a conductive material like nitinol (Naghavi



2003, Verheye 2002a) or an insulating material like polyurethane (Stefanadis 1999). All the currently applied methods require contact between the lumen wall and the thermosensitive element.

Use of an insulating catheter material, like polyurethane, was shown to optimize vulnerable plaque detection. The insulating properties will prevent heat transfer opposed to the thermal properties of a conductive material. The latter causes heat transfer through the catheter, which will be left undetected by the thermosensitive element. Intracoronary thermography catheters should therefore preferentially be made of insulating materials.

Stopping the flow, either by occlusion of the whole vessel or locally by covering the plaque, will contribute to optimal temperature measurement, since heat transfer by convection is prevented. Only a small gap between the lumen wall and the contact surface of the thermography catheter will cause the temperatures to decrease to background values, due to convection by the blood flow, so either full contact between the catheter and the lumen wall or vessel occlusion needs to be assured during the measurement.

Not only the radial location of the catheter is of influence on the temperature measurement. The results from chapter 5 showed the importance of determining the location of the spot at which thermographic measurements should be performed. This should be as near to the vulnerable plaque heat source as possible. To ensure this, one needs to increase the spatial resolution of the measurement as high as possible.

Heat can be generated by very small heat sources, like cell clusters. This results to small spots of high temperature, which require a high spatial sampling of the lumen wall by intracoronary catheters. The currently used catheters sample the lumen wall at one (Stefanadis 1999), four (Verheye 2002a) or five (Naghavi 2003) locations, which leaves large parts of the lumen wall undetected. This implies that vulnerable plaques with focal heat sources might be left undetected with these catheters.

From the results discussed in the previous chapters, it could be concluded that many parameters influence the lumen wall temperature and that there exists no direct relationship between vulnerable plaque heat generation and lumen wall temperature. The influence of blood flow, cap thickness, lipid-density of the lipid core and the presence of vasa vasorum influence the lumen wall temperatures such that relationship cannot be established without information on all of these parameters. Therefore, intracoronary temperature detection needs to be combined with an imaging modality and flow measurements, to obtain information on all these parameters. This combination of techniques could then determine the presence of a vulnerable plaque and its components. Thermographic measurements could then be performed to determine its in-

flammatory state by interpreting the thermographic measurements within this framework of known parameters.

## 7.4 CONCLUSIONS AND FUTURE PERSPECTIVE

The central question in this thesis is whether intracoronary thermography can be used as a vulnerable plaque detection technique. To answer this question correctly and completely, we need to have information on the heat generation, the heat transfer and the heat detection. A number of studies were performed to obtain this information, but despite the extensive research described in this thesis, there are still a number of unanswered key questions.

Regarding the generation of heat, it is still unknown what causes the increased heat production. Some options were given in chapter 2, including the lipid scavenging activities of macrophages and the possibly exothermal processes involved in the breakdown of the extracellular matrix. One of the ways to find out what causes increased heat production is to harvest vulnerable plaques and subsequently isolate different components. These can then be studied with e.g. microcalorimetric methods to obtain information about the heat production.

In the previous section, some recommendations were made with respect to the design of intracoronary catheters. These include combining them with an imaging modality, occluding blood flow during their measurement and the necessity of having a high spatial sampling. The only currently available imaging modality that can provide the necessary additional information, such as cap thickness and presence of lipid core, is optical coherence tomography. Besides the currently applied electrical thermosensitive sensors, other ways to measure temperature exist, which options have not been explored yet. These are e.g. the use of liquid crystals, the use of quartz crystals and temperature dependent fluorescence.

The results in this thesis have provided answers to a number of questions but have also raised questions that need to be answered before a final conclusion on the usefulness of intracoronary thermography for vulnerable plaque detection can be drawn. A conclusive answer to the question whether intracoronary thermography can be applied for vulnerable plaque detection cannot be given yet. Interpretation of intracoronary thermography measurements requires knowledge of the object of measurement, in this case knowledge on what processes cause increased temperatures in a vulnerable plaque. To obtain a relationship between temperature and plaque vulnerability, we need to find out how to measure lumen wall temperatures, leaving no room for doubt when it comes to interpretation of these measurements.



## REFERENCES

(Alberts 1989) Alberts B, Bray D, Lewis J, Raff M, Roberts K, Watson JD. Molecular biology of the cell. New York, NY: Garland Publishing, Inc., 1989.

(Ashforth 1996) Ashforth-Frost S. Quantitative thermal imaging using liquid crystals. *Journal of Biomedical Optics* 1996;1:18-27.

(Bjornheden 1987) Bjornheden T, Bondjers G. Oxygen consumption in aortic tissue from rabbits with diet-induced atherosclerosis. *Arteriosclerosis* 1987;7:238-47.

(Brown 1980) Brown MS, Ho YK, Goldstein JL. The cholesteryl ester cycle in macrophage foam cells. Continual hydrolysis and re-esterification of cytoplasmic cholesteryl esters. *J Biol Chem* 1980;255:9344-52.

(Burke 1997) Burke AP, Farb A, Malcom GT, Liang Y, Smialek J, Virmani R. Coronary risk factors and plaque morphology in men with coronary disease who died suddenly. *N Eng J Med* 1997;336:1276-82.

(Casscells 1996) Casscells W, Hathorn B, David M, Krabach T, Vaughn WK, McAllister HA, Bearman G, Willerson JT. Thermal detection of cellular infiltrates in living atherosclerotic plaques: possible implications for plaque rupture and thrombosis. *Lancet* 1996;347:1447-9.

(Charlebois 2002) Charlebois SJ, Daniels AU, Smith RA. Metabolic heat

production as a measure of macrophage response to particles from orthopedic implant materials. *J Biomed Mater Res* 2002;59:166-75.

(Courtney 2004) Courtney BK, Nakamura M, Tsugita R, Lilly R, Basisht R, Grube E, Honda Y, Yock PG, Fitzgerald PJ. Validation of a thermographic guidewire for endoluminal mapping of atherosclerotic disease: an in vitro study. *Catheter Cardiovasc Interv* 2004;62:221-9.

(Craciunescu 2001) Craciunescu OI, Clegg ST. Pulsatile blood flow effects on temperature distribution and heat transfer in rigid vessels. *J Biomech Eng* 2001;123:500-5.

(Davies 2005) Davies JR, Rudd JF, Fryer TD, Weissberg PL. Targeting the vulnerable plaque: the evolving role of nuclear imaging. *J Nucl Cardiol*;12:234-46.

(Diamantopoulos 2003a) Diamantopoulos L, Liu X, De Scheerder I, Krams R, Li S, Van Cleemput J, Desmet W, Serruys PW. The effect of reduced blood-flow- on the coronary wall temperature: are significant lesions suitable for intravascular thermography? *Eur Heart J* 2003;24:1788-95.

(Diamantopoulos 2003b) Diamantopoulos L. Arterial wall thermography. *J Interv Cardiol* 2003;16:261-6.

(Doriot 2000) Doriot PA, Dorsaz PA, Dorsaz L, De Benedette E, Chate-lain P, Delafontaine P. In-vivo measurement of wall shear stress in human coronary arteries. *Coron Artery Dis* 2000;11:495-502.

(Duck 1990) Duck FA. Physical properties of tissue: a comprehensive reference book. San Diego, CA: Academic Press Limited, 1990.

(Falk 1995) Falk E, Shah PK, Fuster V. Coronary plaque disruption. *Cir-culation* 1995;92:657-71.

(Fayad 2000) Fayad ZA, Fuster V, Fallon JT, Jayasundera T, Worthley SG, Helft G, Aguinaldo JG, Badimon JJ, Sharma SK. Noninvasive in vivo human coronary artery lumen and wall imaging using black-blood magnetic resonance imaging. *Circulation* 2000;102:506-10.

(Ferencik 2006) Ferencik M, Nieman K, Achenbach S. Noncalcified and calcified coronary plaque detection by contrast-enhanced multi-detector

computed tomography: a study of interobserver agreement. *J Am Coll Card* 2006;47:207-9.

(Grattan 1995) Grattan KTV, Zhang ZY. *Fiber optic fluorescence thermometry*. London: Chapman & Hall, 1995.

(ten Have 2004) ten Have AG, Gijssen FJ, Wentzel JJ, Slager CJ, van der Steen AF. Temperature distribution in atherosclerotic coronary arteries: influence of plaque geometry and flow (a numerical study). *Phys Med Biol* 2004;49:4447-62.

(ten Have 2005) ten Have AG, Gijssen FJH, Wentzel JJ, Slager CJ, Serruys PW, van der Steen AFW. Intracoronary thermography: heat generation, transfer and detection. *EuroIntervention* 2005;1:105-14.

(ten Have 2006) ten Have AG, Draaijers EBGT, Gijssen FJH, Wentzel JJ, Slager CJ, Serruys PW, van der Steen AFW. Influence of catheter design on lumen wall temperature distribution in intracoronary thermography. *Journal of Biomechanics* 2006 (accepted for publication).

(Jang 2005) Jang IK, Tearney GJ, MacNeill B, Takano M, Moselewski F, Iftima N, Shishkov M, Houser S, Aretz HT, Halpern EF, Bouma BE. In vivo characterization of coronary atherosclerotic plaque by use of optical coherence tomography. *Circulation* 2005;111:1551-5.

(Kockx 2000) Kockx MM, Middelheim A, Knaapen MWM, Martinet W, De Meyer GRY, Verheye S, Herman AG. Expression of the uncoupling protein UCP-2 in macrophages of unstable human atherosclerotic plaques. *Circulation* 2000;102:12.

(Kolodgie 2004) Kolodgie FD, Virmani R, Burke AP, Farb A, Weber DK, Kutys R, Finn AV, Gold HK. Pathologic assessment of the vulnerable human coronary plaque. *Heart* 2004;90:1385-91.

(Krams 2005) Krams R, Verheye S, van Damme LCA, Tempel D, Mousavi Gourabi B, Boersma E, Kockx MM, Knaapen MWM, Strijder C, van Langenhove G, Pasterkamp G, van der Steen AFW, Serruys PW. In vivo temperature heterogeneity is associated with plaque regions of increased MMP-9 activity. *Eur Heart J* 2005;26:2200-5.

(Langheinrich 2006) Langheinrich AC, Michniewicz A, Sedding DG, Walker G, Beighley PE, Rau WS, Bohle RM, Ritman EL. Correlation of vasa vasorum neovascularization and plaque progression in aortas of apolipoprotein E(-/-)/low-density lipoprotein(-/-) double knockout mice. *Arterioscler Thromb Vasc Biol* 2006;26:347-52.

(Leber 2006) Leber AW, Becker A, Knez A, von Ziegler F, Sirol M, Nikolaou K, Ohnesorge B, Fayad ZA, Becker CR, Reiser M, Steinbeck G, Boekstegers P. Accuracy of 64-slice computed tomography to classify and quantify plaque volumes in the proximal coronary system. *J Am Coll Card* 2006;47:672-7.

(Lendon 1991) Lendon CL, Davies MJ, Born GVR, Richardson PD. Atherosclerotic plaque caps are locally weakened when macrophages density is increased. *Atherosclerosis* 1991;87:87-90.

(Libby 2002) Libby P. Inflammation in atherosclerosis. *Nature* 2002;420:868-74.

(Loike 1981) Loike JD, Silverstein SC, Sturtevant JM. Application of differential scanning microcalorimetry to the study of cellular processes: heat production and glucose oxidation of murine macrophages. *Proc Natl Acad Sci USA* 1981;78:5958-62.

(Lupotti 2003) Lupotti FA, Mastik F, Carlier SG, de Korte CL, van der Giessen WJ, Serruys PW, van der Steen AF. Quantitative IVUS blood flow: validation in vitro, in animals and in patients. *Ultrasound Med Biol* 2003;29:507-15.

(Mackay 2004) Mackay J, Mensah G. The atlas of heart disease and stroke. Geneva: World Health Organization, 2004.

(MacNeill 2004) MacNeill BD, Jang IK, Bouma BE, Iftimia N, Takano M, Yabushita H, Shishkov M, Kauffman CR, Houser SL, Artz HT, DeJoseph D, Halpern ER, Tearney GJ. Focal and multi-focal plaque macrophage distributions in patients with acute and stable presentations of coronary artery disease. *J Am Coll Cardiol* 2004;44:972-9.

(Madjid 2002) Madjid M, Naghavi M, Malik BA, Litovsky S, Willerson JT, Casscells W. Thermal detection of vulnerable plaque. *Am J Cardiol* 2002;90:36L39L.

(Madjid 2004) Madjid M, Zarrabi A, Litovsky S, Willerson JT, Casscells

W. Finding vulnerable atherosclerotic plaques: is it worth the effort? *Arterioscler Thromb Vasc Biol* 2004;24:1775-82.

(Matsui 2001a) Matsui T, Arai T, Sato S, Suzuki M, Ishizuka T, Kikuchi M, Kurita A. Determining the temperature distribution of a model vessel wall under pulsed laser irradiation: an experimental attempt to measure fibrous cap thickness and detect temperature elevation in atherosclerotic lesions. *IEEE Trans Biomed Eng* 2001;48:492-5.

(Matsui 2001b) Matsui T, Arai T, Matsumura K, Ishizuka T, Hgisawa K, Takase B, Sato S, Suzuki M, Kikuchi M, Kurita A. Determining the temperature distribution of swine aorta with simulated atheromatous plaque under pulsed laser irradiation: an experimental attempt to detect the vulnerability of atherosclerosis. *J Med Eng Technol* 2001;25:181-4.

(Moreno 2004) Moreno PR, Purushothaman KR, Fuster V, Echeverri D, Truszczynska H, Sharma SK, Badimon JJ, O'Connor WN. Plaque neovascularization is increased in ruptured atherosclerotic lesions of human aorta: implications for plaque vulnerability. *Circulation* 2004;110:2032-8.

(Naghavi 2003) Naghavi M, Madjid M, Gul K, Siadaty MS, Litovsky S, Willerson JT, Casscells SW. Thermography basket catheter: in vivo measurement of the temperature of atherosclerotic plaques for detection of vulnerable plaques. *Catheter Cardiovasc Interv* 2003;59:52-9.

(Nair 2002) Nair A, Kuban BD, Tuzcu EM, Schoenhagen P, Nissen SE, Vince DG. Coronary plaque classification with intravascular ultrasound radiofrequency data analysis. *Circulation* 2002;106:2200-6.

(Nedergaard 2003) Nedergaard J, Cannon B. The 'novel' 'uncoupling' proteins UCP2 and UCP3: what do they really do? Pros and cons for suggested functions. *Exp Physiol* 2003;88:65-84.

(Newsholme 1989) Newsholme P, Newsholme EA. Rates of utilization of glucose, glutamine and oleate and formation of end-products by mouse peritoneal macrophages in culture. *Biochem J* 1989;261:211-8.

(Nissen 2001) Nissen SE, Yock P. Intravascular ultrasound: novel pathophysiological insights and current clinical applications. *Circulation* 2001;103:604-16.

(Palou 1998) Palou A, Pico C, Bonet ML, Oliver P. The uncoupling protein, thermogenin. *Int J Biochem Cell Biol* 1998;30:7-11.

(Pasterkamp 1999) Pasterkamp G, Schoneveld AH, van der Wal AC, Hijnen DJ, van Wolveren WJ, Plomp S, Teepen HL, Borst C. Inflammation of the atherosclerotic cap and shoulder of the plaque is a common and locally observed feature in unruptured plaques of femoral and coronary arteries. *Arterioscler Thromb Vasc Biol* 1999;19:54-8.

(van de Poll 2002) van de Poll SW, Romer TJ, Puppels GJ, van der Laarse A. Imaging of atherosclerosis. Raman spectroscopy of atherosclerosis. *J Cardiovasc Risk* 2002;9:255-61.

(Rocha e Silva 1978) Rocha e Silva M. A brief survey of the history of inflammation. *Agents Actions* 1978;8:45-9.

(Schaar 2003) Schaar JA, de Korte CL, Mastik F, Strijder C, Pasterkamp G, Boersma E, Serruys PW, van der Steen AFW. Characterizing vulnerable plaque features with intravascular elastography. *Circulation* 2003;108:2636-41.

(Schaar 2004a) Schaar JA, Muller JE, Falk E, Virmani R, Fuster V, Serruys PW, Colombo A, Stefanadis C, Casscells WS, Moreno PR, Maseri A, van der Steen AF. Terminology for high-risk and vulnerable coronary artery plaques. Report of a meeting on the vulnerable plaque, Juni 17 and 18, 2003, Santorin, Greece. *Eur Heart J* 2004;25:1077-82.

(Schaar 2004b) Schaar JA, Regar E, Mastik F, McFadden EP, Saia F, Disco C, de Korte CL, de Feyter PJ, van der Steen AFW, Serruys PW. Incidence of high-strain patterns in human coronary arteries: assessment with three-dimensional intravascular palpography and correlation with clinical presentation. *Circulation* 2004;109:1965-71.

(Schmermund 2003) Schmermund A, Rodermann J, Erbel R. Intracoronary thermography. *Herz* 2003;28:505-12.

(Schwartz 2003) Schwartz RS, Bayes-Genis A, Lesser JR, Sangiorgi M, Henry TD, Conover CA. Detecting vulnerable plaque using peripheral blood: inflammatory and cellular markers. *J Interv Cardiol* 2003;16:213-42.

(Shinnar 1999) Shinnar M, Fallon JT, Wehrli S, Levin M, Dalmacy D, Fayad ZA,



Badimon JJ, Harrington M, Harrington E, Fuster V. The diagnostic accuracy of ex vivo MRI for human atherosclerotic plaque characterization. *Arterioscler Thromb Vasc Biol* 1999;19:2756-61.

(St Clair 1976) St Clair RW. Cholesteryl ester metabolism in atherosclerotic arterial tissue. *Ann N Y Acad Sci* 1976;275:228-37.

(Stary 1992) Stary HC, Blankenhorn DH, Chandler AB, Glagov S, Insull Jr. W, Richardson M, Rosenfeld ME, Schaffer SA, Schwartz CJ, Wagner WD, Wissler RW. A definition of the intima of human arteries and of its atherosclerosis-prone regions. *Circulation* 1992;85:391-405.

(Stary 1994) Stary HC, Cahndler AB, Glagov S, Guyton JR, Insull Jr. W, Rosenfeld ME, Schaffer SA, Schwartz CJ, Wagner WD, Wissler RW. A definition of initial, fatty streak, and intermediate lesions of atherosclerosis. *Arterioscler Thromb* 1994;14:840-56.

(Stary 1995) Stary HC, Chandler AB, Dinsmore RE, Fuster V, Glagov S, Insull Jr. W, Rosenfeld ME, Schwartz CJ, Wagner WD, Wissler RW. A definition of advanced types of atherosclerotic lesions and a histological classification of atherosclerosis. *Circulation* 1995;92:1355-74.

(Stary 2000) Stary HC. Natural history and histological classification of atherosclerotic lesions. *Arterioscler Thromb Vasc Biol* 2000;20:1177-8.

(Stefanadis 1998) Stefanadis C, Toutouzas P. In vivo local thermography of coronary artery atherosclerotic plaques in humans. *Ann Intern Med* 1998;129:1079-80.

(Stefanadis 1999) Stefanadis C, Diamantopoulos L, Vlachopoulos C, Tsiamis E, Dernellis J, Toutouzas K, Stefanadi E, Toutouzas P. Thermal heterogeneity within human atherosclerotic coronary arteries detected in vivo: a new method of detection by application of a special thermography catheter. *Circulation* 1999;99:1965-71.

(Stefanadis 2000) Stefanadis C, Diamantopoulos L, Dernellis J, Economou E, Tsiamis E, Toutouzas K, Vlachopoulos C, Toutouzas P. Heat production of atherosclerotic plaques and inflammation assessed by the acute phase proteins in acute coronary syndromes. *J Mol Cell Cardiol* 2000;32:43-52.

(Stefanadis 2001) Stefanadis C, Toutouzas K, Tsiamis E, Stratos C, Vavuranakis M, Kallikazaros I, Panagiotakos D, Toutouzas P. Increased local temperature in human coronary atherosclerotic plaques: an independent predictor of clinical outcome in patients undergoing a percutaneous coronary intervention. *J Am Coll Cardiol* 2001;37:1277-83.

(Stefanadis 2002) Stefanadis C, Toutouzas K, vavuranakis M, Tsiamis E, Tousoulis D, Panagiotakos DB, Vaina S, Pitsavos C, Toutouzas P. Statin treatment is associated with reduced thermal heterogeneity in human atherosclerotic plaques. *Eur Heart J* 2002;23:1664-9.

(Stefanadis 2003a) Stefanadis C, Toutouzas K, Vavuranakis M, Tsiamis E, Vaina S, Toutouzas P. New balloon-thermography catheter for in vivo temperature measurements in human coronary atherosclerotic plaques: a novel approach for thermography? *Catheter Cardiovasc Interv* 2003;58:344-50.

(Stefanadis 2003b) Stefanadis C, Toutouzas K, Tsiamis E, Mitropoulos I, Tsioufis C, Kallikazaros I, Pitsavos C, Toutouzas P. Thermal heterogeneity in stable human coronary atherosclerotic plaques is underestimated in vivo: the "cooling effect" of blood flow. *J Am Coll Cardiol* 2003;41:403-8.

(Sung 1997) Sung HW, Chen WY, Tsai CC, Hsu HL. In vitro study of enzymatic degradation of biological tissues fixed by glutaraldehyde or epoxy compound. *J Biomater Sci Polym Ed* 1997;8:587-600.

(Takahashi 2002) Takahashi K, Takeya M, Sakashita N. Multifunctional roles of macrophages in the development and progression of atherosclerosis in humans and experimental animals. *Med Electron Microsc* 2002;35:179-203.

(Thóren 1990) Thóren SA, Monti M, Holma B. Heat conduction microcalorimetry of overall metabolism in rabbit alveolar macrophages in monolayers and in suspensions. *Biochim Biophys Acta* 1990;1033:305-10.

(Toutouzas 2000) Toutouzas K, Stefanadis C, Vavuranakis M, Tsiamis E, Tsioufis C, Pitsavos C, Toutouzas P. Arterial remodeling in acute coronary syndromes: Correlation of IVUS characteristics with temperature of the culprit lesion. *Circulation* 2000;102:707.

(Toutouzas 2001) Toutouzas K, Stefanadis C, Tsiamis E, Vavuranakis M, Tsioufis C, Tsekoura D, Vaina S, Toutouzas P. The temperature of atheroscle-

rotic plaques is correlated with matrix metalloproteinases concentration in patients with acute coronary syndromes. *J Am Coll Cardiol* 2001;37:356A.

(Toutouzas 2004) Toutouzas K, Vaina S, Tsiamis E, Vavuranakis M, Mitropoulos J, Bosinakou E, Toutouzas P, Stefanadis C. Detection of increased temperature of the culprit lesion after recent myocardial infarction: the favorable effect of statins. *Am Heart J* 2004;148:783-8.

(Toutouzas 2006) Toutouzas K, Drakopoulou M, Mitropoulos J, Tsiamis E, Vaina S, Vavuranakis M, Markou V, Bosinakou E, Stefanadis C. Elevated plaque temperature in non-culprit de novo atheromatous lesions of patients with acute coronary syndromes. *J Am Coll Cardiol* 2006;47:301-6.

(Verheye 2002a) Verheye S, De Meyer GRY, Van Langenhove G, Knaapen MWM, Kockx MM. In vivo temperature heterogeneity of atherosclerotic plaques is determined by plaque composition. *Circulation* 2002;105:1596-601.

(Verheye 2002b) Verheye S, Diamantopoulos L, Serruys PW, Van Langenhove G. Imaging of atherosclerosis. Intravascular imaging of the vulnerable atherosclerotic plaque: spotlight on temperature measurement. *J Cardiovasc Risk* 2002;9:247-54.

(Verheye 2002c) Verheye S, Van Langenhove G, Diamantopoulos L, Serruys PW, Vermeersch P. Temperature heterogeneity is nearly absent in angiographically normal or mild atherosclerotic coronary segments: Interim results from a safety study. *Am J Cardiol* 2002;90:24h.

(Verheye 2004) Verheye S, De Meyer GR, Krams R, Kockx MM, Van Damme LC, Mousavi Gourabi B, Knaapen MW, Van Langenhove G, Serruys PW. Intravascular thermography: Immediate functional and morphological vascular findings. *Eur Heart J* 2004;25:158-65.

(Virmani 2000) Virmani R, Kolodgie FD, Burke AP, Farb A, Schwartz SM. Lessons from sudden coronary death. A comprehensive morphological classification scheme for atherosclerotic lesions. *Arterioscler Thromb Vasc Biol* 2000;20:1262-75.

(van der Wal 1994) van der Wal AC, Becker AE, van der Loos CM, Das PK. Site of intimal rupture or erosion of thrombosed coronary atherosclerotic plaques is characterized by an inflammatory process irrespective of the

dominant plaque morphology. *Circulation*;89:36-44.

(Wang 2000) Wang SS, VanderBrink BA, Regan J, Carr K, Link MS, Hornoud MK, Foote CM, Estes NA, Wang PJ. Microwave radiometric thermometry and its potential applicability to ablative therapy. *J Interv Card Electrophysiol* 2000;4:295-300.

(Webster 2002) Webster M, Stewart J, Ruygrok P, Ormiston J, Schott D, Gray B, Fraser A. Intracoronary thermography with a multiple thermocouple catheter: Initial human experience. *Am J Cardiol* 2002;90:24h.

(Welch 1995) Welch AJ, van Gemert MJC. Optical-thermal response of laser-irradiated tissue. New York, NY: Plenum Press, 1995.

(WHO 2003) World Health Organization. Global Health: today's challenges. In: *The World Health Report 2002 – Shaping the Future*. Geneva: World Health Organization, 2003.

(Wlodarczyk 1999) Wlodarczyk W, Hentschel M, Wust P, Noeske R, Hosten N, Rinneberg H, Felix R. Comparison of four magnetic resonance methods for mapping small temperature changes. *Phys Med Biol* 1999;44:607-24.

(Yabushita 2002) Yabushita H, Bouma BE, Houser SL, Aretz HT, Jang IK, Schlendorf KH, Kauffman CR, Shishkov M, Kang DH, Halpern EF, Tearney GJ. Characterization of human atherosclerosis by optical coherence tomography. *Circulation* 2002;106:1640-5.

(Yuan 2004) Yuan C, Kerwin WS. MRI of atherosclerosis. *J Magn Res Im* 2004;19:710-9.

(Zarrabi 2002) Zarrabi A, Gul K, Willerson JT, Casscells W, Naghavi M. Intravascular thermography: a novel approach for detection of vulnerable plaque. *Curr Opin Cardiol* 2002;17:656-62.



## SAMENVATTING

Coronaire hart- en vaatafwijkingen kosten jaarlijks wereldwijd aan 7,2 miljoen mensen het leven en zijn daarmee de belangrijkste doodsoorzaak. Afwijkingen aan de kransslagaderen, de aderen die het hart van bloed voorzien, kunnen ischemie veroorzaken, welke vaak het gevolg is van vergevorderde stadia van atherosclerose. Atherosclerose is een progressieve ontstekingsreactie, en wordt gekarakteriseerd door vetophopingen en vorming van fibreus weefsel in de grote vaten. De vulnerabele plaque is een van de ontwikkelingsstadia van atherosclerose. Een type vulnerabele plaque onderscheidt zich van andere door de aanwezigheid van een lipide opeenhoping die van het bloed wordt gescheiden door een dunne fibreuze kap. Rondom de vetophoping bevinden zich macrofagen, vaak in de kap en in de schouder gebieden van de kap. Het is aangetoond dat een ruptuur van dit type vulnerabele plaque de belangrijkste oorzaak is van hartaanvallen, en het is dus noodzakelijk dit type plaque te detecteren zodat ze tijdig behandeld kunnen worden.

Intracoronaire thermografie is een relatief nieuwe methode die mogelijk vulnerabele plaques kan detecteren door middel van thermografische technieken. Dit vakgebied vindt zijn oorsprong in een publicatie van Casscells et al (Casscells 1996), waarin thermische heterogeniteit werd aangetoond in weefsel van halsslagaderen. Deze heterogeniteit kon gekoppeld worden aan verhoogde celdichtheid en van deze cellen hadden de meeste cellen de eigenschappen van macrofagen. Na deze eerste publicatie zijn veel verschillende studies over intracoronaire thermografie gepubliceerd. De studies die zijn gerapporteerd verschillen echter in studie opzet, de gebruikte catheters en het

subject. Zowel in vivo als ex vivo data zijn gerapporteerd, dieren en mensen zijn bestudeerd en de catheters die zijn gebruikt verschillen in ontwerp. Door de vele variaties is het dan ook niet verbazingwekkend dat de gemeten temperaturen uiteenlopen. Verklaringen voor deze variaties zijn het onderwerp van hoofdstuk 2, waarin een overzicht wordt gegeven van de gepubliceerde data en ze worden benaderd vanuit een fysisch perspectief.

Om een beter beeld te krijgen van wat van invloed is op intracoronaire thermografische metingen, hebben wij numerieke simulaties verricht. Deze simulaties zijn het onderwerp van de hoofdstukken 3, 4 en 5. In hoofdstuk 3 werd onderzocht hoe de geometrie van de warmte bron van invloed is op het temperatuur profiel aan de vaatwand. De afmetingen van de warmtebron werden zowel in circumferentiële, longitudinale en radiële richting gevarieerd. Tevens werden verschillende warmteproducties van de bron beschouwd. Ook de invloed van bloedstroming op het temperatuurprofiel is bestudeerd. De maximale temperatuursverschillen, de maximale temperatuur aan de vaatwand minus de achtergrondtemperatuur, waren hoger wanneer de warmtebron groter was. De maximale temperatuursverschillen varieerden voor de verschillende geometrieën, en waren het hoogst voor de circumferentiële en de longitudinale warmtebronnen. De bloedstroom zorgde voor een substantiële afkoeling van de vaatwand, en de mate van invloed verschilde voor de warmtebron geometriën. De invloed was het grootst voor de circumferentiële bronnen en het kleinst voor de longitudinale bronnen. Wanneer de kap dikker werd, werden de maximale temperatuursverschillen kleiner, maar de invloed van de bloedstroom groter.

In hoofdstuk 4 is de warmtebron gekoppeld aan een meer realistische plaque geometrie. De warmtebron werd toegekend aan de kap, aan de schoudergebieden van de kap en aan een dunne laag weefsel rondom de lipide ophoping. Tevens werd gekeken naar wat het resultaat is wanneer al deze drie gebieden de warmtebron vormden. In dit hoofdstuk werd ook ingegaan op de invloed die de vasa vasorum heeft op het temperatuurprofiel aan de vaatwand. Tevens werd onderzocht wat de invloed is van een isolerende vetophoping. De resultaten toonden aan dat de locatie van de warmtebron het meest van invloed was op het profiel van de temperatuursverdeling aan de vaatwand. Deze invloed was het sterkst wanneer de warmtebron in de schoudergebieden van de plaque was gelokaliseerd, wat tot een zeer focale temperatuursverhoging leidde. De maximale temperatuur aan de vaatwand werd voornamelijk bepaald door de warmteproductie van de bron en het afkoelingseffect van het bloed. De isolerende werking van de vetophoping verhoogde de temperaturen aan de vaatwand wanneer de warmtebron in de kap was gelokaliseerd, en de aanwezigheid van vasa vasorum verlaagde de vaatwand temperaturen.

Dat de invloed van de catheter op het warmteprofiel niet verwaarloosd kan worden is de conclusie van hoofdstuk 5. Hierin werden een aantal ontwerp parameters van het catheterontwerp getoetst. De diameter van de catheter werd gevarieerd, het materiaal waarvan de catheter is gemaakt werd gevarieerd tussen polyurethaan en nitinol en ook naar de positie van de catheter ten opzichte van de warmtebron is gekeken. De locatie waar het thermisch gevoelige element, zoals een thermokoppel of een thermistor, geplaatst moet worden voor optimale vulnerabele plaque detectie verschilde voor catheters gemaakt van polyurethaan en van nitinol. De aanwezigheid van een polyurethaan catheter, een isolerend materiaal, verhoogde de temperaturen aan de vaatwand wanneer deze gepositioneerd was dicht bij de warmtebron. Een nitinol catheter, een geleidend materiaal, daarentegen verlaagde de temperaturen. Het thermisch gevoelige element kan het beste geplaatst worden aan het eind van de nitinol catheter, terwijl voor een polyurethaan catheter het element het beste op een kleine afstand van het cathetereinde geplaatst kan worden. Wanneer de catheter de warmtebron niet volledig bedekte, reduceerden de gemeten temperaturen tot de achtergrondtemperatuur. Hetzelfde was het geval wanneer er een dunne laag bloed tussen de vaatwand en de catheter stroomde. Het is dus van groot belang dat het thermisch gevoelige element in contact komt met de warmtebron. Het afsluiten van de bloedstroom verhoogde de temperaturen, en dit effect was het grootst voor de nitinol catheter.

Een thermografische in vivo studie is het onderwerp van hoofdstuk 6. Hiervoor is gebruik gemaakt van een muismodel waarin vergevorderde atherosclerotische plaques opgewekt kunnen worden. De plaques zijn bestudeerd met een infrarood camera. Met de gebruikte experimentele opstelling is het gebleken dat dit type plaque thermische heterogeniteit vertoont. De gemeten temperatuursverschillen zijn gekoppeld aan de macrofaag en lipide hoeveelheden die gevonden zijn met histologische kleuringen. De data zijn geanalyseerd zowel per muis, per plaque en per histologische dwarsdoorsnede. De analyse van deze data leverde geen eenduidige relatie op tussen macrofagen en temperatuursverschillen.

Gezien de nieuwheid van intracoronaire thermografische detectie van vulnerabele plaques, valt er nog veel te onderzoeken. Om de kennis omtrent de warmte producerende processen in vulnerabele plaques te vergroten zou men ze calorimetrisch kunnen bestuderen. Op deze manier zou meer inzicht verworven kunnen worden in de thermische activiteit van macrofagen, maar ook in andere mogelijke oorzaken van thermische heterogeniteit, zoals de afbraak van de extracellulaire matrix en de invloed van ontkoppelings proteïnen. Uit de numerieke simulaties blijkt verder dat ook het catheterontwerp moet worden verbeterd. De spatiale resolutie van de catheters moet worden vergroot,

het thermosensitieve element kan worden vervangen door andere uitleesmogelijkheden, bijvoorbeeld optische elementen, en de combinatie met een beeldverwerkings methode kan nog worden bestudeerd. In hoofdstuk 7 wordt hierop verder ingegaan.





## DANKWOORD

Iedereen die, op welke wijze dan ook, heeft bijgedragen aan de totstandkoming van dit proefschrift, wil ik op deze plaats van harte bedanken. In het bijzonder wil ik Frank Gijsen, Frits Mastik, Hans Schuurbijs, Kees Slager en Jolanda Wentzel bedanken, zonder wiens begeleiding, technische ondersteuning en overweldigend enthousiasme dit proefschrift niet zou zijn geschreven.

Collega's, vrienden en familie hebben op zeer uiteenlopende manieren bijgedragen aan dit proefschrift. Mijn dank aan alle collega's voor de collegialiteit tijdens de afgelopen jaren en aan mijn VWO-vriendinnen, UT-vriend(inn)en, Ouwe Koeien, volleybalvrienden en familie voor alle onmisbare ontspanning.

Mijn ouders, broer en Nico wil ik bedanken voor hun eindeloze geduld en alle steun en liefde die ik van hen heb ontvangen.

Antoinette ten Have  
Rotterdam, juli 2006





# CURRICULUM VITAE

1987-1994	VWO, RKSG Titus Brandsma, Bolsward, the Netherlands VWO, Bogerman College, Sneek, the Netherlands
1991-1992	Maumee High School, Maumee OH, U.S.A.
1994-2000	MSc Applied Physics Twente University, Enschede, the Netherlands
1999	Internship Unidad de Biofísica y Bioingeniería Facultad de Medicina, Universitat de Barcelona, Barcelona, Spain
2000	Master Thesis at Department of Biomedical Optics Twente University, Enschede, the Netherlands
2000-2001	Internship at The Van Oudenaarden Biophysics Lab Massachusetts Institute of Technology, Cambridge MA, U.S.A.
2001-2006	PhD Biomedical Engineering Thoraxcenter, Erasmus MC, Rotterdam, the Netherlands